NASA-CR-200693

FINAL REPORT FOR
NASA Grant NAG 5-2109

Parametric Robust Control and System Identification:
Unified Approach

L.H. Keel

Center of Excellence in Information Systems

Tennessee State University

330 Tenth Avenue North

Nashville, TN 37203-3401

Tel: (615) 963-7025,   Fax: (615) 963-7027

E-mail: keel@gauss.tnstate.edu

Submitted to

NASA Goddard Space Flight Center

Greenbelt, MD 20771

NASA Technical Officer: Dr. Harold P. Frisch

Code 714.1

Space Technology Division

Report Period: October 1, 1992 - December 14, 1995

March 25, 1996

Contents

1 SUMMARY

During the period of this support, a new control system design and analysis method has been studied. This approach deals with control systems containing uncertainties that are represented in terms of its transfer function parameters. Such a representation of the control system is common and many physical parameter variations fall into this type of uncertainty. Techniques developed here are capable of providing nonconservative analysis of such control systems with parameter variations. We have also developed techniques to deal with control systems when their state space representations are given rather than transfer functions. In this case, the plant parameters will appear as entries of state space matrices. Finally, a system modeling technique to construct such systems from the raw input - output frequency domain data has been developed.

2 LIST OF PUBLICATIONS SUPPORTED BY NAG 5-2109

Book

1. S.P. Bhattacharyya, H. Chapellat and L.H. Keel, *Robust Control: The Parametric Approach*, Prentice-Hall, 1995.

Refereed Journal Papers and Book Chapters

1. S.P. Bhattacharyya and L.H. Keel, "Robust Stability and Control of Linear and Multilinear Interval Systems," *Control and Dynamic Systems*, Vol. 51, Part 2, pp. 31 - 77, Academic Press, 1992.

2. L.H. Keel, J. Shaw and S.P. Bhattacharyya, "Robust Control of Interval Systems," in *Robust Control*, pp. 24 - 31, Springer Verlag, 1992.

3. S. Ahmad, L.H. Keel, and S.P. Bhattacharyya, "Robust PID Control and Lead-Lag Compensation for Linear Interval Systems," *Robustness of Dynamic Systems with Parameter Uncertainties*, pp. 251 - 260, Birhauser Press, 1992.

4. H. Chapellat, L.H. Keel, and S.P. Bhattacharyya, "Robustness Properties of Multilinear Interval Systems," *Robustness of Dynamic Systems with Parameter Uncertainties*, pp. 73 - 80, Birhauser Press, 1992.

5. S.P. Bhattacharyya and L.H. Keel, "Comments on 'Extreme Point Results for Robust Stabilization of Interval Plants with First Order Compensators", *IEEE Transactions on Automatic Control*, Vol. 38, No. 11, pp. 1734 - 1735, 1993.

6. J.-S. Lew, J.-N. Juang, and R.W. Longman, "Comparison of Several System Identification Methods for Flexible Structures," *ASME Journal of Sound and Vibration*, Vol. 167, No. 3, 1993.

7. L.H. Keel and S.P. Bhattacharyya, "Control System Design for Parametric Uncertainty," *International Journal of Robust and Nonlinear Control*, Vol. 4, pp. 87 - 100, 1994.

8. H. Chapellat, L.H. Keel, and S.P. Bhattacharyya, "Extremal Robustness of Multilinear Interval Systems," *Automatica*, Vol. 30, No. 6, pp. 1037 - 1042, 1994.

9. L.H. Keel and S.P. Bhattacharyya, "Robust Parametric Classical Control Design," *IEEE Transactions on Automatic Control*, Vol. 39, No. 7, pp. 1524 - 1530, 1994.

10. J.S. Lew, L.H. Keel, and J-N Juang "Quantification of Model Error via an Interval Model with Nonparametric Error Bound," *AIAA Journal of Guidance, Controls, and Dynamics*, Vol. 17, No. 6, pp. 1212 - 1218, 1994.

11. L.H. Keel and S.P. Bhattacharyya, "Robust Stability of Interval Matrices: A Computational Approach," *International Journal of Control*, Vol.62, No. 6, pp. 1491 - 1506, 1995

12. J.-S. Lew, "Using Transfer Function Parameter Changes for Damage Detection of Structures," *AIAA Journal*, Vol. 33, No. 11, pp. 2189 - 2193, 1995.

13. L.H. Keel and S.P. Bhattacharyya, "Phase Properties of Hurwitz Polynomials," *IEEE Transactions on Automatic Control*, Vol. 41, No. 6, 1996 (To appear)

14. T.L. Link, J.S. Lew, E. Garcia, and L.H. Keel, "Vibration Suppression of Flexible Structures with Parametric Uncertainty Using Interval Control Systems," *IEEE Transactions on Control Systems Technology*, Vol. 4, No. 3, 1996 (To apear)

Refereed Conference Papers

1. L.H. Keel and S.P. Bhattacharyya, "Stability Margins for Multilinear Interval Systems via Phase Conditions: A Unified Approach," *Proceedings of the 1993 American Control Conference*, San Francisco, CA, 1993.

2. L.H. Keel and S.P. Bhattacharyya, "Vertex Results in Robust Stability," *Proceedings of the 1993 IFAC World Congress*, Sydney, Australia, 1993.

3. L.H. Keel and S.P. Bhattacharyya, "Parametric Stability Margin for Multilinear Interval Control Systems," *Proceedings of the 1993 American Control Conference*, San Francisco, CA, 1993.

4. L.H. Keel, "Invariance of Matrix Inertia under Parameter Variations," *Third SIAM Conference on Linear Algebra: Signals, Systems, Control*, Seattle, WA, 1993.

5. J.S. Lew, L.H. Keel, and J-N. Juang, "Quantification of Model Error via an Interval Model with Nonparametric Error Bound," *Proceedings of the 1993 AIAA Guidance, Navigation, and Control Conference*, Montery, CA, 1993.

6. S. Bhattacharyya, L.H. Keel, and S.P. Bhattacharyya, "Robust Stabilizer Synthesis for Interval Plants Using Nevanlina-Pick Theory," *Proceedings of the 32nd IEEE Conference on Decision and Control*, San Antonio, TX, 1993.

7. J.-S. Lew, "Application of Singular Value Decomposition for Static Equilibrium Analysis of Mechanical Systems," *Processdings of the 1993 ASME Design Automation Conference*, Albuquerque, NM, 1993.

8. J.S. Lew, T.L. Link, E. Garcia, and L.H. Keel, "Interval Model Identification for Flexible Structures with Uncertain Parameters," *Proceedings of the 1994 AIAA/ASME Adaptive Structures Forum*, Hilton Head, SC, 1994.

9. L.H. Keel, J.S. Lew, and S.P. Bhattacharyya, "System Identification Using Interval Dynamic Models," *.Proceedings of the 1994 American Control Conference*, Baltimore, MD, 1994.

10. T.L. Link, J.S. Lew, E. Garcia, and L.H. Keel, "Robustness Verification for Flexible Structures via Interval Control Systems," *Proceedings of 1994 AIAA Conference on Guidance, Navigation, and Control*, Scollsdale, AZ, 1994.

11. L.H. Keel and S.P. Bhattacharyya, "Robust Stability of Interval Matrices: A Computational Approach," *Proceedings of the 1994 Asian Control Conference*, Tokyo, Japan, 1994.

12. S.P. Bhattacharyya and L.H. Keel, "Robust Stability and Control," *Proceedings of the 3rd IFAC Symposium on Advances in Control Education*, Tokyo, Japan, 1994.

13. J.-S. Lew, "Comparison of Interval Modeling Techniques for Structures with Uncertain Parameters," *Proceedings of the 5th International Conference on Adaptive Structures*, Technomic Publishing, 1995.

14. J.-S, Lew, "Using Transfer Function Parameter Changes for Damage Detection of Structures," *Proceedings of the AIAA/ASME Adaptive Structures Forum*, Washington, DC, 1995.

15. L.H. Keel and S.P. Bhattacharyya, "Phase Properties of Hurwitz Polynomials," *Proceedings of the 34th IEEE Conference on Decision and Control*, New Orleans, LA, December 13 - 15, 1995.

16. J.-S. Lew, "Torque Converter Clutch Slip Control with Fliction Uncertainty," *Proceedings of the 1996 SAE International Congress & Exposition*, Detroit, MI, February 26 - 29, 1996.

17. Y.C. Kim and L.H. Keel, "Robust Stabilization of a Magnetic Levitation Vehicle," *Proceedings of the 1st International Symposium on Intelligent Automation and Control*, Montpellier, France, May 27 - 30, 1996 (To appear).

3 INTRODUCTION

The subject of robust control began to receive worldwide attention since the late 1970's. In particular, since the seminal theorem of Kharitonov, the problem of robustness under parametric uncertainty became one of the major subjects in which researchers heavily invested their efforts. Through this project, we aimed to achieve meaningful analysis and design mechanisms for a system whose uncertainties are modeled as parameters of the transfer function coefficients. At present the theory is capable of determining the largest parametric stability margin in various forms of measures, the worst case gain and phase margins, the worst case unstructured (H_∞) stability margin, and the nonlinear sector bounded stability margin while the given parametric uncertainty is simultaneously presented. These novel analysis techniques are equally applicable to systems whose transfer function coefficients are linear or multilinear functions of parameters subject to perturbations. These results have also been tailored to solve the problem when the state space representation of the system rather than transfer function is given. In this case, some entries of state space matrices are considered as perturbed parameters.

Moreover, the techniques developed here overcome the difficulties that are encountered by the traditional frequency domain classical domain analysis and design when multiple parameter variations are presented. We have successfully developed new tools that enable us to construct Bode, Nyquist, and Nicholes templates for the control system containing multiple parameter variations. Using these innovative techniques, designers now have access to information which is vital to the design of control systems. As a result, the Matlab based toolbox for Robust Parametric Control has been implemented, and the final stage of testing is being conducted. A portion of this toolbox is available through a Mathworks' anonymous ftp site for those interested in this research. The results have also been extended to the problem of system identification. Our technique effectively constructs a parameterized transfer function from the given set of input - output pairs of data that represents the behavior of the system to be modeled.

For the past three years of this NASA support, numerous important publications have been generated. Our recent book, *Robust Control: The Parametric Approach* published by Prentice Hall Publishing Company, contains the details of this research.

The remainder of this report is organized as follows: In section 4, we describe the basic mathematics used in robust stability problems for interval systems. These results are further extended to achieve frequency domain properties of such systems. In conjunction with this frequency domain information, design and analysis techniques which are similar to those used in classical control are described in detail. In section 5, the result of Section 4 is improved to deal with more complex systems (multilinear interval systems). All the results developed in the framework of interval systems are extended to this class of systems. The main tool we have employed here is the Mapping Theorem. Section 6 shows an interval system modeling technique, and it is successfully applied to a large space structure with variable load. This section demonstrates successful application of the results. Finally, using the results obtained for multilinear interval systems, some techniques are presented which determine robust stability of the system when the state space representation is given.

4   ROBUST CONTROL VIA INTERVAL SYSTEMS

Frequency response methods play a fundamental role in the fields of control, communications and signal processing. Classical control focuses on the frequency domain properties of control systems and has developed design methods based on simple but powerful graphical tools such as the Nyquist plot, Bode plots, and Nichols Chart. These techniques are well known and are popular with practicing engineers. However, they were developed for a fixed nominal system and in general are inapplicable when several uncertain parameters are present. In these situations it is necessary to evaluate the frequency domain behaviour of the *entire family* of systems in order to effectively carry out analysis and design.

A brute force approach to this problem (grid the uncertainty set) can be avoided by assuming a certain amount of structure for the perturbations even if such an assumption introduces some conservatism. In this section we shall consider the class of linear interval systems where the uncertain parameters lie in intervals and appear linearly in the numerator and denominator coefficients of the transfer functions. For example, the family of transfer functions

$$\mathbf{G}(s) = \frac{4s^3 + \alpha_2 s^2 + \alpha_1 s + 5}{s^4 + 10\beta_3 s^3 + \beta_2 s^2 + (\beta_1 + 2\gamma_1)s}$$

where $\alpha_2, \alpha_1, \beta_3, \beta_2, \beta_1, \gamma_1$ vary in independent intervals is a linear interval system containing six interval parameters. In this example, the uncertainty template $\mathbf{G}(j\omega)$ at each frequency ω is a complex plane set generated by the parameter vector ranging over the six dimensional parameter box. With the results to be developed in this section we will be able to replace $\mathbf{G}(s)$ by a subset of systems $\mathbf{G}_E(s)$. This extremal subset will allow us to constructively generate the *exact* boundary of the uncertainty template by means of a set of *one parameter* problems. These extremal systems will allow us to exactly calculate the boundaries of the Bode, Nyquist and Nichols plots of all transfer functions in the control system. They also can be used to calculate the worst case gain, phase, and parametric stability margins over the uncertain set of parameters. The utility of these concepts in control system design is illustrated by giving examples which robustify classical design techniques by incorporating parametric uncertainty.

We begin by considering an interval plant connected to a fixed feedback controller and develop the appropriate mathematical machinery for this system. The generalized Kharitonov segments serve to define the extremal systems. Using these systems, we calculate the boundaries of the image sets of various system transfer functions evaluated at $s = j\omega$. These include the characteristic polynomial, open and closed loop transfer functions, sensitivity and complementary sensitivity and disturbance transfer functions. We also evaluate the worst case stability margins using these extremal systems. These results depend on some simple geometric facts regarding the sum and quotients of complex plane sets. We then generalize these results to the larger class of linear interval systems using essentially the same geometric ideas.

4.1   INTERVAL CONTROL SYSTEMS

Consider the feedback system shown in Figure 1 with
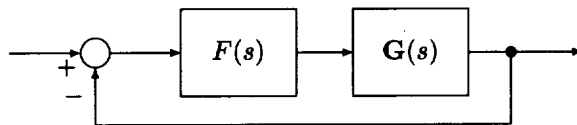
Figure 1: A unity feedback interval control system

$$F(s) := \frac{F_1(s)}{F_2(s)}, \qquad G(s) := \frac{N(s)}{D(s)}. \tag{1}$$

We suppose that $F(s)$ is fixed but $G(s)$ contains uncertain real parameters which appear as the coefficients of $N(s)$ and $D(s)$. Write

$$D(s) := a_0 + a_1 s + a_2 s^2 + a_3 s^3 + \cdots + a_{n-1} s^{n-1} + a_n s^n$$
$$N(s) := b_0 + b_1 s + b_2 s^2 + b_3 s^3 + \cdots + b_{m-1} s^{m-1} + b_m s^m \tag{2}$$

5

where $a_k \in [a_k^-, \bar{a}_k^+]$, for $k \in \underline{n} := \{1, \cdots, n\}$ and $b_k \in [b_k^-, \bar{b}_k^+]$, for $k \in \underline{m}$. Let us define the interval polynomial sets

$$\mathbf{D}(s) := \{D(s) \ : \ a_0 + a_1 s + a_2 s^2 + \cdots + a_n s^n, \ a_k \in [a_k^-, a_k^+], \ \text{for} \ k \in \underline{n}\}$$

$$\mathbf{N}(s) := \{N(s) \ : \ b_0 + b_1 s + b_2 s^2 + \cdots + b_m s^m, \ b_k \in [b_k^-, b_k^+], \ \text{for} \ k \in \underline{m}\}$$

and the corresponding set of *interval systems*:

$$\mathbf{G}(s) := \left\{ \ \frac{N(s)}{D(s)} \ : \ (N(s), D(s)) \in (\mathbf{N}(s) \mathrm{x} \mathbf{D}(s)) \ \right\}. \tag{3}$$

We refer to the unity feedback system in Figure 1 as an *interval control system*. For simplicity, we will use the notational convention

$$\mathbf{G}(s) = \frac{\mathbf{N}(s)}{\mathbf{D}(s)} \tag{4}$$

to denote the family (3). The characteristic polynomial of the system is

$$\delta(s) := F_1(s)N(s) + F_2(s)D(s) \tag{5}$$

and the set of system characteristic polynomials can be written as

$$\mathbf{\Delta}(s) := F_1(s)\mathbf{N}(s) + F_2(s)\mathbf{D}(s). \tag{6}$$

The control system is robustly stable if each polynomial in $\mathbf{\Delta}(s)$ is of the same degree and is Hurwitz.

Let $\mathcal{K}_N(s)$ and $\mathcal{K}_D(s)$ denote Kharitonov polynomials associated with $\mathbf{N}(s)$ and $\mathbf{D}(s)$, and let $\mathcal{S}_N(s)$ and $\mathcal{S}_D(s)$ denote the corresponding sets of Kharitonov segments. Recall that these segments are pairwise convex combinations of Kharitonov polynomials sharing a common even or odd part. Define the *extremal subsets*, using the above notational convention:

$$\mathbf{G}_{\mathrm{E}}(s) := \frac{\mathcal{K}_N(s)}{\mathcal{S}_D(s)} \cup \frac{\mathcal{S}_N(s)}{\mathcal{K}_D(s)} \qquad \text{(extremal systems)} \tag{7}$$

$$\mathbf{G}_{\mathrm{K}}(s) := \frac{\mathcal{K}_N(s)}{\mathcal{K}_D(s)} \qquad \text{(Kharitonov systems)}. \tag{8}$$

We shall say that $F(s)$ satisfies the *vertex condition* if the polynomials $F_i(s)$ are of the form

$$F_i(s) := s^{t_i}(a_i s + b_i)U_i(s)R_i(s), \quad i = 1, 2 \tag{9}$$

where t_i are nonnegative integers, a_i, b_i are arbitrary real numbers, $U_i(s)$ is an anti-Hurwitz polynomial, and $R_i(s)$ is an even or odd polynomial. We recall the result given by GKT.

Theorem 1. *The control system of Figure 1 is robustly stable that is stable for all $G(s) \in \mathbf{G}(s)$ if and only if it is stable for all $G(s) \in \mathbf{G}_{\mathrm{E}}(s)$. If in addition $F(s)$ satisfies the vertex condition, robust stability holds if the system is stable for each $G(s) \in \mathbf{G}_{\mathrm{K}}(s)$.*

The GKT thus reduces the problem of verifying robust stability over the multiparameter set $\mathbf{G}(s)$ to a set of one parameter stability problems over $\mathbf{G}_E(s)$ in general, and under the special conditions on $F(s)$ stated, to the vertex set $\mathbf{G}_K(s)$. In the rest of this section we shall show that the systems $\mathbf{G}_{\mathrm{E}}(s)$ and $\mathbf{G}_{\mathrm{K}}(s)$ enjoy many other useful boundary and extremal properties. They can be constructively used to carry out frequency response calculations in control system analysis and design. In fact, it will turn out that most of the important system properties such as worst case stability and performance margins over the set of uncertain parameters can be determined by replacing $G(s) \in \mathbf{G}(s)$ by the elements of $G(s) \in \mathbf{G}_{\mathrm{E}}(s)$. In some special cases one may even replace $G(s)$ by the elements of $\mathbf{G}_{\mathrm{K}}(s)$. The results are first developed for interval plants for the sake of simplicity. They hold for the more general class of linear interval systems as indicated in section 4.5.

4.2   FREQUENCY DOMAIN PROPERTIES

In order to carry out frequency response analysis and design incorporating robustness with respect to parameter uncertainty we need to be able to determine the complex plane images of various parametrized sets. In this section we will develop some computationally efficient procedures to generate such sets. We shall first consider the complex plane images of $\mathbf{\Delta}(s)$ and $\mathbf{G}(s)$ at $s = j\omega$. These sets, called uncertainty templates, are denoted $\mathbf{\Delta}(j\omega)$ and $\mathbf{G}(j\omega)$. Since $\mathbf{N}(s)$ and $\mathbf{D}(s)$ are

interval families, $\mathbf{N}(j\omega)$ and $\mathbf{D}(j\omega)$ are axis parallel rectangles in the complex plane. $F_1(j\omega)\mathbf{N}(j\omega)$ and $F_2(j\omega)\mathbf{D}(j\omega)$ are likewise rotated rectangles in the complex plane. Thus $\mathbf{\Delta}(j\omega)$ is the complex plane sum of two rectangles whereas $\mathbf{G}(j\omega)$ is the quotient of two rectangles. We assume here that $0 \notin \mathbf{D}(j\omega)$. If this assumption fails to hold we can always "indent" the $j\omega$ axis to exclude those values of ω which violate the assumption. Therefore, throughout this section we will make the standing assumption that the denominator of any quotients exclude zero.

The next lemma will show us how to evaluate the sum and quotient of two complex plane polygons Q_1 and Q_2 with vertex sets V_1 and V_2, and edge sets E_1 and E_2, respectively. Let $\partial(\cdot)$ denote the boundary of the complex plane set $(\cdot)$.

Lemma 1. (a) $\partial(Q_1 + Q_2) \subset (V_1 + E_2) \cup (E_1 + V_2)$, (b) $\partial\left(\frac{Q_1}{Q_2}\right) \subset \frac{E_1}{V_2} \cup \frac{V_1}{E_2}$.

This lemma shows us the interesting fact that the boundaries of sums and quotients of two polygons can be determined by sums and quotients of the corresponding vertex-edge pairs. Figure 2 illustrates that the boundaries of the sum of two four sided polygons are obtained by generating the sum of all segment-edge pairs. Similarly, Figure 3 shows the sum of two general polygons.

It can be shown that the inverse image of a line segment which excludes the origin, is an arc of a circle passing through the origin. This is shown in Figure 4. Therefore the inverse image of a polygon is bounded by such arcs as shown in Figure 5. To determine $\mathbf{\Delta}(j\omega)$ and $\mathbf{G}(j\omega)$ we note that the vertices of $\mathbf{N}(j\omega)$ and $\mathbf{D}(j\omega)$ correspond to the Kharitonov polynomials whereas the edges correspond to the Kharitonov segments. The set of points $\mathcal{K}_N(j\omega)$ are therefore the vertices of $\mathbf{N}(j\omega)$ and the four lines $\mathcal{S}_N(j\omega)$ are the edges of $\mathbf{N}(j\omega)$. $F_1(j\omega)\mathbf{N}(j\omega)$ is also a polygon with vertices $F_1(j\omega)\mathcal{K}_N(j\omega)$ and edges $F_1(j\omega)\mathcal{S}_N(j\omega)$. Similarly, $F_2(j\omega)\mathcal{K}_D(j\omega)$ and $F_2(j\omega)\mathcal{S}_D(j\omega)$ are the vertices and edges of the polygon $F_2(j\omega)\mathbf{D}(j\omega)$. The $j\omega$ image of the extremal systems $\mathbf{G}_E(s)$ defined earlier exactly coincides with these vertex-edge pairs. Let

$$(\mathbf{N}(s)\mathrm{x}\mathbf{D}(s))_E := (\mathcal{K}_N(s)\mathrm{x}\mathcal{S}_D(s)) \cup (\mathcal{S}_N(s)\mathrm{x}\mathcal{K}_D(s)). \tag{10}$$

Recall that the *extremal systems* are

$$\mathbf{G}_E(s) := \left\{ \frac{N(s)}{D(s)} \ : \ (N(s), D(s)) \in (\mathbf{N}(s)\mathrm{x}\mathbf{D}(s))_E \right\} := \frac{\mathcal{K}_N(s)}{\mathcal{S}_D(s)} \cup \frac{\mathcal{S}_N(s)}{\mathcal{K}_D(s)} \tag{11}$$

and define

$$\mathbf{\Delta}_E(s) := \{F_1(s)N(s) + F_2(s)D(s) \ : \ (N(s), D(s)) \in (\mathbf{N}(s)\mathrm{x}\mathbf{D}(s))_E\}. \tag{12}$$

We can now state an important result regarding the boundary of image sets.

Theorem 2. (**Boundary Generating Property**)

a) $\partial\mathbf{\Delta}(j\omega) \subset \mathbf{\Delta}_E(j\omega)$ b) $\partial\mathbf{G}(j\omega) \subset \mathbf{G}_E(j\omega)$

Example 1. Consider the problem of determining the frequency template of the interval plant

$$G(s) = \frac{n(s)}{d(s)} = \frac{b_1 s + b_0}{a_2 s^2 + a_1 s + a_0}$$

where the parameters vary as follows:

$$a_0 \in [1, 2], \quad a_1 \in [2, 3], \quad a_2 \in [2, 3], \quad b_0 \in [1, 2], \quad b_1 \in [2, 3].$$

The Kharitonov polynomials of $d(s)$ and $n(s)$ are:

$$K_d^1(s) = 3s^2 + 2s + 1, \quad K_d^2(s) = 3s^2 + 3s + 1, \quad K_d^3(s) = 2s^2 + 2s + 2, \quad K_d^4(s) = 2s^2 + 3s + 2$$

and

$$K_n^1(s) = 2s + 1, \quad K_n^2(s) = 3s + 1, \quad K_n^3(s) = 2s + 2, \quad K_n^4(s) = 3s + 2.$$

Thus, the boundary of the entire frequency domain template is obtained by the frequency evaluation of the following 32 systems:

$$\frac{K_n^i(s)}{\lambda K_d^j(s) + (1 - \lambda)K_d^k(s)} \ , \quad \text{and} \quad \frac{\lambda K_n^j(s) + (1 - \lambda)K_n^k(s)}{K_d^i(s)},$$

for

$$i = 1, 2, 3, 4; \quad (j, k) \in \{(1, 2), (1, 3), (2, 3), (3, 4)\}.$$

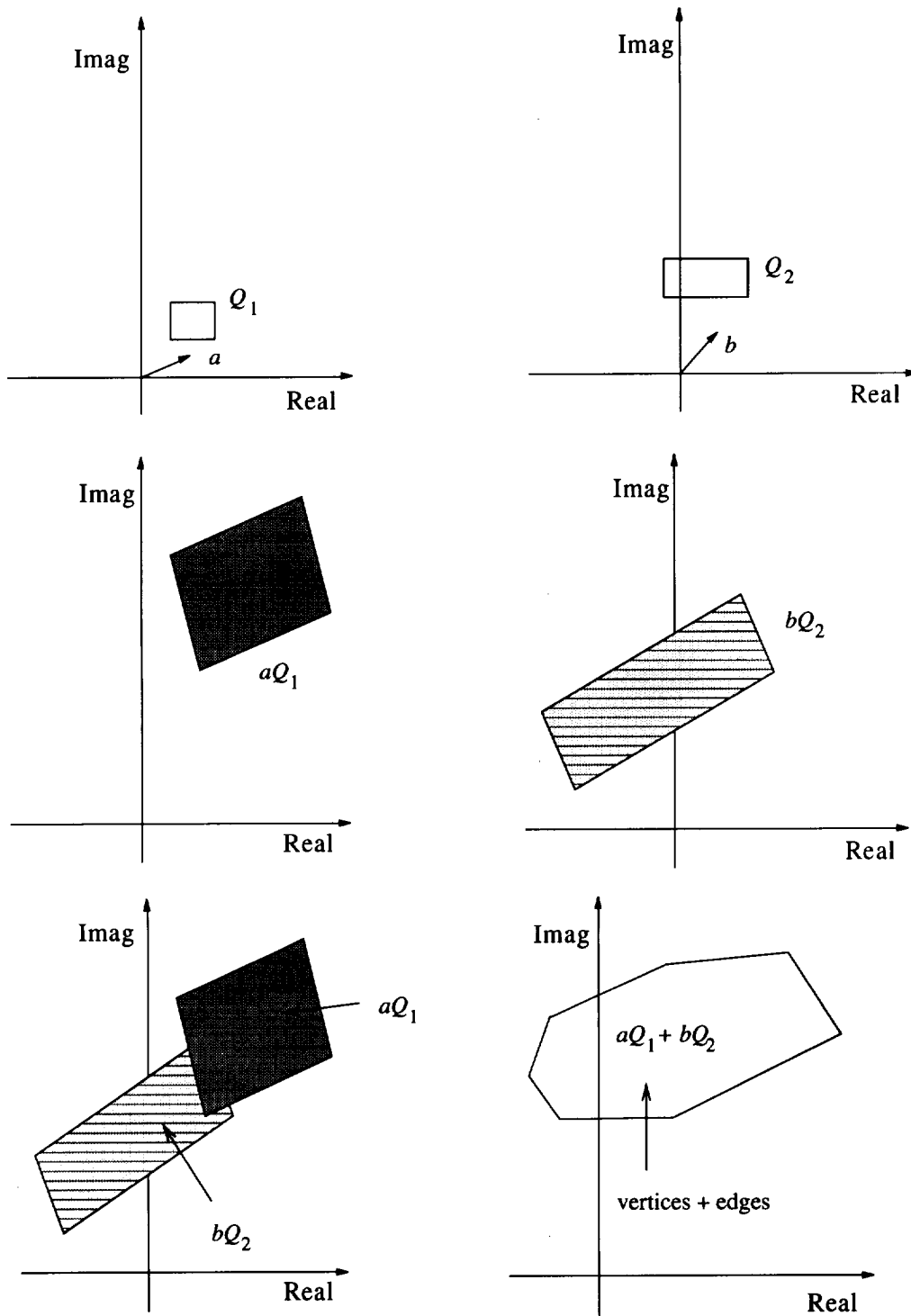Figure 6 shows the template $\mathbf{G}(j\omega)$ at $\omega = 1$.

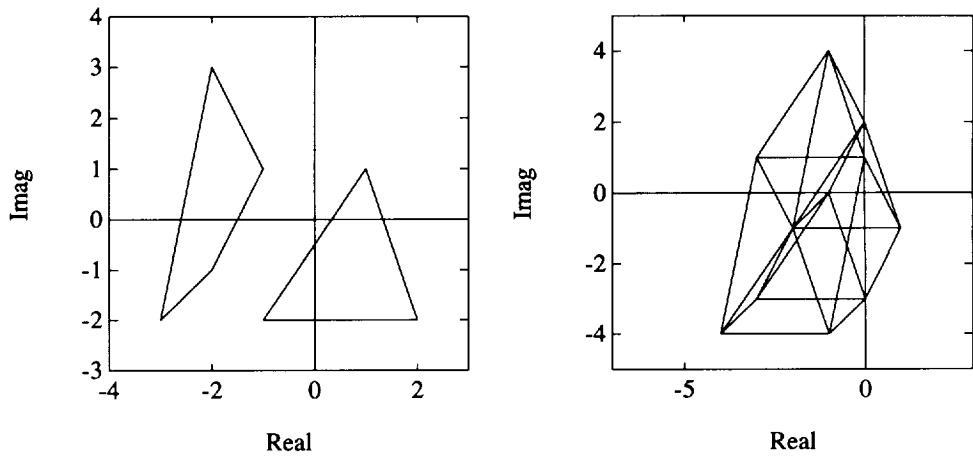Figure 2: Illustration of sum of two polygons
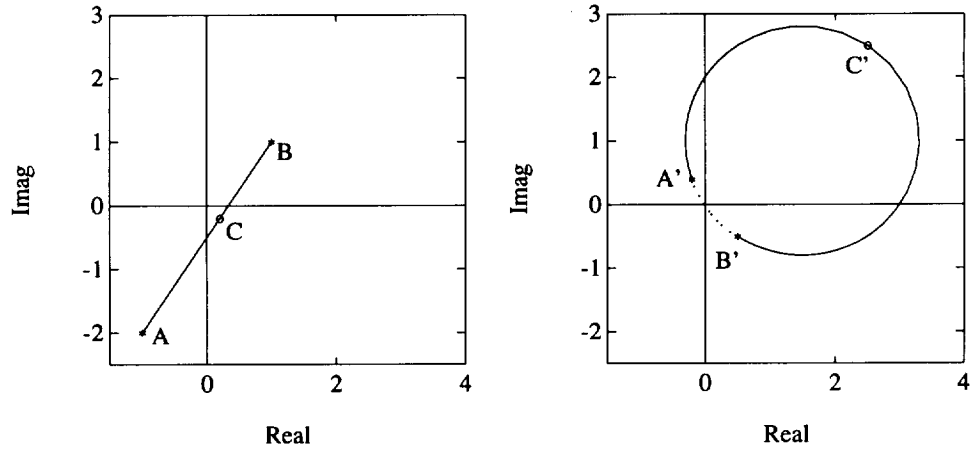
Figure 3: Sum of two polygons
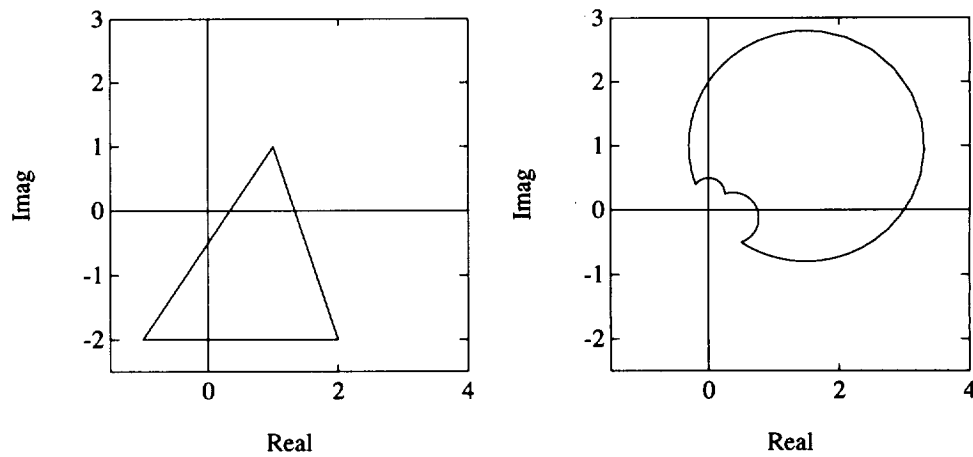

Figure 4: Line and inverse of line

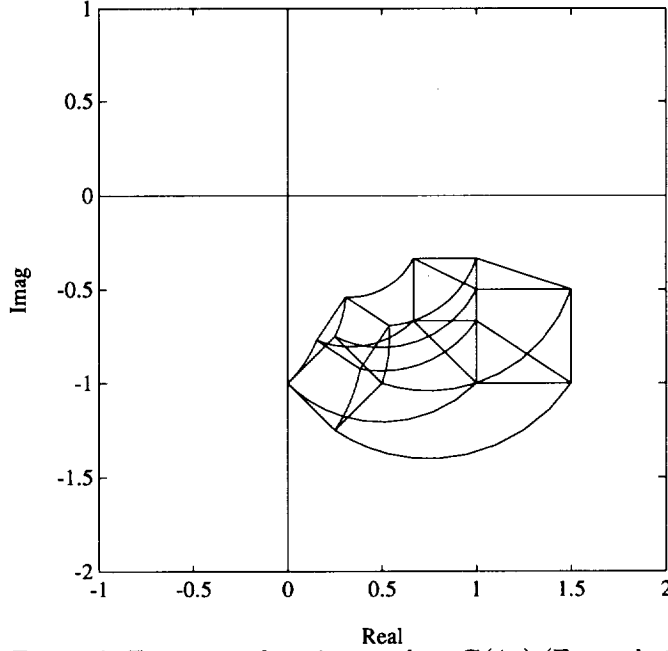Figure 5: Polygon and the inverse of polygon

9

Figure 6: Frequency domain template $\mathbf{G}(j\omega)$ (Example 1)

4.2.1 Closed Loop Transfer Functions

Referring now to the control system in Figure 1, we consider the following transfer functions of interest in analysis and design problems:

$$\frac{y(s)}{u(s)} = G(s), \qquad \frac{u(s)}{e(s)} = F(s)$$

$$T^o(s) := \frac{y(s)}{e(s)} = F(s)G(s), \qquad T^e(s) := \frac{e(s)}{r(s)} = \frac{1}{1 + F(s)G(s)} \qquad (13)$$

$$T^u(s) := \frac{u(s)}{r(s)} = \frac{F(s)}{1 + F(s)G(s)}, \qquad T^y(s) := \frac{y(s)}{r(s)} = \frac{F(s)G(s)}{1 + F(s)G(s)}.$$

As $G(s)$ ranges over the uncertainty set $\mathbf{G}(s)$ the transfer functions $T^o(s)$, $T^y(s)$, $T^u(s)$, $T^e(s)$ range over corresponding uncertainty sets $\mathbf{T}^o(s)$, $\mathbf{T}^y(s)$, $\mathbf{T}^u(s)$, and $\mathbf{T}^e(s)$, respectively. In other words,

$$\mathbf{T}^o(s) := \{F(s)G(s) \ : \ G(s) \in \mathbf{G}(s)\}, \quad \mathbf{T}^e(s) := \left\{ \frac{1}{1 + F(s)G(s)} \ : \ G(s) \in \mathbf{G}(s) \right\} \quad (14)$$

$$\mathbf{T}^u(s) := \left\{ \frac{F(s)}{1 + F(s)G(s)} \ : \ G(s) \in \mathbf{G}(s) \right\}, \quad \mathbf{T}^y(s) := \left\{ \frac{F(s)G(s)}{1 + F(s)G(s)} \ : \ G(s) \in \mathbf{G}(s) \right\}.$$

We will now show that the boundary generating property of the extremal subsets shown in Theorem 2 carries over to each of the system transfer functions listed above. In fact, we will show that the boundary of the image set at $s = j\omega$, the Nyquist plot and Bode plot boundaries of each of the above sets are all generated by the subset $\mathbf{G}_E(s)$. Introduce the subsets of (14) obtained by replacing $\mathbf{G}(s)$ by $\mathbf{G}_E(s)$:

$$\mathbf{T}^o_E(s) := \{F(s)G(s) \ : \ G(s) \in \mathbf{G}_E(s)\}, \quad \mathbf{T}^e_E(s) := \left\{ \frac{1}{1 + F(s)G(s)} \ : \ G(s) \in \mathbf{G}_E(s) \right\}(15)$$

$$\mathbf{T}^u_E(s) := \left\{ \frac{F(s)}{1 + F(s)G(s)} \ : \ G(s) \in \mathbf{G}_E(s) \right\}, \quad \mathbf{T}^y_E(s) := \left\{ \frac{F(s)G(s)}{1 + F(s)G(s)} \ : \ G(s) \in \mathbf{G}_E(s) \right\}.$$

The main result can now be stated.

Theorem 3. *For every $\omega \geq 0$,*

$(a)\partial\mathbf{T}^o(j\omega) \subset \mathbf{T}^o_E(j\omega), \quad (b)\partial\mathbf{T}^e(j\omega) \subset \mathbf{T}^e_E(j\omega), \quad (c)\partial\mathbf{T}^u(j\omega) \subset \mathbf{T}^u_E(j\omega), \quad (d)\partial\mathbf{T}^y(j\omega) \subset \mathbf{T}^y_E(j\omega)$

10

Remark 1. This result shows that at every $\omega \geq 0$, the boundary of the image set of each transfer function in (14) is contained in the corresponding image set of the extremal systems. We point out that in the definition of the interval plant $\mathbf{G}(s)$ we assumed that the numerator and denominator parameters were independent. This assumption obviously does not hold any longer when we deal with say, $\mathbf{T}^y(s)$ where the numerator and denominator depend on some common parameters. It is therefore useful to know that the boundary generating property of the set $\mathbf{G}_E(s)$ carries over nevertheless. In a later section we will show that the boundary generating property of the set $\mathbf{G}_E(s)$ will hold much more generally.

Example 2. Consider the system given in Example 1. Let us assume that $F(s) = 1$ and that we wish to calculate $\mathbf{T}^y(j\omega)$.

$$\mathbf{T}^y(s) = \left\{ \frac{G(s)}{1 + G(s)} : G(s) \in \mathbf{G}(s) \right\}.$$

For this example, we have

$$T^y(s) = \frac{b_1 s + b_0}{a_2 s^2 + (a_1 + b_1)s + (a_0 + b_0)}$$

where $a_0 \in [1,2]$, $a_1 \in [2,3]$, $a_2 \in [2,3]$, $b_0 \in [1,2]$, $b_1 \in [2,3]$.

The denominator and numerator polynomials are dependent on some of the same perturbing parameters. However, Theorem 3 handles this dependency. Since $\partial \mathbf{T}^y(j\omega) \subset \mathbf{T}^y_E(j\omega)$, it is enough to construct the following template:

$$\mathbf{T}^y_E(j\omega) = \left\{ \frac{G(j\omega)}{1 + G(j\omega)} : G(j\omega) \in \mathbf{G}_E(j\omega) \right\}.$$

In other words, we simply replace $\mathbf{G}(s)$ by $\mathbf{G}_E(s)$ in $\mathbf{T}^y$. Thus we need to construct the image of the following transfer functions for $\lambda \in [0,1]$:

$$\frac{K_n^i(j\omega)}{\lambda K_d^k(j\omega) + (1-\lambda)K_d^l(j\omega) + K_n^i(j\omega)}, \quad \text{and} \quad \frac{\lambda K_n^k(j\omega) + (1-\lambda)K_n^l(j\omega)}{\lambda K_n^k(j\omega) + (1-\lambda)K_n^l(j\omega) + K_d^i(j\omega)}$$

for $i = 1, 2, 3, 4$ and $(k, l) \in \{(1, 2), (1, 3), (2, 3), (3, 4)\}$. The sets of Kharitonov polynomials corresponding to the denominator and numerator polynomials are defined in Example 1. The frequency domain template at $\omega = 1$ is shown in Figure 7.
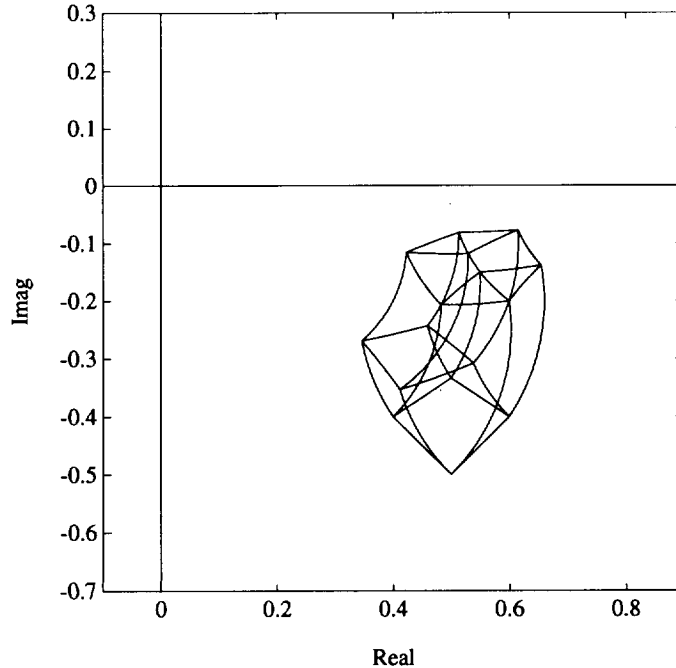

Figure 7: Frequency domain template $\mathbf{T}^y(j\omega)$ (Example 2)

11

4.3 NYQUIST, BODE, AND NICHOLS ENVELOPES

In the previous section we established that at a fixed frequency the image set template of various transfer function set can be constructed from the corresponding extremal transfer function set $\mathbf{G}_E(s)$. In control system design it is important to see the behaviour of these transfer function families for all frequency. Denote the Nyquist plot of the family $\mathbf{G}(s)$ as

$$\mathbf{G} = \cup_{0 \leq \omega < \infty} \mathbf{G}(j\omega). \tag{16}$$

The boundary of $\mathbf{G}$ is the Nyquist envelope of $\mathbf{G}$. Similarly, the Nyquist plots of $\mathbf{T}^o(s)$, $\mathbf{T}^e(s)$, $\mathbf{T}^u(s)$, and $\mathbf{T}^y(s)$ are denoted respectively by $\mathbf{T}^o$, $\mathbf{T}^e$, $\mathbf{T}^u$, and $\mathbf{T}^y$. From the boundary property of Theorem 3, it follows that the envelopes of these Nyquist plots are generated by the extremal systems.

Theorem 4. (Nyquist Envelope)
The Nyquist plots of each of the transfer function sets $\mathbf{T}^o(s)$, $\mathbf{T}^y(s)$, $\mathbf{T}^u(s)$, and $\mathbf{T}^e(s)$ are bounded by their corresponding extremal subsets:

$$(a)\partial\mathbf{G} \subset \mathbf{G}_E, \quad (b)\partial\mathbf{T}^o \subset \mathbf{T}_E^o, \quad (c)\partial\mathbf{T}^y \subset \mathbf{T}_E^y, \quad (d)\partial\mathbf{T}^u \subset \mathbf{T}_E^u, \quad (e)\partial\mathbf{T}^e \subset \mathbf{T}_E^e. \tag{17}$$

The Bode envelopes of each of the system transfer functions $\mathbf{G}(s)$, $\mathbf{T}^o(s)$, $\mathbf{T}^e(s)$, $\mathbf{T}^u(s)$, and $\mathbf{T}^y(s)$ can also be constructed if we can determine the maximum and minimum values of the magnitude and phase of the family of systems at each frequency. From the boundary relations given in Theorem 3, it again follows that these maximum and minimum values occur over the subset $\mathbf{G}_E(s)$. This leads us to the following result.

Theorem 5. (Bode Envelope)
The Bode magnitude and phase envelopes of each of the transfer function sets $\mathbf{G}(s)$, $\mathbf{T}^o(s)$, $\mathbf{T}^e(s)$, $\mathbf{T}^u(s)$, $\mathbf{T}^y(s)$ are generated respectively by the extremal subsets, $\mathbf{G}_E(s)$, $\mathbf{T}_E^o(s)$, $\mathbf{T}_E^e(s)$, $\mathbf{T}_E^u(s)$, $\mathbf{T}_E^y(s)$.

It is instructive to interpret this result from the geometric point of view. Consider the Bode plot of the interval family $\mathbf{G}(s)$. For a fixed ω^*, the image of the interval transfer function is the quotient of two convex polygons in the complex plane where the polygons represent the images of the numerator and denominator polynomial families. This is depicted in Figure 8.
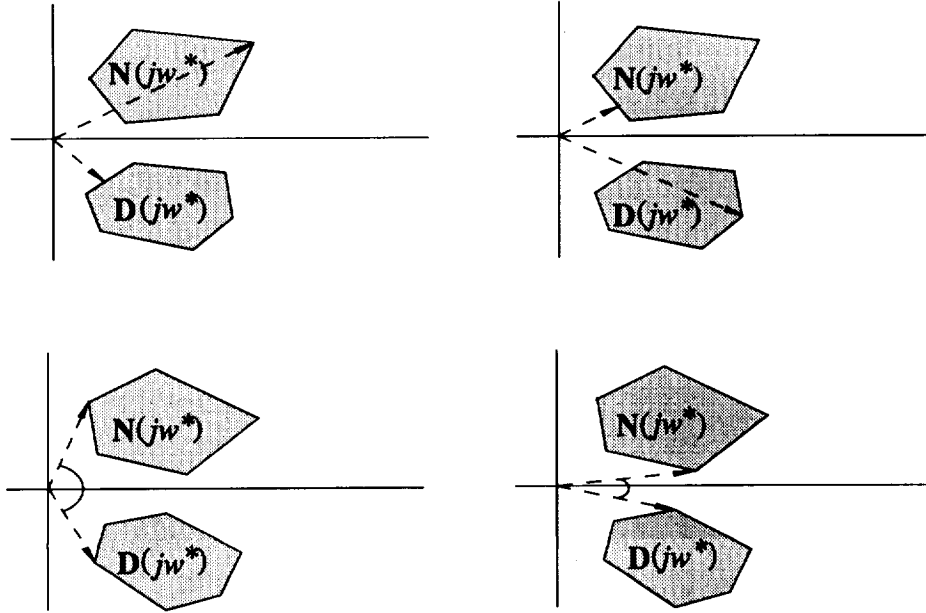

Figure 8: Extremal magnitude and phase of $\mathbf{N}(j\omega^*)$ and $\mathbf{D}(j\omega^*)$

12

From Figure 8(a) and (b), we can see that the maximum and minimum magnitudes of $G(j\omega^*)$ occur on one of the vertex-segment combinations of these polygons. Since the parameters in the numerator and denominator are independent we have:

$$\text{(a)} \quad \max\left|\frac{N(j\omega^*)}{D(j\omega^*)}\right| = \frac{\max|N(j\omega^*)|}{\min|D(j\omega^*)|} \qquad \text{(b)} \quad \min\left|\frac{N(j\omega^*)}{D(j\omega^*)}\right| = \frac{\min|N(j\omega^*)|}{\max|D(j\omega^*)|}.$$

While the maximum magnitude always occurs at a vertex the minimum can occur on an edge. The maximum and minimum points will generate the extreme points of the Bode magnitude envelope at the frequency ω^*. On the other hand, as shown in Figure 8(c) and (d), the extreme points on the phase envelope are always generated by vertex-vertex pairs:

$$\text{(c)} \quad \max\arg\frac{N(j\omega^*)}{D(j\omega^*)} = \max\arg N(j\omega^*) - \min\arg D(j\omega^*)$$

$$\text{(d)} \quad \min\arg\frac{N(j\omega^*)}{D(j\omega^*)} = \min\arg N(j\omega^*) - \max\arg D(j\omega^*).$$

The relations given in the Theorem above are useful in constructing the Bode magnitude and phase envelopes as well as Nyquist envelopes. In classical control design techniques, the Nichols Chart is also a popular computational tool. For a fixed transfer function, the Nichols Chart is a plot of the magnitude versus the phase with frequency as a running parameter. When a family of parametrized systems is involved, we get at each frequency a *magnitude-phase template*. When this template is swept over all frequencies, we get the Nichols Envelope of the family. By using the boundary property of Theorem 3 it can be seen that the Nichols Envelope is also generated by the extremal systems.

Theorem 6. (Nichols Envelope)
The Nichols Envelope of each of the transfer function sets $G(s)$, $T^o(s)$, $T^e(s)$, $T^u(s)$, $T^y(s)$ *are generated respectively by the extremal subsets,* $G_E(s)$, $T_E^o(s)$, $T_E^e(s)$, $T_E^u(s)$, $T_E^y(s)$.

The Nichols template is obtained by mapping the points of the Nyquist plane (see Figure 9) into the Nichols plane (see Figure 10). This gives the exact Nichols template.
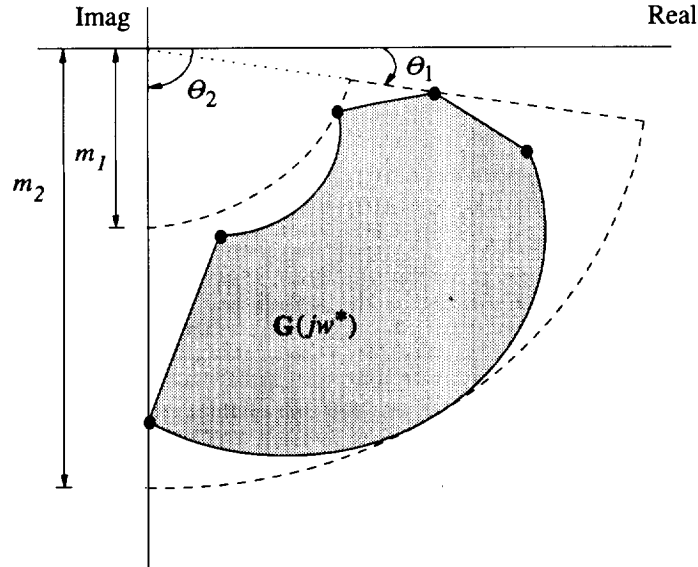
Figure 9: A Nyquist template

The Nichols envelope can also be generated approximately from the Bode magnitude and phase envelopes of the family. At each frequency we draw a rectangle in the magnitude-phase plane (Nichols plane). The dashed rectangle shown in Figure 10 corresponds to the magnitude and phase ranges obtained from the Bode envelopes. When these overbounded images of $G(j\omega)$ templates are swept over frequency, we obtain the approximate Nichols envelope which contains the actual envelope. We illustrate these computations with an example.
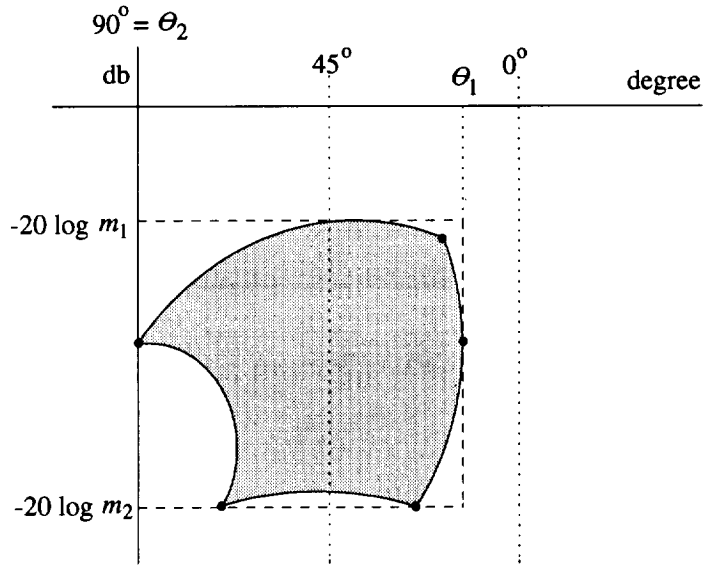
Figure 10: A Nichols template

Example 3. Consider the plant and controller

$$G(s) = \frac{b_1 s + b_0}{a_2 s^2 + a_1 s + a_0} \qquad C(s) = \frac{s^2 + 2s + 1}{s^4 + 2s^3 + 2s^2 + s}$$

where the plant parameters vary as

$$b_1 \in [0.1, 0.2], \quad b_0 \in [0.9, 1.1], \quad a_2 \in [0.9, 1.0], \quad a_1 \in [1.8, 2.0], \quad a_0 \in [1.9, 2.1].$$

Figures 11, 12, and 13 show the frequency domain plots for this example.
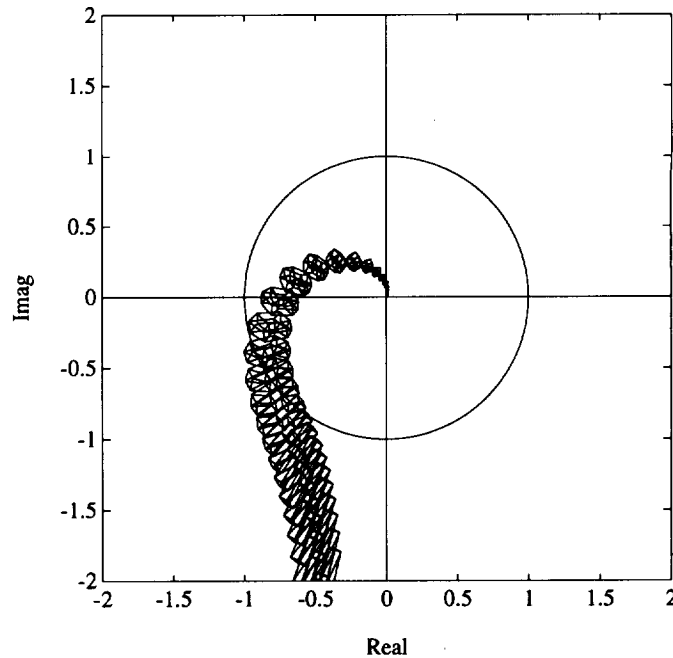
Figure 11: Nyquist templates (Example 3)

14
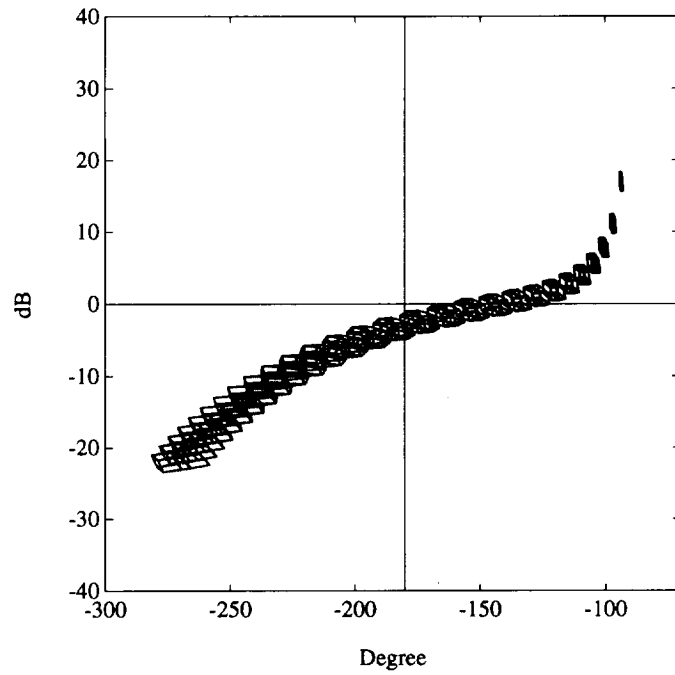
Figure 12: Nichols envelope (Example 3)
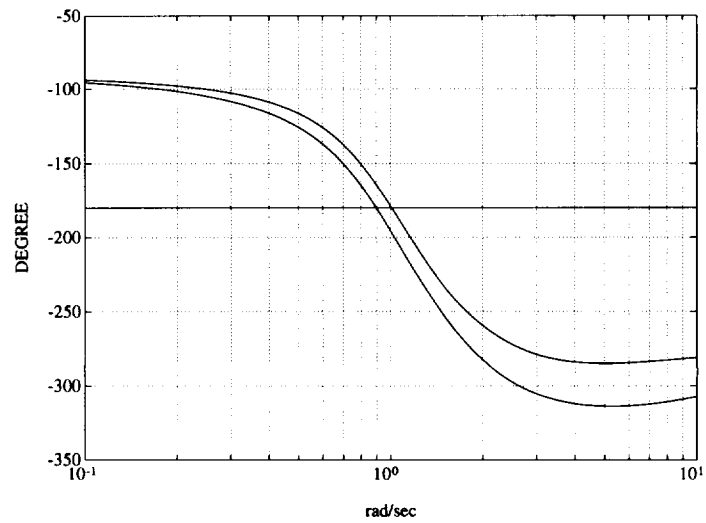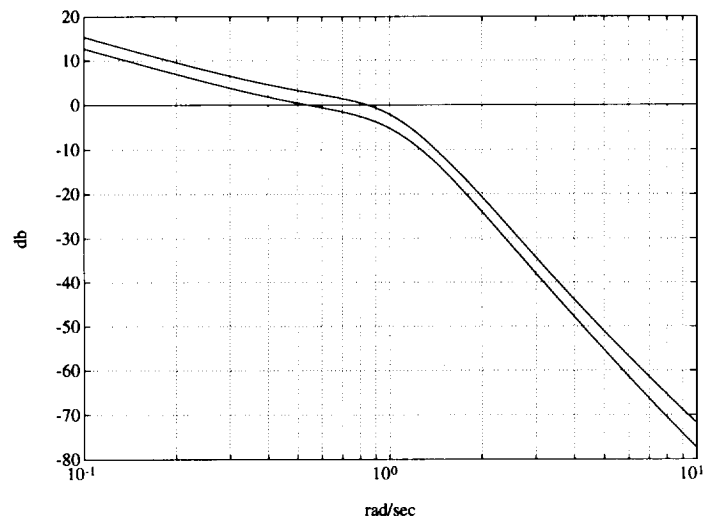
Figure 13: Bode envelopes (Example 3)

15

4.3.1 Conservatism of the Envelopes

For a fixed system, all of the above three frequency plots provide the same information on the system. However, for the case of a parametrized family of systems, the situation is quite different. The Nyquist and Nichols plots of a fixed system can be regarded as a string in the Nyquist or Nichols plane. For a parametrized family of systems, the Nyquist or Nichols plots therefore consists of a family of strings. However, the envelope of the plot is, in general, not a string that belongs to the family. In other words, there is no system in the family which generates the entire boundary of the envelope itself. On the other hand, every point on the boundary of the envelope has a string passing through it as shown in Figures 14 and 15.
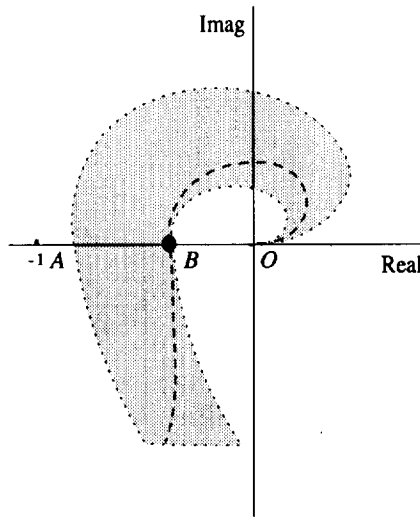

Figure 14: Nyquist envelope and Nyquist plots of individual member systems
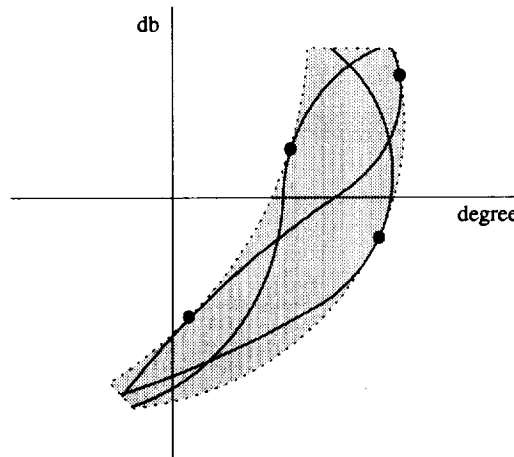
Figure 15: Nichols envelope and Nichols plots of individual member systems

The Bode envelopes in fact correspond to an overbound of the image of the complex plane set $G(j\omega)$ at each frequency ω. Considering Figure 16, we also see that each point on the boundaries of the envelopes came from a true member system of the family. From the Bode envelopes, we notice that the smallest gain margin of the family is K. However, the member system passing through the "•" point in the magnitude plot does not correspond to the phase crossover point "•" in the phase plot. Due to this phenomena, the true smallest gain margin might be bigger than K. A similar argument can be made for the case of the smallest phase margin (see Figure 17). This is because of the *independent* evaluation of the magnitude and phase envelopes of the family. In other words, despite the fact that each point on the boundaries of the Bode magnitude and phase envelopes, comes from some parameter in the family, the latter envelopes taken jointly, represent only the approximate set which corresponds to the dashed box in Figure 10 and equivalently, the dashed portion of the disc in Figure 9. Therefore, the smallest gain and phase margins read from

16
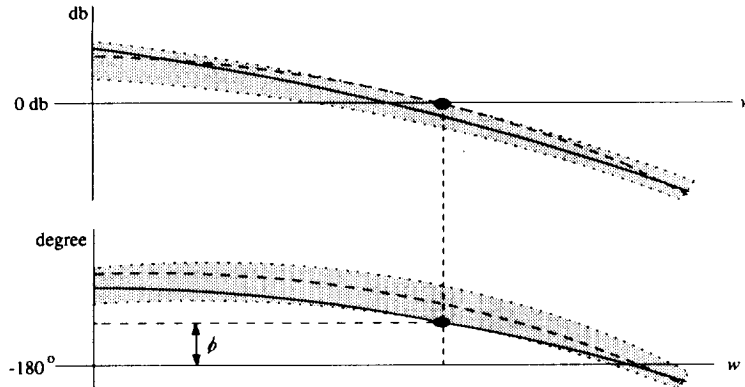
Figure 16: Bode envelopes and guaranteed phase margin
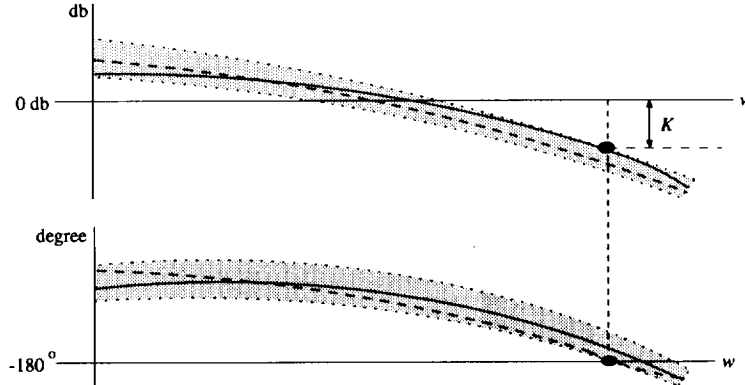
Figure 17: Bode envelopes and guaranteed gain margin

the Bode envelopes would be conservative, with the degree of conservatism depending upon how big the actual image inside the dashed box is (see Figure 10).

Remark 2. The above boundary results remain valid if $F_i(s)$ are complex functions rather than real polynomials. This is useful in applications. For example, in systems containing time-delay $F_i(s)$ could contain terms such as e^{-Ts}. Also many robust performance problems reduce to verifying robust stability under real parameter perturbations using complex compensators.

4.4 EXTREMAL STABILITY MARGINS

In this section, we deal with the calculation of guaranteed stability margins. We will first consider the gain and phase margins at the loop breaking point "m" shown in Figure 18. When $G(s)$
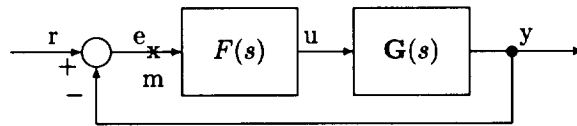
Figure 18: A unity feedback system

contains parameter uncertainty the worst case values of gain and phase margins over the parameter uncertainty set are important measures of robust performance. We show that these worst case margins in fact occur over the subset of extremal plants $\mathbf{G_E}(s)$.

4.4.1 Guaranteed Gain and Phase Margins

Suppose that $F(s)$ robustly stabilizes the family $\mathbf{G}(s)$. The gain margin of the system for a fixed $G(s) \in \mathbf{G}(s)$ is defined to be the smallest value K_G for which

$$(1 + K)F_1(s)N(s) + F_2(s)D(s)$$

17

remains stable for all $K \in [0, K_G)$. Similarly, the phase margin of the system for a fixed $G(s) \in \mathbf{G}(s)$ is defined to be the smallest value θ_G for which

$$e^{j\theta}F_1(s)N(s) + F_2(s)D(s)$$

remains stable for all $\theta \in [0, \theta_G)$. The worst case gain and phase margins are:

$$K^* := \inf_{G(s)\in\mathbf{G}(s)} K_G \qquad \theta^* := \inf_{G(s)\in\mathbf{G}(s)} \theta_G. \qquad (18)$$

Theorem 7. (Extremal Gain and Phase Margin)

I)

$$K^* = \inf_{G(s)\in\mathbf{G_E}(s)} K_G, \qquad \theta^* = \inf_{G(s)\in\mathbf{G_E}(s)} \theta_G.$$

II) If $F_i(s)$ are real and satisfy the vertex conditions specified in part II of GKT, then we have

$$K^* = \inf_{G(s)\in\mathbf{G_K}(s)} K_G$$

The proof of this theorem readily follows from the fact that $\Delta(j\omega)$ and $\Delta_E(j\omega)$ share identical boundaries. Moreover, when $F_i(s)$ satisfy the vertex conditions the proof follows from the fact that $\Delta(s)$ is stable if and only if $\Delta_K(s)$ is stable.

4.4.2 Worst Case Parametric Stability Margin

We now consider the worst case parametric stability margin. We assume as before that $F(s)$ robustly stabilizes $\mathbf{G}(s)$. The parameter $\mathbf{p}$ of dimension t consists of the coefficients of $\mathbf{N}(s)$ and $\mathbf{D}(s)$ and varies in the hypercube $\mathbf{\Pi}$. We will rewrite $\delta(s)$ in (5) as $\delta(s, \mathbf{p})$ to emphasize its dependence on the parameter $\mathbf{p}$. Let $\mathbf{\Pi_E}$ denote the parameter subset of $\mathbf{\Pi}$ corresponding to the extremal systems $\mathbf{G_E}(s)$. Let $\mathbf{\Pi_K}$ denote the parameter subset of $\mathbf{\Pi}$ corresponding to the extremal systems $\mathbf{G_K}(s)$.

Let $\| \cdot \|$ denote any norm in $\mathbf{R}^t$ and let $\mathcal{P}_\mathbf{u}$ denote the set of points $\mathbf{u}$ in $\mathbf{R}^t$ for which $\delta(s, \mathbf{u})$ is unstable or loses degree (relative to its generic degree over $\mathbf{\Pi}$). Let

$$\rho(\mathbf{p}) = \inf_{\mathbf{u}\in\mathcal{P}_\mathbf{u}} \|\mathbf{p} - \mathbf{u}\|_p$$

denote the radius of the stability ball (measured in the norm $\| \cdot \|$) and centered at the point $\mathbf{p}$. This number serves as the stability margin associated with the point $\mathbf{p}$ and indicates its distance from instability. If the box $\mathbf{\Pi}$ is stable we can associate a stability margin, denoted $\rho(\mathbf{p})$, with each point in $\mathbf{\Pi}$. A natural question to ask then is: What is the worst case value of the parametric stability margin over $\mathbf{\Pi}$ and what is the point where it occurs? An answer to this question gives an indication of how close one can get to instability over the box $\mathbf{\Pi}$.

Define a mapping from $\mathbf{\Pi}$ to the set of all positive real numbers:

$$\mathbf{\Pi} \xrightarrow{\rho} \mathcal{R}^+\backslash\{0\}, \qquad \mathbf{p} \longrightarrow \rho(\mathbf{p})$$

Our question stated in terms of functions is: Has the function $\rho(\mathbf{p})$ a minimum and is there a precise point in $\mathbf{\Pi}$ where it is reached? The answer is provided by the following theorem:

Theorem 8. (Extremal Parametric Stability Margin)

I) The minimum value over $\mathbf{\Pi}$ of $\rho(\mathbf{p})$ is reached at a point on the extremal set $\mathbf{\Pi_E}$.

II) If $F_i(s)$ satisfy the vertex conditions, the minimum value of $\rho(\mathbf{p})$ is reached at a point on the extremal set $\mathbf{\Pi_K}$.

Example 4. Consider the unity feedback control system with

$$G(s) = \frac{a_1 s + a_0}{b_2 s^2 + b_1 s + b_0} \quad \text{and} \quad F(s) = \frac{s^2 + 2s + 1}{s^4 + 2s^3 + 2s^2 + s}$$

where

$$a_1 \in [0.15 - \epsilon, 0.15 + \epsilon], \quad a_0 \in [1 - \epsilon, 1 + \epsilon],$$
$$b_2 \in [0.95 - \epsilon, 0.95 + \epsilon], \quad b_1 \in [1.9 - \epsilon, 1.9 + \epsilon], \quad b_0 \in [2 - \epsilon, 2 + \epsilon].$$

We wish to find the largest excursion of parameters allowed or equivalently the maximum value of ϵ for which closed loop stability is preserved. The image set plot at $\epsilon = 0.128$, shown in Figure 19, reveals that the phase difference reaches $180°$ at $\epsilon \approx 0.128$ (Figure 20). It is clear that any value of ϵ smaller than 0.128 results in smaller image sets than the ones shown in Figure 19. Moreover, if we sweep the frequency the connected image sets will form an envelope which does not contain the origin for $\epsilon = 0.128$. Therefore, an envelope corresponding to any value of ϵ smaller than 0.128 cannot contain the origin. Thus, we conclude that the feedback system remains stable under the perturbations bounded by this maximum value of ϵ.
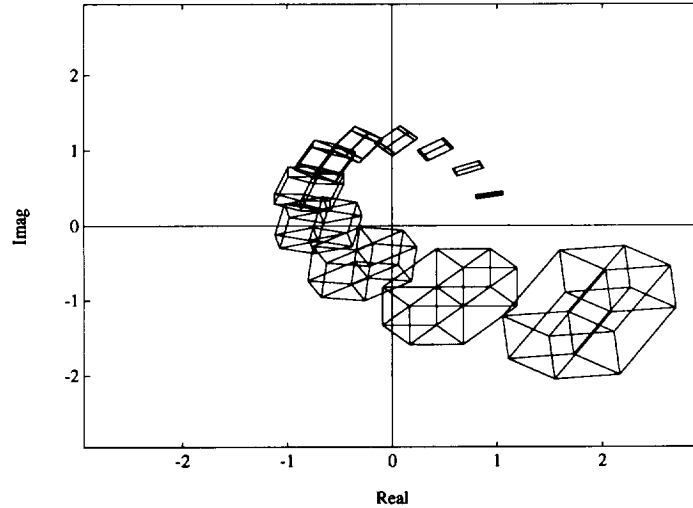
Figure 19: Image set plot at $\epsilon = 0.128$ (Example 4)
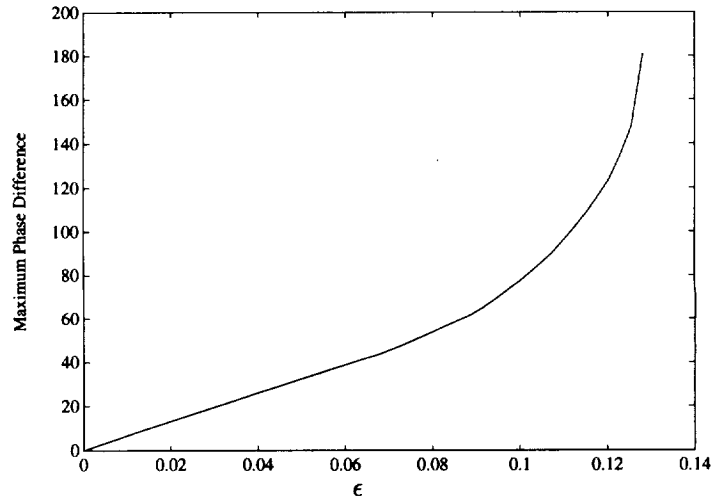
Figure 20: Phase plot (Example 4)

4.5   LINEAR INTERVAL CONTROL SYSTEMS

The results given so far in this section assume that $G(s)$ is an interval plant, namely the ratio of interval polynomials. Each of the results given shows that a particular calculation involving $G(\cdot)$ can be replaced by the corresponding calculation over the one parameter subsets $G_E(\cdot)$. This sort of simplification actually carries over to the more general class of *linear interval systems* $G(s)$ defined below. Instead of repeating all the previous results, we show in this section how to construct the extremal subsets $G_E(s)$ and leave the details of the proofs to the reader.

We still consider the unity feedback system shown in Figure 1 with

$$F(s) := \frac{F_1(s)}{F_2(s)}, \qquad G(s) := \frac{N(s)}{D(s)}. \tag{19}$$

19

We suppose that $F(s)$ is fixed, $G(s)$ is subject to parametric uncertainty and is now of the form

$$N(s) := L_1(s)A_1(s) + L_2(s)A_2(s) + \cdots + L_u(s)A_u(s)$$
$$D(s) := M_1(s)B_1(s) + M_2(s)B_2(s) + \cdots + M_v(s)B_v(s) \tag{20}$$

with $A_i(s)$ and $B_j(s)$ being *independent* interval polynomials. Write

$$A_i(s) := a_0^i + a_1^i s + a_2^i s^2 + a_3^i s^3 + \cdots + a_{n_i-1}^i s^{n_i-1} + a_{n_i} s^{n_i}$$
$$B_j(s) := b_0^j + b_1^j s + b_2^j s^2 + b_3^j s^3 + \cdots + b_{d_j-1}^j s^{d_j-1} + b_{d_j}^j s^{d_j} \tag{21}$$

where $a_k^i \in [a_k^{i-}, a_k^{i+}]$, for $k \in \underline{n_i}$ and $b_k^j \in [b_k^{j-}, b_k^{j+}]$, for $k \in \underline{d_j}$, and $L_i(s)$ and $M_j(s)$ are fixed polynomials in s. Let

$$\underline{A}(s) := [A_1(s), A_2(s), \cdots, A_u(s)], \quad \underline{B}(s) := [B_1(s), B_2(s), \cdots, B_v(s)]. \tag{22}$$

Let us define the sets

$$\mathbf{A}_i(s) := \{A_i(s) \ : \ a_0^i + a_1^i s + a_2^i s^2 + \cdots + a_{n_i}^i s^{n_i}, \ a_k^i \in [a_k^{i-}, a_k^{i+}], \text{ for } k \in \underline{n_i}\}$$
$$\mathbf{B}_j(s) := \{B_j(s) \ : \ b_0^j + b_1^j s + b_2^j s^2 + \cdots + b_{d_j}^j s^{d_j}, \ b_k^j \in [b_k^{j-}, b_k^{j+}], \text{ for } k \in \underline{d_j}\}$$

$$\mathbf{N}(s) := \left\{ \sum_{i=1}^u L_i(s)A_i(s) \ : \ (A_1(s), \cdots, A_u(s)) \in \mathbf{A}_1(s) \times \cdots \times \mathbf{A}_u(s) \right\}$$

$$\mathbf{D}(s) := \left\{ \sum_{i=1}^v M_i(s)B_i(s) \ : \ (B_1(s), \cdots, B_v(s)) \in \mathbf{B}_1(s) \times \cdots \times \mathbf{B}_v(s) \right\}$$

and the corresponding set of uncertain systems

$$\mathbf{G}(s) := \left\{ \frac{N(s)}{D(s)} \ : \ (N(s), D(s)) \in (\mathbf{N}(s) \mathrm{x} \mathbf{D}(s)) \right\} := \frac{\mathbf{N}(s)}{\mathbf{D}(s)} \tag{23}$$

is called a *linear interval system*. The Kharitonov polynomials and segments associated with $\mathbf{A}_i(s)$ are denoted $\mathcal{K}_{A_i}(s)$ and $\mathcal{S}_{A_i}(s)$, respectively. $\mathcal{K}_{B_k}(s)$ and $\mathcal{S}_{B_k}(s)$ are defined similarly. Now let us define

$$\mathbf{A}_K(s) := \mathcal{K}_{A_1}(s) \times \cdots \times \mathcal{K}_{A_u}(s), \qquad \mathbf{B}_K(s) := \mathcal{K}_{B_1}(s) \times \cdots \times \mathcal{K}_{B_v}(s) \tag{24}$$

and

$$\mathbf{A}_E^k(s) := \mathcal{K}_{A_1}(s) \times \cdots \times \mathcal{K}_{A_{k-1}}(s) \times \mathcal{S}_{A_k}(s) \times \mathcal{K}_{A_{k+1}}(s) \cdots \times \mathcal{K}_{A_u}(s),$$
$$\mathbf{B}_E^j(s) := \mathcal{K}_{B_1}(s) \times \cdots \times \mathcal{K}_{B_{j-1}}(s) \times \mathcal{S}_{B_j}(s) \times \mathcal{K}_{B_{j+1}}(s) \cdots \times \mathcal{K}_{B_v}(s) \tag{25}$$

for $k \in \underline{u}$ and $j \in \underline{v}$. Let

$$\mathbf{A}_E(s) := \cup_{i=1}^u \mathbf{A}_E^i(s), \qquad \mathbf{B}_E(s) := \cup_{i=1}^v \mathbf{B}_E^i(s). \tag{26}$$

Now introduce

$$\mathbf{N}_K(s) := \left\{ N(s) \ : \ N(s) = \sum L_i(s)A_i(s), (A_1(s), \cdots, A_u(s)) \in \mathbf{A}_K(s) \right\}$$
$$\mathbf{N}_E(s) := \left\{ N(s) \ : \ N(s) = \sum L_i(s)A_i(s), (A_1(s), \cdots, A_u(s)) \in \mathbf{A}_E(s) \right\}. \tag{27}$$

Similar definitions hold for $\mathbf{D}_K(s)$ and $\mathbf{D}_E(s)$, and the extremal subsets are:

$$(\mathbf{N}(s) \mathrm{x} \mathbf{D}(s))_E := (\mathbf{N}_K(s) \mathrm{x} \mathbf{D}_E(s)) \cup (\mathbf{N}_E(s) \mathrm{x} \mathbf{D}_K(s)). \tag{28}$$

The extremal subset of the family $\mathbf{G}(s)$ is:

$$\mathbf{G}_E(s) := \left\{ \frac{N(s)}{D(s)} \ : \ (N(s), D(s)) \in (\mathbf{N}(s) \mathrm{x} \mathbf{D}(s))_E \right\} := \frac{\mathbf{N}_K(s)}{\mathbf{D}_E(s)} \cup \frac{\mathbf{N}_E(s)}{\mathbf{D}_K(s)}. \tag{29}$$

In words the extremal set is obtained by fixing all the A_i, B_j at Kharitonov vertices except one and letting this one range over the Kharitonov segments. We remark here that in the more general case where some of the A_i and B_j happen to be identical the same procedure for constructing the extremal subset will work except that this constraint must be imposed on $\mathbf{G}_E(s)$.

With the above definitions we can verify that $\mathbf{N}(j\omega)$ and $\mathbf{D}(j\omega)$ are polygons. The vertices of $\mathbf{N}(j\omega)$ are contained in the set $\mathbf{N}_K(j\omega)$ and the edges of $\mathbf{N}(j\omega)$ are contained in $\mathbf{N}_E(j\omega)$. Similar relations hold for $\mathbf{D}(j\omega)$. From this, it follows easily that for the class of linear interval systems $G(s)$ defined in (20) - (23) each of the statements given in Theorems 1 - 8 remains valid with $\mathbf{G}_E(s)$ defined as in (29). The conditions are constructive because here again $\mathbf{G}_E(s)$ is a set of one parameter families. We illustrate the above calculations in the example below.

Example 5. Consider the linear interval system

$$G(s) = \frac{L_1(s)A_1(s)}{M_1(s)B_1(s) + M_2(s)B_2(s)} = \frac{5(\gamma_1 s + \gamma_0)}{s(\alpha_3 s^3 + \alpha_2 s^2) + (\beta_2 s^2 + \beta_1 s)}$$

where $\gamma_1 \in [0.40, 1.60]$, $\gamma_0 \in [19.40, 20.60]$, $\alpha_3 \in [0.40, 1.60]$, $\alpha_2 \in [7.40, 8.60]$, $\beta_2 \in [31.4, 32.6]$, $\beta_1 \in [74.45, 75.65]$. Here, we illustrate the construction of Bode, Nyquist, and Nichols templates. First we write the Kharitonov polynomials of $A_1(s)$, $B_1(s)$, and $B_2(s)$:

$$K_{A_1}^1(s) = 1.6s^3 + 8.6s^2 \qquad K_{A_1}^2(s) = 0.4s^3 + 8.6s^2 \qquad K_{A_1}^3(s) = 1.6s^3 + 7.4s^2$$

$$K_{A_1}^4(s) = 0.4s^3 + 7.4s^2 \qquad K_{B_1}^1(s) = 32.6s^2 + 74.45s \qquad K_{B_1}^2(s) = 32.6s^2 + 75.65$$

$$K_{B_1}^3(s) = 31.4s^2 + 74.45s \qquad K_{B_1}^4(s) = 31.4s^2 + 75.65s \qquad K_{B_2}^1(s) = 0.4s + 19.4s$$

$$K_{B_2}^2(s) = 1.6s^2 + 19.4s \qquad K_{B_2}^3(s) = 0.4s^2 + 20.6s \qquad K_{B_1}^4(s) = 1.6s^2 + 20.6s$$

Then the extremal systems we will deal with are

$$\frac{L_1(s)\left(\lambda K_{A_1}^i(s) + (1-\lambda)K_{A_1}^k(s)\right)}{M_1(s)K_{B_1}^l(s) + M_2(s)K_{B_2}^j(s)},$$

$$\frac{L_1(s)K_{A_1}^i(s)}{M_1(s)\left(\lambda K_{B_1}^k(s) + (1-\lambda)K_{B_1}^l(s)\right) + M_2(s)K_{B_2}^j(s)}, \qquad \frac{L_1(s)K_{A_1}^i(s)}{M_1(s)K_{B_1}^j(s) + M_2(s)\left(\lambda K_{B_2}^k(s) + (1-\lambda)K_{B_2}^l(s)\right)},$$

for $i, j = 1, 2, 3, 4$; $(k, l) \in \{(1, 2), (1, 3), (2, 4), (3, 4)\}$. Figures 21, 23 and 22 show the Nyquist, Bode and Nichols envelopes of the system respectively.
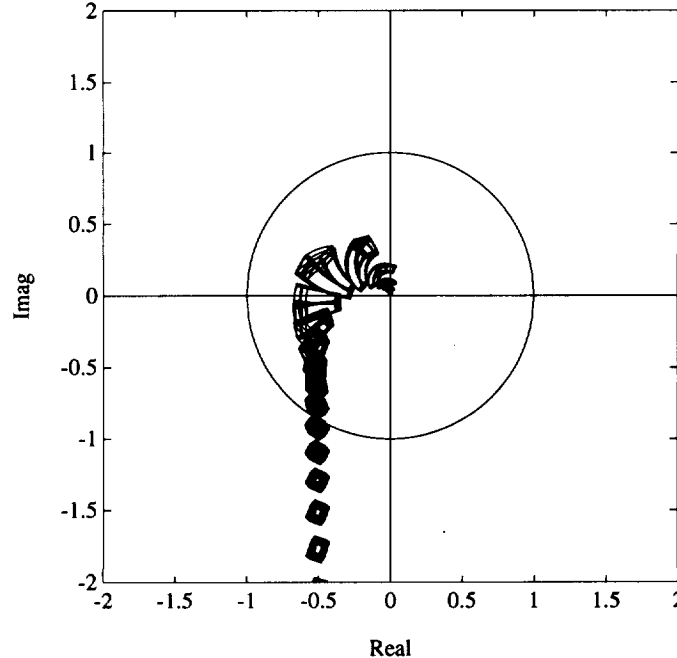

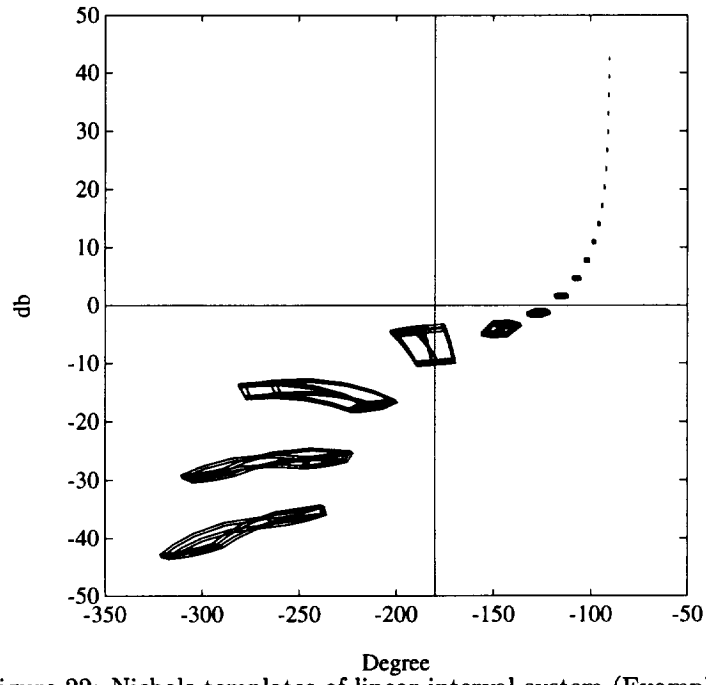Figure 21: Nyquist templates of linear interval system (Example 5)

21

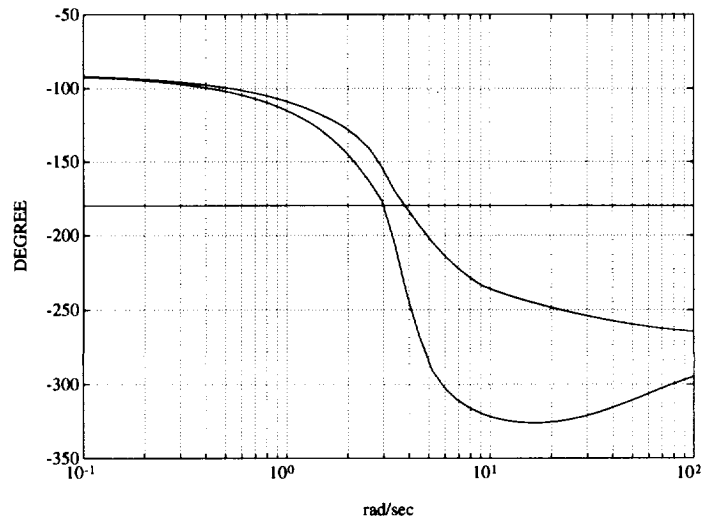Figure 22: Nichols templates of linear interval system (Example 5)
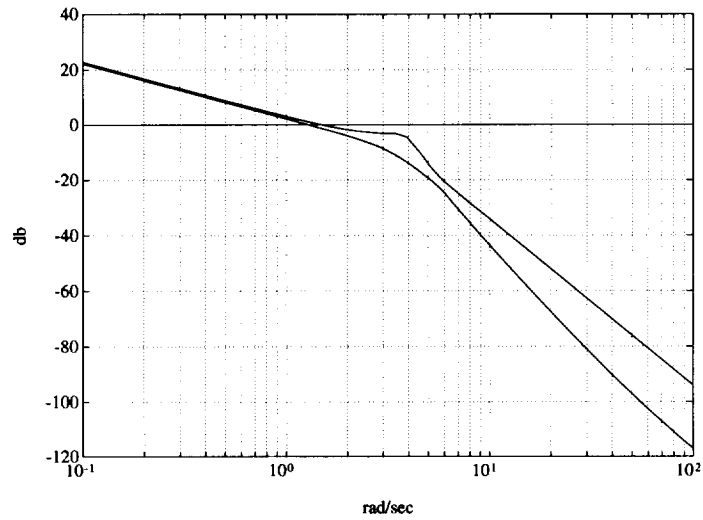

Figure 23: Bode envelopes of linear interval system (Example 5)

22

4.6 POLYTOPIC SYSTEMS

In many models containing parametric uncertainty the only convenient representation is one where each independent parameter is explicitly displayed. In this case, we write

$$G(s) := \frac{a_1 L_1(s) + a_2 L_2(s) + \cdots + a_u L_u(s)}{b_1 M_1(s) + b_2 M_2(s) + \cdots + b_v M_v(s)} \tag{30}$$

and let

$$\mathbf{G}(s) := \left\{ G(s) \ : \ a_i^- \le a_i \le a_i^+, \ b_j^- \le b_j \le b_j^+, \ i \in \underline{u}, \ j \in \underline{v} \right\} \tag{31}$$

denote the family of uncertain systems. Let

$$\mathbf{p} := [a_1, a_2, \cdots, a_u, b_1, b_2, \cdots, b_v] \tag{32}$$

denote the parameter vector and

$$\Pi := \left\{ \mathbf{p} \ : \ a_i^- \le a_i \le a_i^+, \ b_j^- \le b_j \le b_j^+, \ i \in \underline{u}, \ j \in \underline{v} \right\} \tag{33}$$

the uncertainty polytope. Write (30) as $G(s, \mathbf{p})$ to emphasize its dependence on $\mathbf{p}$. For convenience we refer to the family of systems $G(s, \mathbf{p}) : \mathbf{p} \in \Pi$ represented in the form (30) as a *polytopic system*. Of course a polytopic system is just a special case of a linear interval system with the uncertain polynomials being of degree zero.

Let Π_E denote the exposed edges of Π and introduce the extremal systems

$$\mathbf{G}_E(s) := \left\{ G(s, \mathbf{p}) \ : \ \mathbf{p} \in \Pi_E \right\}. \tag{34}$$

Now suppose that s^* is an arbitrary point in the complex plane, where the image set $\mathbf{G}(s^*)$ needs to be found. In the Hurwitz case we might have $s^* = j\omega$ and in a discrete time control system, for example, s^* could be a point on the unit circle. We have the following result.

Theorem 9.

$$\partial \mathbf{G}(s^*) \subset \mathbf{G}_E(s^*).$$

All the results of Theorems 1 to 8 carry over to this general case with the extremal set $\mathbf{G}_E(s)$ being defined by (34). The more general case where some a_i, b_j are identical can be handled by imposing the same constraint on $\mathbf{G}_E(s)$.

4.7 LINEAR FRACTIONAL TRANSFORMATIONS OF INTERVAL SYSTEMS

We have thus far assumed that our uncertain system is described by an interval system, a linear interval system, or a polytopic system model. In each of these cases we developed extremal and boundary results under the assumption that the numerator and denominator parameter sets are *disjoint* or that they perturb *independently*. On the other hand, we saw that these extremal and boundary results carry over to all the feedback system transfer functions even though, in some of these, the numerator and denominator do contain *common* uncertain parameters. A natural question to ask therefore is: What is a useful general model with interval parametric uncertainty, incorporating dependencies between numerator and denominator parameters, for which boundary or extremal results can be obtained? It turns out that a very broad class of systems of this type can be encompassed under the class of *linear fractional transformations* of an linear interval system.

Therefore, let us suppose that $\mathbf{G}(s)$ is a linear interval system (see (23)) with independent uncertain interval polynomials $A_i(s), B_j(s)$ and let $\mathbf{G}_E(s)$ denote the extremal subset as defined in Section 4.5. Let $P(s), Q(s), R(s), S(s)$ be four arbitrary fixed functions and consider the transformation

$$H(s) = \frac{P(s)G(s) + Q(s)}{R(s)G(s) + S(s)}.$$

We suppose that the transformation is well defined $(R(s)G(s) + S(s) \ne 0)$ and refer to such a transformation as a *linear fractional transformation*. Obviously $H(s)$ contains, in general, common interval parameters in the numerator and denominator even though $G(s)$ has only independent parameters in the numerator and denominator. As before let

$$\mathbf{H}(s) := \left\{ \frac{P(s)G(s) + Q(s)}{R(s)G(s) + S(s)} : G(s) \in \mathbf{G}(s) \right\}$$

and let

$$\mathbf{H}_E(s) := \left\{ \frac{P(s)G(s) + Q(s)}{R(s)G(s) + S(s)} : G(s) \in \mathbf{G}_E(s) \right\}.$$

We show below that under mild conditions on the set $P(s), Q(s), R(s), S(s)$ the boundary of the set $\mathbf{H}(j\omega)$ is generated by the extremal set $\mathbf{G}_E(j\omega)$.

Theorem 10. *If*

$$P(j\omega)S(j\omega) - Q(j\omega)R(j\omega) \neq 0$$

we have

$$\partial\mathbf{H}(j\omega) \subset \mathbf{H}_E(j\omega).$$

Remark 3. With this result in hand it is easy to see that all the extremal and boundary results stated in this section carry over to linear fractional transformations of linear interval systems. The practical implication of this result is that by adjusting the set $P(s), Q(s), R(s), S(s)$ we can account for a large class of interdependencies between the perturbations. It is easy to show that all the transfer functions that occur in a closed loop system can be shown to be linear fractional transformations of $G(s)$ which satisfy the restriction stated in the theorem above. Thus it is not surprising that the extremal results stated in Theorem 3 hold. Finally, we point out that the boundary generating property of $\mathbf{G}_E(s)$ continues to hold for any further linear fractional transformations applied to $H(s)$.

Example 6. Let us consider the block diagram shown in Figure 24.
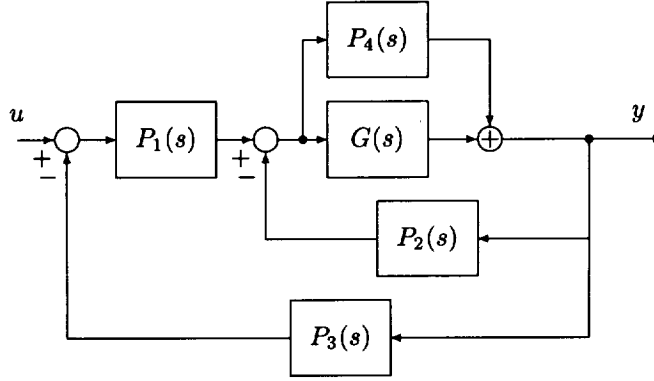
Figure 24: A feedback system

The closed loop transfer function of the system is

$$\frac{y(s)}{u(s)} = \frac{P_1(s)P_4(s) + P_1(s)G(s)}{1 + [P_1(s)P_3(s) + P_2(s)]\,P_4(s) + [P_1(s)P_3(s) + P_2(s)]\,G(s)} = H(s).$$

If $G(s)$ belongs to an interval transfer function family $\mathbf{G}(s)$, then the family of output transfer functions is

$$\mathbf{H}(s) = \left\{ \frac{P_1(s)P_4(s) + P_1(s)G(s)}{1 + [P_1(s)P_3(s) + P_2(s)]\,P_4(s) + [P_1(s)P_3(s) + P_2(s)]\,G(s)} : G(s) \in \mathbf{G}(s) \right\}$$

$$= \left\{ \frac{\overbrace{P_1(s)}^{P(s)}G(s) + \overbrace{P_1(s)P_4(s)}^{Q(s)}}{\underbrace{[P_1(s)P_3(s) + P_2(s)]}_{R(s)}G(s) + \underbrace{1 + [P_1(s)P_3(s) + P_2(s)]\,P_4(s)}_{S(s)}} : G(s) \in \mathbf{G}(s) \right\}.$$

Thus, if

$$P(j\omega)S(j\omega) - Q(j\omega)R(j\omega) \neq 0,$$

we have

$$\partial\mathbf{H}(j\omega) \subset \mathbf{H}_E(j\omega).$$

The point is, that even though $\mathbf{H}(s)$ is *not* an interval transfer function, the boundary of $\mathbf{H}(j\omega)$ is captured by replacing $\mathbf{G}(s)$ by the elements of the extremal set $\mathbf{G}_E(s)$ which is a considerable saving. Similar results hold for the Nyquist and Bode envelopes, and in fact all extremal properties of $\mathbf{H}(s)$ will occur on the subset $\mathbf{H}_E(s)$.

4.8 ROBUST PARAMETRIC CLASSICAL DESIGN

We illustrate the utility of the above tools in extending the design techniques of classical control to systems containing parameter uncertainty. The requirement of robust design is that the design specifications must be satisfied over the entire parameter set. Thus the worst case values must be acceptable. Since these worst case values occur over the extremal set $\mathbf{G}_E(s)$, it suffices to verify that the specifications are met over this set.

4.8.1 Guaranteed Classical Design

Example 7. Consider the interval plant

$$\mathbf{G}(s) = \frac{n_0}{d_3 s^3 + d_2 s^2 + d_1 s + d_0}$$

with $n_0 \in [10, 20]$, $d_3 \in [0.06, 0.09]$, $d_2 \in [0.2, 0.8]$, $d_1 \in [0.5, 1.5]$, $d_0 = 0$. The objective is to design a controller so that the closed loop system

a) is robustly stable under all parameter perturbations,

b) possesses a guaranteed phase margin of at least 45°. In other words the worst case phase margin over the set of uncertain parameters must be better than 45°, and

c) possesses a bandwidth greater than or equal to 0.1 [rad/sec] with a reasonable value of resonant peak M_p.

We simply follow the standard classical control design techniques with the new tools developed here. First we construct the Bode envelopes of the open loop interval plant $\mathbf{G}(s)$. From the magnitude and phase envelopes, we observe that the worst case phase margin of 50° is achieved if the gain crossover frequency ω_c' is at 0.5 [rad/sec]. In order to bring the magnitude envelope down to 0 [dB] at the new crossover frequency ω_c', the phase lag compensator of the form

$$C(s) = \frac{1 + aTs}{1 + Ts}, \quad a < 1$$

must provide the amount of attenuation equal to the minimum value of the magnitude envelope at ω_c':

$$\max_{G(j\omega_c') \in \mathbf{G}(j\omega_c')} |G(j\omega_c')| = -20 \log_{10} a [dB].$$

Thus, we have $a = 0.01$. Now we choose the corner frequency $\frac{1}{aT}$ to be one decade below ω_c':

$$\frac{1}{aT} = \frac{\omega_c'}{10} \bigg|_{\omega_c' = 0.5}$$

and we have $T = 2000$. Finally, the resulting phase lag compensator becomes

$$C(s) = \frac{1 + 20s}{1 + 2000s}.$$

Here we give some analysis to check whether the controller $C(s)$ satisfies the given design requirements. The robust stability of the closed loop system with the controller $C(s)$ may be easily determined by applying Theorem 1. Moreover by GKT since we use a first order controller it is only necessary to check the stability of the following vertex polynomials:

$$(1 + 2000s)K_d^i(s) + (1 + 20s)K_n^j(s), \qquad i = 1, 2, 3, 4; j = 1, 2$$

where

$$K_n^1(s) := 10 \qquad K_n^2(s) := 20$$
$$K_d^1(s) := 0.5s + 0.8s^2 + 0.09s^3 \qquad K_d^2(s) := 1.5s + 0.8s^2 + 0.06s^3$$
$$K_d^3(s) := 0.5s + 0.2s^2 + 0.09s^3 \qquad K_d^4(s) := 1.5s + 0.2s^2 + 0.06s^3.$$

The eight polynomials above are stable and this shows that the closed loop system remains stable under all parameter perturbations within the given ranges. Figure 25 shows the frequency response (Bode envelopes) of $\mathbf{G}(s)$ (uncompensated system) and $C(s)\mathbf{G}(s)$ (compensated system).
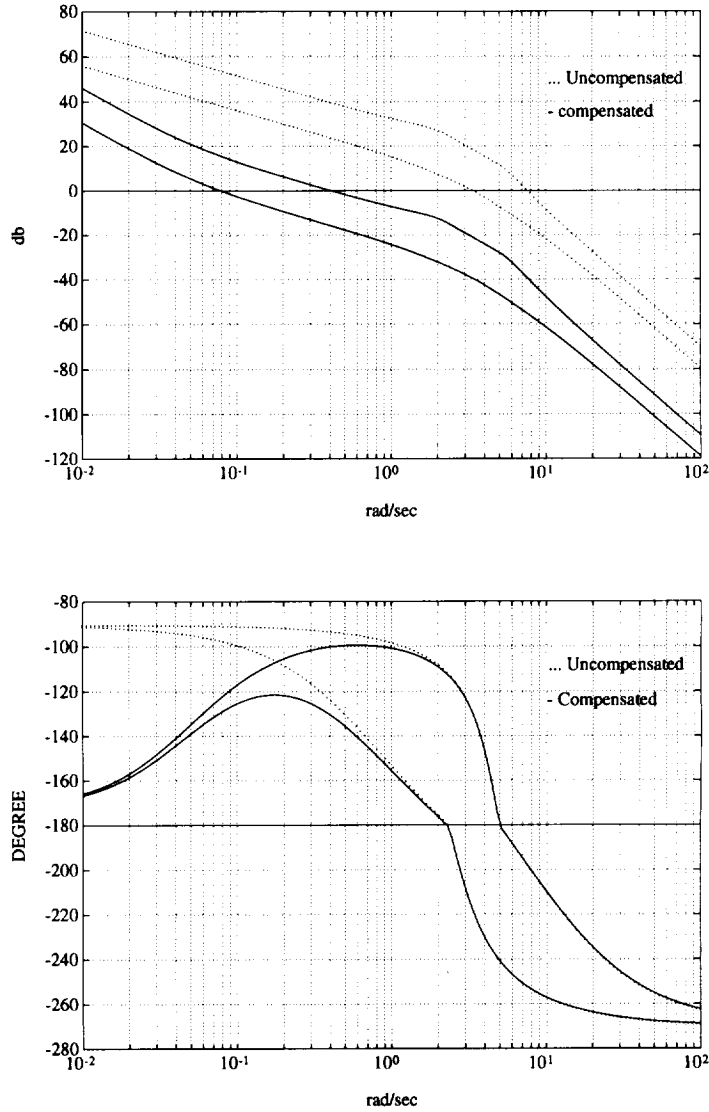
Figure 25: Bode envelopes of $\mathbf{G}(s)$ and $C(s)\mathbf{G}(s)$ (Example 7)

Clearly, the guaranteed phase margin requirement of 45° is satisfied. The guaranteed gain margin of the system is 12 db. The closed loop response $|\mathbf{M}(j\omega)|$ called $\mathbf{T}^y(j\omega)$ in (14) is shown in Figure 26 where

$$\mathbf{M}(j\omega) := \mathbf{M}(s)|_{s=j\omega} := \left\{ M(s) \ : \ \frac{C(s)G(s)}{1 + C(s)G(s)}, \ \ G(s) \in \mathbf{G}(s) \right\}. \tag{35}$$

Note that the $|\mathbf{M}(j\omega)|$ envelope shown in this figure is calculated from the result of Theorem 4. Figure 26 shows that the M_p of every system in the family lies between 1.08 and 1.3886. This also shows that the bandwidth of every system in the family lies in between 0.12 and 0.67 [rad/sec]. Thus, the design objective is achieved. Figure 27 shows the Nyquist plot of $C(s)\mathbf{G}(s)$. The center of the M-circle in Figure 27 is

$$\left(\frac{M_p^2}{1 - M_p^2}, 0 \right) = \left(\frac{1.3886^2}{1 - 1.3886^2}, 0 \right) = (-2.0772, 0)$$

and the radius of the circle is

$$r = \left| \frac{M_p}{1 - M_p^2} \right| = 1.496.$$

26
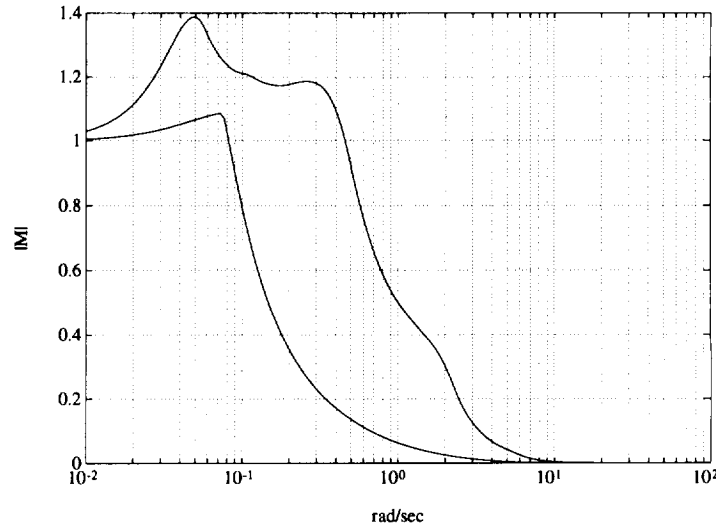
Figure 26: Closed-loop frequency response (Example 7)
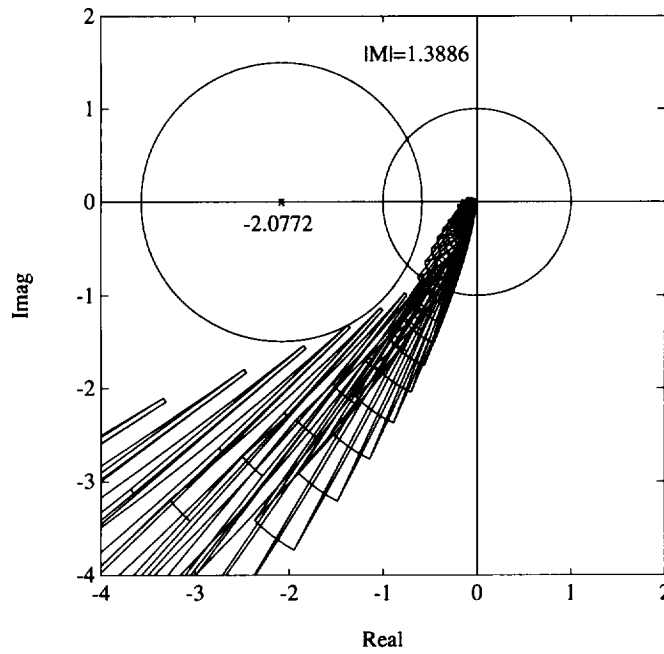
Figure 27: Nyquist envelope of $C(s)\mathbf{G}(s)$ with M-circle (Example 7)

Example 8. (**Lead-lag Compensation**) We give an example of lead-lag compensation design utilizing the developments described above. Let us consider the interval plant

$$G(s) = \frac{a_0}{b_3 s^3 + b_2 s^2 + b_1 s + b_0}$$

with coefficients bounded as follows: $a_0 \in [5,7]$, $b_3 \in [.09,.11]$, $b_2 \in [.9,1.2]$, $b_1 \in [.8,1.5]$, $b_0 \in [.1,.3]$. The objective of the design is to guarantee that the entire family of systems has a phase margin of at least $60°$ and a gain margin of at least 30dB. From Figure 28, we observe that the phase margin $70°$ which is equal to the desired phase margin of $60°$ plus some safety factor can be obtained if the new gain-crossover frequency ω_c' is at 0.35 [rad/sec]. This means that the phase-lag compensator must reduce the maximum magnitude of $\mathbf{G}(j\omega_c')$ over the interval family to 0 [db]. Thus, we solve

$$-20 \log_{10} a = \max_{G(j\omega_c') \in \mathbf{G}(j\omega_c')} |G(j\omega_c')| = 28[\text{db}]$$

and we have $a = 0.0398$. In order that the phase lag of the compensator does not affect the phase at the new gain-crossover frequency ω_c', we choose the value of $1/aT$ to be at one decade below ω_c'. Thus,

$$T = \frac{10}{a\omega_c'} = \frac{10}{(0.0398)(0.35)} = 717.875.$$

27
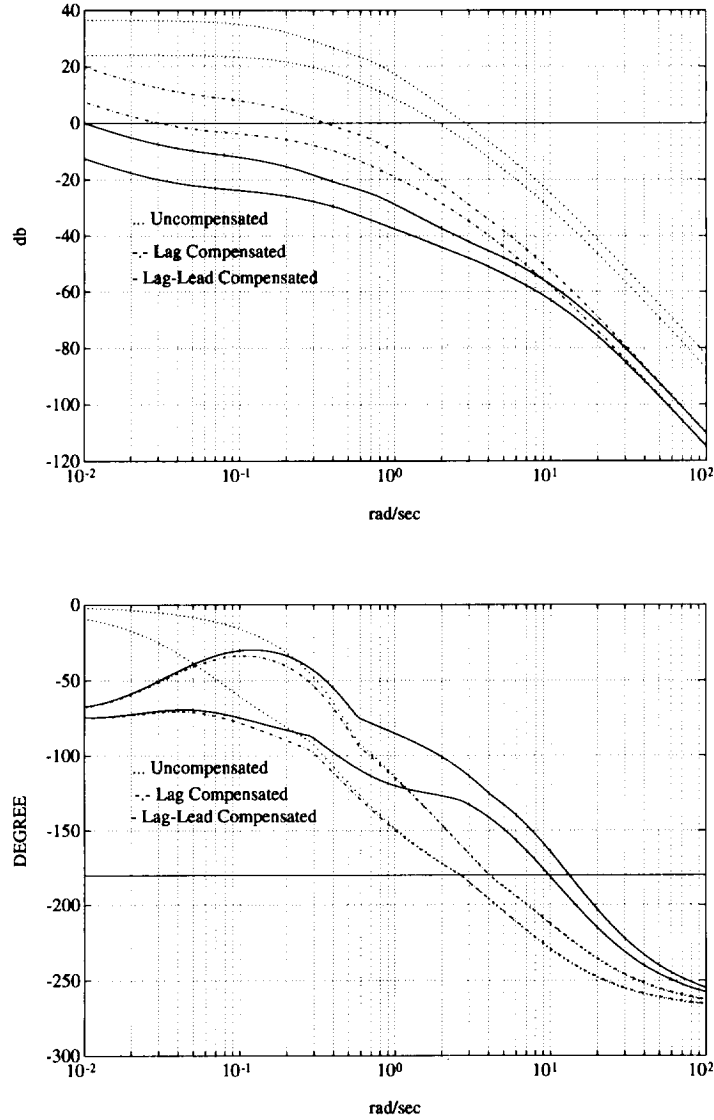
Figure 28: Bode envelopes (Example 8)

Therefore, the lag compensator obtained is

$$C_1(s) = \frac{1 + aTs}{1 + Ts} = \frac{28.5714s + 1}{717.875s + 1}.$$

We have now achieved approximately 70° of guaranteed phase margin and 25dB of guaranteed gain margin. To achieve the desired gain margin, we now wish to move the phase-crossover frequency ω_c'' to 4.7 [rad/sec]. If the magnitude plot does not move, we can achieve the gain margin of 35db at this frequency. Thus, we solve

$$-10\log_{10} a = -(35 - 25) = -10[\text{db}]$$

and we have $a = 10$. Then,

$$\frac{1}{T} = \sqrt{a}\omega_c'' = \sqrt{10}(4.7) = 14.86$$

and $T = 0.0673$. Therefore, the cascaded lead compensator is

$$C_2(s) = \frac{1}{a}\frac{1 + aTs}{1 + Ts} = \frac{1}{10}\frac{(10)(0.0673)s + 1}{0.0673s + 1} = \frac{s + 1.485}{s + 14.859}.$$

28

From Figure 28, we verify that the compensated system provides approximately 105° of guaranteed phase margin and 50dB of guaranteed gain margin. Therefore, the controller

$$C(s) = C_2(s)C_1(s) = \frac{s+1.5}{s+15}\frac{28.5714s+1}{717.682s+1}$$
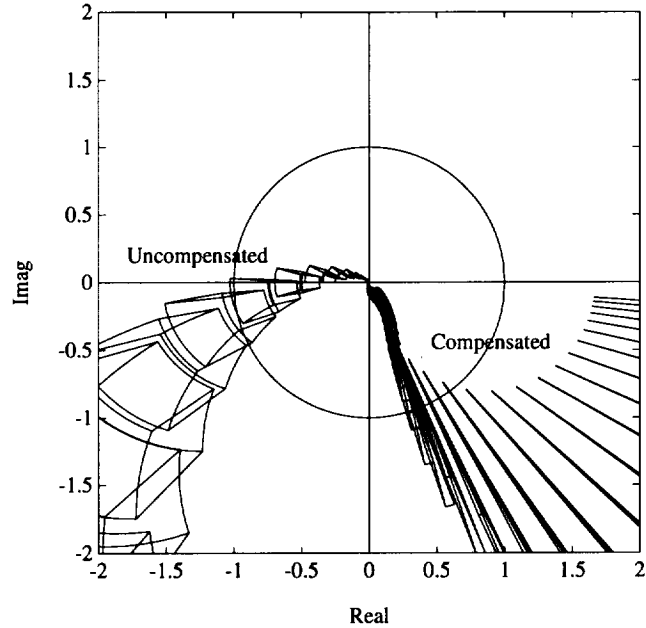
Figure 29: Nyquist envelope (Example 8)
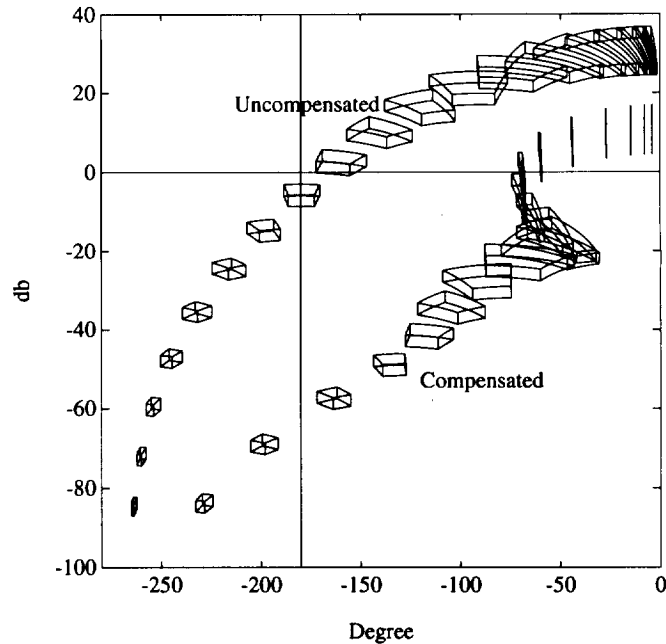
Figure 30: Nichols templates (Example 8)

attains the design specifications robustly. Figures 29, 30 and 28 show the Nyquist, Nichols and Bode envelopes of the uncompensated and compensated systems.

Example 9. (**PI Compensation**) Consider the plant

$$G(s) = \frac{n_1 s + 1}{.02s^4 + d_3 s^3 + d_2 s^2 + .04s}$$

with its coefficients bounded by given intervals as follows:

$$n_1 \in [.35, .45], \quad d_3 \in [.25, .35], \quad b_2 \in [.9, 1.1]$$

The objective of the design is to guarantee that the entire family of closed loop systems has a phase margin of at least 45°.

Here we design a PI compensator of the form

$$C(s) = K_P + \frac{K_I}{s}.$$

From Figure 32 we see that the new gain-crossover frequency ω_c' should be moved to 0.034 [rad/sec]. Since the maximum magnitude at ω_c' is 55 [db], we let

$$G_p(j\omega_c') := \max_{G(j\omega_c') \in \mathbf{G}(j\omega_c')} |G(j\omega_c')| = -20 \log_{10} K_p = 54.89[\text{db}]$$

from which

$$K_P = 10^{-|G_p(j\omega_c')|[\text{db}]/20} = 10^{-54.89/20} = 0.0018.$$

In order that the phase lag of the PI compensator not effect the phase of the compensated system at ω_c', we choose the corner frequency K_I/K_P to be one decade below ω_c'. Thus,

$$K_I = \frac{\omega_c'}{10} K_P = \frac{0.034}{10}(0.0018) = 6.12 \times 10^{-6}.$$

Therefore, the PI compensator obtained is

$$C(s) = \frac{6.12 \times 10^{-6} + .0018s}{s}.$$

Figure 31 shows the Nyquist envelope while Figures 32 and 33 show the Bode and Nichols envelopes of the uncompensated and compensated systems. We can see that the phase margin specifications are robustly achieved.
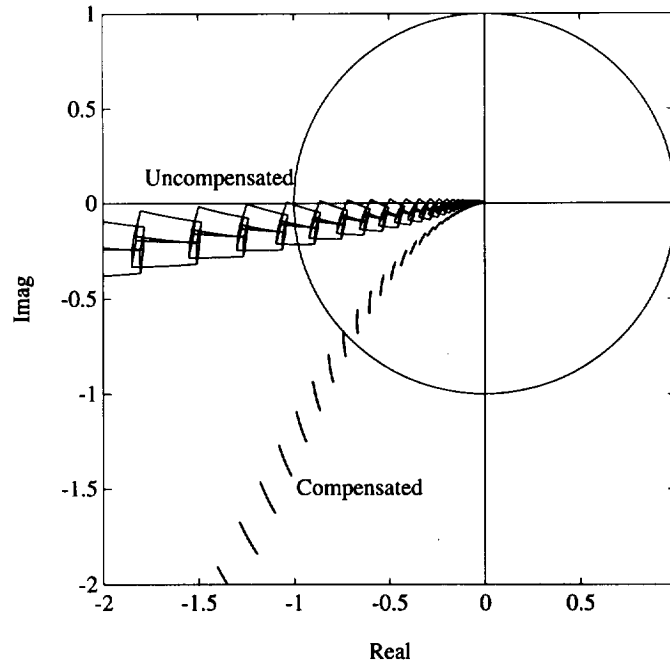
Figure 31: Nyquist envelope (Example 9)

30
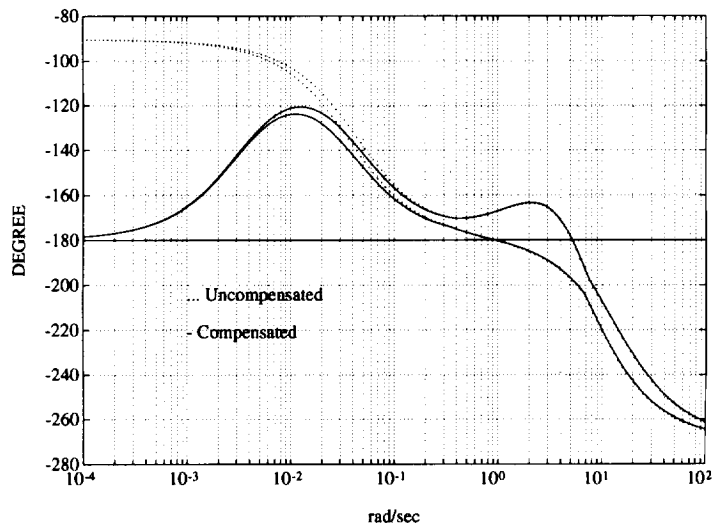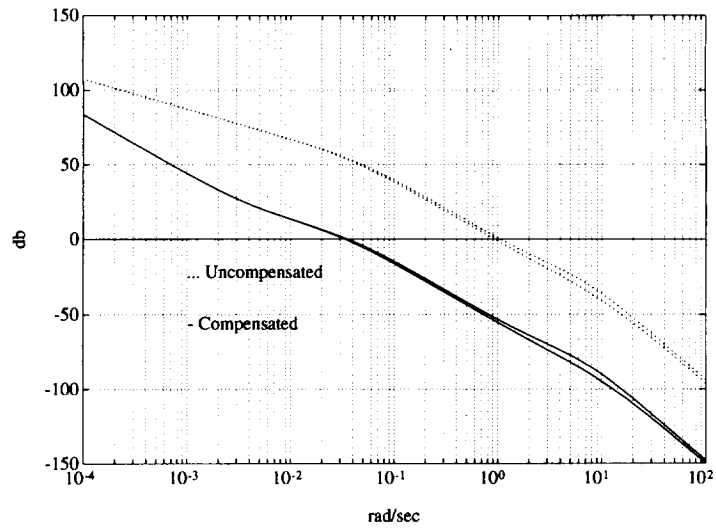
Figure 32: Bode envelopes (Example 9)
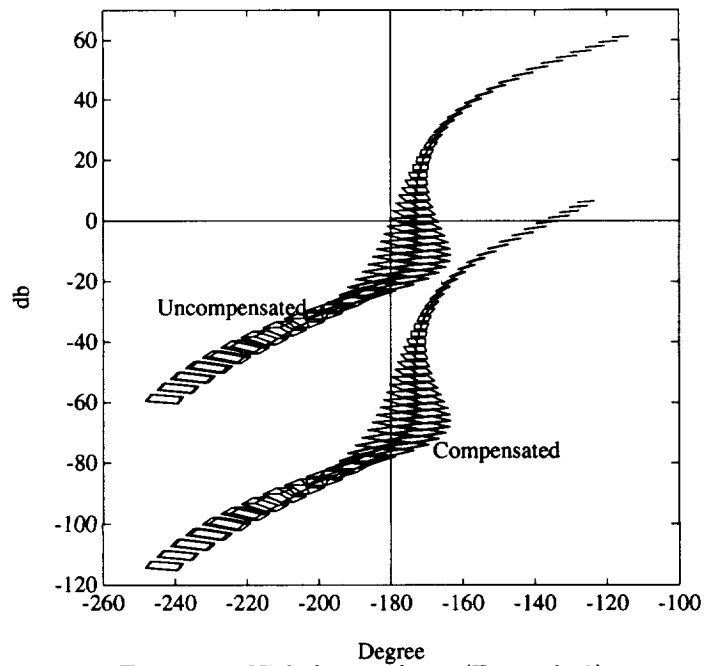
Figure 33: Nichols templates (Example 9)

4.8.2 Optimal Controller Parameter Selection

In the design problem, we interchange the role of plant and controller, and consider a family of controllers stabilizing a fixed plant $G(s)$. The design problem here is to select from the controller family the *best* parameter value according to some criterion. This type of problem is common in practice. Let us consider for example that this parameter selection is to be made to maximize gain margin or phase margin. The set of controller parameters may be given in terms of bounded values. In other words, we have a interval family of controllers stabilizing a fixed plant. To maximize the gain margin (or phase margin) over this set, we explore the boundary results given earlier.

In Section 4.3 we showed that the minimum gain margin (or phase margin) occurs over the extremal set. In practice, the maximum gain margin (or phase margin) will also frequently occur over the same set. To see this, we argue as follows. The Nyquist boundary of the system cuts the real axis over the range A to B (see Figure 34 and Figure 35).
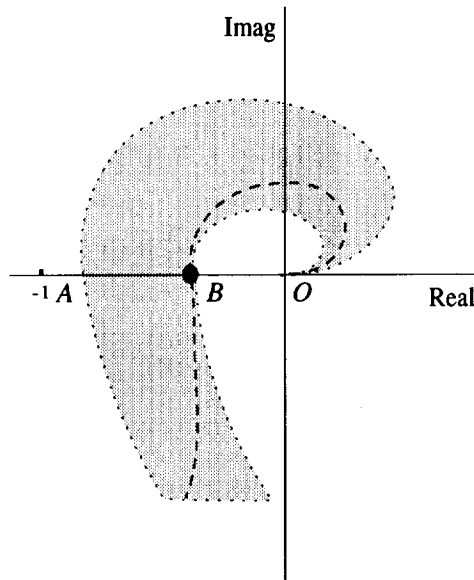
Figure 34: A system that delivers the maximum gain margin
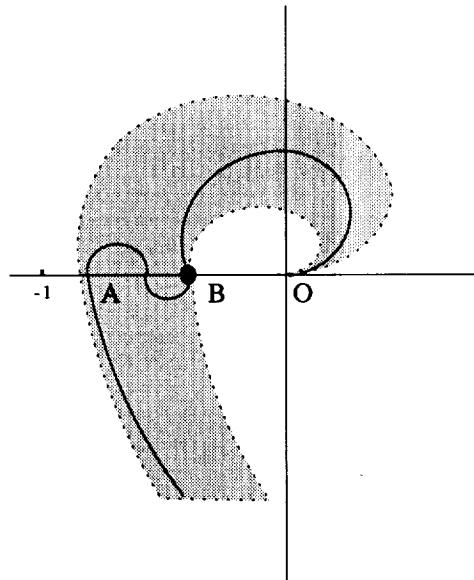
Figure 35: A system that does not deliver the maximum gain margin

The point A corresponds to the minimum gain margin of the family. The point B is a potential candidate for the maximum gain margin (gain margin $= 1/OB$). Corresponding to the point B, there

32

exists a set C_B of admissible (parameters lie within the given intervals) controllers whose Nyquist plots pass through the point B. Suppose that one of these controllers is such that the Nyquist plot does *not* cut the real axis at any other point (see Figure 34). It is clear that this controller delivers the maximum gain margin ($1/OB$) and is the optimally robust gain margin controller in the family. We can see that the maximum gain margin will be unrealizable only if each and every controller in C_B happens to cut the real axis at another point also (see Figure 35). Based on the above arguments, we suggest the following design procedure. First, check whether the given family of interval controllers stabilizes the plant $G(s)$ by using the GKT. If so, we use this set of controllers. Otherwise, we determine the parametric stability margin around the nominal values of controller parameters and create the largest interval stabilizing controller family around this nominal. From this controller set we can find the controller parameters that provide the maximum gain or phase margin. This can be done by generating the Nyquist envelope of the family using the development discussed earlier. If the margin obtained is not satisfactory, we reset the controller parameters to the new nominal corresponding to the point B and create a new interval stabilizing family. We repeat this procedure until a satisfactory margin is achieved or the improvement of the margin is negligibly small. The set of stabilizing interval controllers can be determined by many different methods; for example the locus introduced by Tsypkin and Polyak may be used. Of course, there is no guarantee that a globally optimum design will be achieved by this method. However, a satisfactory robust design will often result.

Example 10. Consider the feedback system with the plant transfer function

$$G(s) := \frac{250}{.025s^2 + 1.75s + 30}$$

and controller transfer function

$$C(s) := \frac{\alpha s + 1}{s^2 + \beta s + \gamma}.$$

The nominal values of controller parameters are $\alpha_0 = 5$, $\beta_0 = 2$, $\gamma_0 = 1$.

The phase margin of the given system with the nominal values of controller parameters is $19.55°$. The objective is to tune the three controller parameters so that the resulting system has a phase margin of approximately $45°$. We first find the ℓ_2 parametric stability margin r_1 around the nominal values of parameters $(\alpha_0, \beta_0, \gamma_0)$ by using the method proposed by Tsypkin and Polyak. From this value of r_1, which was obtained as $r_1 = 1$, we create the family of stabilizing controllers in the form of an interval transfer function $\mathbf{C}_1(s)$. Using this interval controller family, we create the corresponding Nyquist envelope which shows the maximum obtainable phase margin of $29.85°$. Using the formulas developed previously, we select the parameter values $(\alpha_1, \beta_1, \gamma_1)$, and consequently the controller $C(s, \alpha_1, \beta_1, \gamma_1) \in \mathbf{C}_1(s)$ that produces the maximum phase margin of $29.85°$. Since the resulting controller $C(s, \alpha_1, \beta_1, \gamma_1)$ does not satisfy the given requirement, we proceed with a second iteration. The parametric stability margin around $(\alpha_1, \beta_1, \gamma_1)$ we found is again 1. We now create a new interval family $\mathbf{C}_2(s)$ of stabilizing controllers. Using the same procedure as before, we find the controller $C_2(s, \alpha_2, \beta_2, \gamma_2) \in \mathbf{C}_2(s)$. This produces the maximum phase margin of $43.76°$. In the table below we present the successive designs through several iterations and Figure 36 shows the Nyquist plot of the optimal system for each iteration.

iteration	parameter ranges	parameter selected	phase margin
i	(α, β, γ)	$(\alpha_i, \beta_i, \gamma_i)$	
0	–	$(5, 2, 1)$	$19.55°$
1	$([4,6], [1,3], [0,2])$	$(4, 3, 2)$	$29.85°$
2	$([3,5], [2,4], [1,3])$	$(3, 4, 1)$	$43.76°$

4.8.3 Discrete Time Control Systems

The frequency templates of discrete interval control systems can also be constructed similarly. We still use the basic geometric facts regarding the addition, multiplication and division of complex plane image sets discussed here; however, the main simplifying tool used in the case of continuous systems, the GKT, is no longer applicable here. We illustrate this by an example.

Example 11. Consider the discrete-time feedback system shown in Figure 37. Let the interval plant $\mathbf{G}(z)$ and the controller $C(z)$ be

$$\mathbf{G}(z) = \frac{z + \alpha}{z^2 + \beta z + \gamma} \quad \text{and} \quad C(z) = \frac{-0.2z - 0.35}{z + 3}$$

33
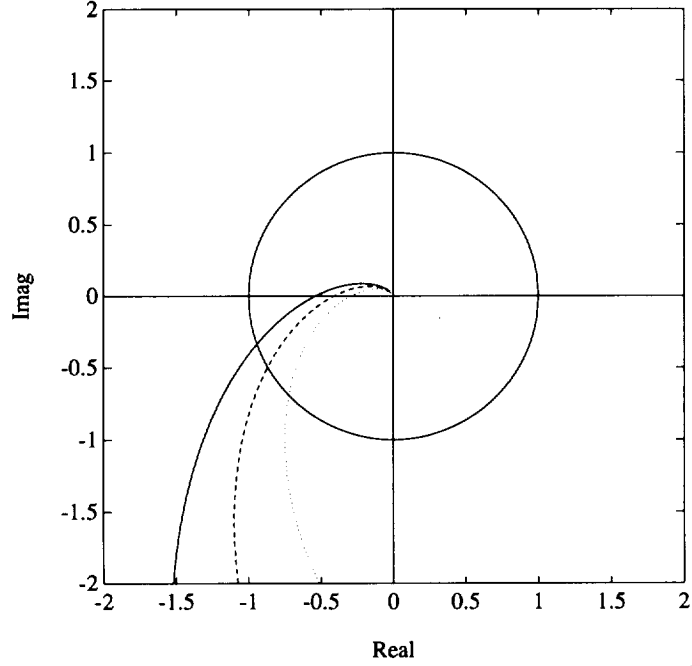
Figure 36: Nyquist plots of optimal systems (Example 10)
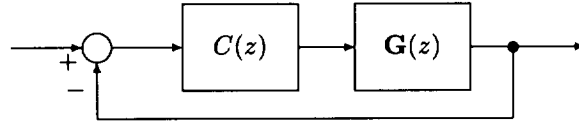
Figure 37: A discrete time feedback system (Example 11)

where
$$\alpha \in [0.8, 1.2] := [\alpha^-, \alpha^+], \quad \beta \in [1.8, 2.2] := [\beta^-, \beta^+], \quad \gamma \in [2.8, 3.2] := [\gamma^-, \gamma^+].$$

Then we have the extremal subset $\mathbf{G}_E(z)$ consisting of the following 12 systems:

$$G_{E_1}(z) = \frac{z + (\lambda\alpha^- + (1-\lambda)\alpha^+)}{z^2 + \beta^- z + \gamma^-}, \quad G_{E_2}(z) = \frac{z + (\lambda\alpha^- + (1-\lambda)\alpha^+)}{z^2 + \beta^+ z + \gamma^-}$$

$$G_{E_3}(z) = \frac{z + (\lambda\alpha^- + (1-\lambda)\alpha^+)}{z^2 + \beta^- z + \gamma^+}, \quad G_{E_4}(z) = \frac{z + (\lambda\alpha^- + (1-\lambda)\alpha^+)}{z^2 + \beta^+ z + \gamma^+}$$

$$G_{E_5}(z) = \frac{z + \alpha^-}{z^2 + (\lambda\beta^- + (1-\lambda)\beta^+)z + \gamma^-} \quad G_{E_6}(z) = \frac{z + \alpha^-}{z^2 + (\lambda\beta^- + (1-\lambda)\beta^+)z + \gamma^+}$$

$$G_{E_7}(z) = \frac{z + \alpha^+}{z^2 + (\lambda\beta^- + (1-\lambda)\beta^+)z + \gamma^-} \quad G_{E_8}(z) = \frac{z + \alpha^+}{z^2 + (\lambda\beta^- + (1-\lambda)\beta^+)z + \gamma^+}$$

$$G_{E_9}(z) = \frac{z + \alpha^-}{z^2 + \beta^- z + (\lambda\gamma^- + (1-\lambda)\gamma^+)} \quad G_{E_{10}}(z) = \frac{z + \alpha^-}{z^2 + \beta^+ z + (\lambda\gamma^- + (1-\lambda)\gamma^+)}$$

$$G_{E_{11}}(z) = \frac{z + \alpha^+}{z^2 + \beta^- z + (\lambda\gamma^- + (1-\lambda)\gamma^+)} \quad G_{E_{12}}(z) = \frac{z + \alpha^+}{z^2 + \beta^+ z + (\lambda\gamma^- + (1-\lambda)\gamma^+)}$$

where in each case λ ranges over $[0, 1]$.

By searching over the family $\mathbf{G}_E(z)$ with $z = e^{j\omega T}$ for $\omega \in [0, \infty)$ and a fixed T, we can obtain the frequency templates of the system. For illustration, the Bode envelopes of the above discrete time feedback system are given in Figure 38 for $T = 1$. The Nyquist and Nichols envelopes can also be generated similarly.

34
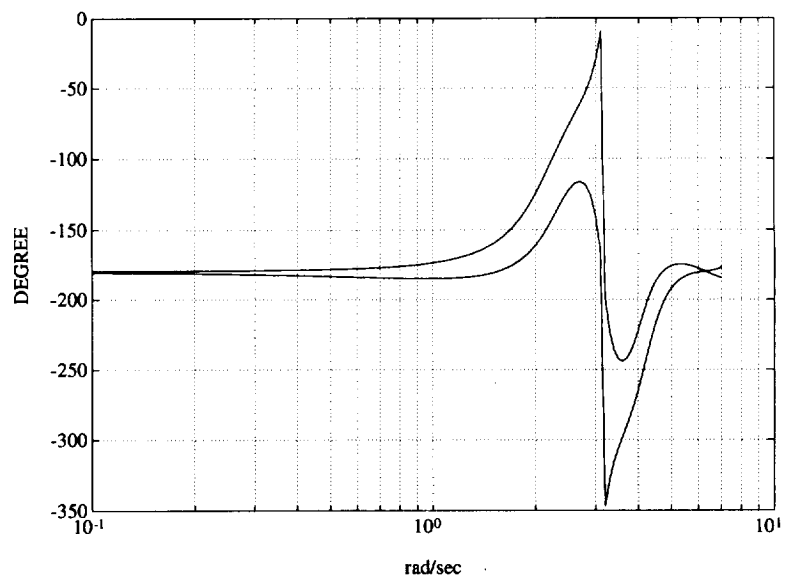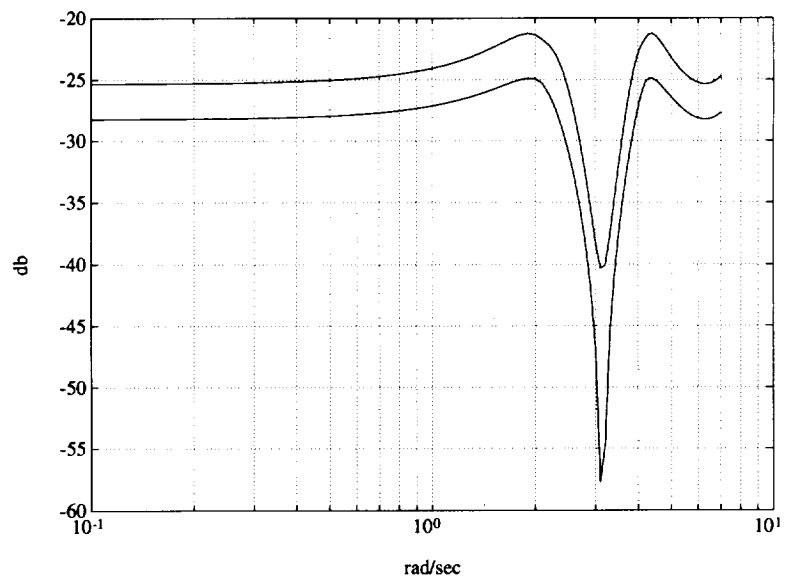
Figure 38: Bode envelopes (Example 11)

5 MULTILINEAR INTERVAL SYSTEMS

Consider the feedback configuration shown in Figure 39. $F(s)$ is a fixed controller and $G_1(s)$ and
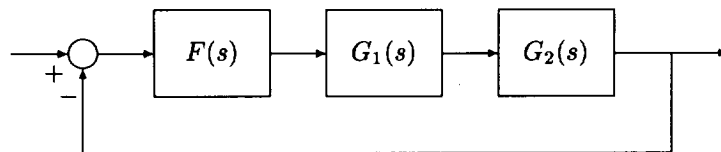
Figure 39: Interconnected Feedback System

$G_2(s)$ are independent subsystems containing parameter uncertainty. Let

$$F(s) := \frac{F_1(s)}{F_2(s)}, \quad G_1(s) := \frac{P_{11}(s)}{P_{21}(s)}, \quad G_2(s) := \frac{P_{12}(s)}{P_{22}(s)}. \tag{36}$$

If the subsystems $G_1(s)$ and $G_2(s)$ contain independent parameters it is reasonable to model them as *interval* or *linear interval* systems $\mathbf{G}_i(s)$, $i = 1, 2$. The characteristic polynomial of this feedback system is:

$$\delta(s) := F_1(s)P_{11}(s)P_{12}(s) + F_2(s)P_{21}(s)P_{22}(s). \tag{37}$$

The open loop transfer function

$$T^o(s) = F(s)G_1(s)G_2(s) = \frac{F_1(s)P_{11}(s)P_{12}(s)}{F_2(s)P_{21}(s)P_{22}(s)}$$

and the closed loop transfer function

$$T^c(s) = \frac{F(s)G_1(s)G_2(s)}{1 + F(s)G_1(s)G_2(s)} = \frac{F_1(s)P_{11}(s)P_{12}(s)}{F_1(s)P_{11}(s)P_{12}(s) + F_2(s)P_{21}(s)P_{22}(s)}.$$

These transfer functions have numerator and denominator polynomials that are multilinear functions of interval polynomials. In addition, the numerator and denominator in $T^o(s)$ have independent interval polynomials (parameters), but in $T^c(s)$ the numerator and denominator contain *common* interval polynomials.

For this class of systems we are interested in the following types of questions:

1) Does $F(s)$ robustly stabilize the system or not?

2) If $F(s)$ does robustly stabilize the system, what are the worst case gain margin, phase margin, parametric stability margin, H_∞ stability margin and performance measured in terms of H_∞ norms, as the parameters range over the uncertainty set?

3) How can one construct the Bode magnitude and phase, and Nyquist plots of various transfer function sets such as $T^o(s)$ and $T^c(s)$ generated by the uncertain parameters?

These questions were addressed in the previous sedction for an arbitrary stability region using the Mapping Theorem as a computational tool. In this section, we focus on the case of Hurwitz stability and show how the Generalized Kharitonov Theorem (GKT) can be extended to this multilinear case to provide a great deal of simplification and computational efficiency. We first derive a multilinear version of GKT. This generalization provides us with an extremal test set for multilinear interval systems, with drastically reduced dimension of the parameter space, from which all the above questions can be answered. It will tell us, essentially that as long as the dependencies are multilinear, worst case stability margins and performance can be calculated for an arbitrary control system containing interval subsystems by replacing each interval subsystem $\mathbf{G}^i(s)$ by the corresponding extremal set of systems $\mathbf{G}_E^i(s)$. The polytopic approximation derived in the last section can then be used on this extremal set to give a highly efficient computational solution to the design and analysis questions posed above. In the next section we describe the extension of GKT to the multilinear case.

36

5.1 MULTILINEAR INTERVAL POLYNOMIALS

To avoid notational complexity, we first consider the simplest multilinear polynomial form motivated by (37). We consider the Hurwitz stability of the characteristic polynomial family of the form

$$\delta(s) := F_1(s)P_{11}(s)P_{12}(s) + F_2(s)P_{21}(s)P_{22}(s) \tag{38}$$

where $F_i(s)$ are fixed real polynomials and $P_{ij}(s)$ are real interval polynomials with *independently* varying parameters. Let **p** denote the ordered set of coefficients of the polynomials $\{P_{11}(s), P_{12}(s)P_{21}, (s)P_{22}(s)\}$. We assume that each coefficient varies in an independent interval, or equivalently that **p** varies in an axis-parallel box Π. The dimension of the parameter space here is equal to the number of independently varying parameters contained in these polynomials. We let $\mathbf{P}_{ij}(s)$ denote the interval polynomial family and $\mathcal{K}_{ij}(s)$ and $\mathcal{S}_{ij}(s)$ denote the respective Kharitonov polynomials and Kharitonov segments. The family of uncertain polynomials is represented as

$$\mathbf{\Delta}(s) := F_1(s)\mathbf{P}_{11}(s)\mathbf{P}_{12}(s) + F_1(s)\mathbf{P}_{21}(s)\mathbf{P}_{22}(s). \tag{39}$$

Define

$$\mathbf{\Delta}_{\mathrm{E}}^1(s) := F_1(s)\mathcal{S}_{11}(s)\mathcal{S}_{12}(s) + F_2(s)\mathcal{K}_{21}(s)\mathcal{K}_{22}(s), \quad \mathbf{\Delta}_{\mathrm{E}}^2(s) := F_1(s)\mathcal{K}_{11}(s)\mathcal{K}_{12}(s) + F_2(s)\mathcal{S}_{21}(s)\mathcal{S}_{22}(s)$$

and introduce the extremal manifolds

$$\mathbf{\Delta}_{\mathrm{E}}(s) := \mathbf{\Delta}_{\mathrm{E}}^1(s) \cup \mathbf{\Delta}_{\mathrm{E}}^2(s). \tag{40}$$

Lemma 2. *Under the assumption that every polynomial in $\mathbf{\Delta}(s)$ is of the same degree and the parameters (coefficients) in the interval polynomials $\mathbf{P}_{11}(s)$, $\mathbf{P}_{12}(s)$, $\mathbf{P}_{21}(s)$, $\mathbf{P}_{22}(s)$ are independent, $\mathbf{\Delta}(s)$ is Hurwitz stable if and only if $\mathbf{\Delta}_{\mathrm{E}}(s)$ is Hurwitz stable.*

For the general case, we have the *multilinear interval polynomial*

$$\mathbf{\Delta}(s) = F_1(s)\mathbf{P}_{11}(s)\cdots\mathbf{P}_{1r_1}(s) + \cdots + F_m(s)\mathbf{P}_{m1}(s)\cdots\mathbf{P}_{mr_m}(s) \tag{41}$$

where $F_i(s)$ are fixed and $P_{ij}(s)$ are interval polynomial families. The arguments used in the earlier case carry over to this case and the result will be presented without repeating the proof. We define

$$\mathbf{\Delta}_{\mathrm{E}}^l(s) := F_1(s)\mathcal{K}_{11}(s)\cdots\mathcal{K}_{1r_1}(s) + \cdots + F_{l-1}(s)\mathcal{K}_{l-1,1}(s)\cdots\mathcal{K}_{l-1,r_{l-1}}(s)$$
$$+ F_l(s)\mathcal{S}_{l,1}(s)\cdots\mathcal{S}_{l,r_l}(s) + F_{l+1}\mathcal{K}_{l+1,1}(s)\cdots\mathcal{K}_{l+1,r_{l+1}} + \cdots + F_m(s)\mathcal{K}_{m,1}(s)\cdots\mathcal{K}_{m,r_m}(s) \tag{42}$$

and introduce the *extremal manifolds*

$$\mathbf{\Delta}_{\mathrm{E}}(s) := \cup_{l=1}^m \mathbf{\Delta}_{\mathrm{E}}^l(s). \tag{43}$$

Theorem 11. *Under the assumption that every polynomial in $\mathbf{\Delta}(s)$ is of the same degree and the parameters (coefficients) in the interval polynomials $\mathbf{P}_{ij}(s)$ are independent, $\mathbf{\Delta}(s)$ is Hurwitz stable if and only if $\mathbf{\Delta}_{\mathrm{E}}(s)$ is Hurwitz stable.*

Remark 4. The theorem is also valid when some of the polynomials $F_i(s)$ are complex or quasipolynomials This follows from the corresponding fact that GKT holds when some of the fixed polynomials $F_i(s)$ are replaced by complex polynomials or quasipolynomials.

The next example illustrates the construction of the set of manifolds.

Example 12. (**Extremal Manifolds for Multilinear Systems**) Consider the characteristic polynomial
$$\delta(s) = F_1(s)P_{11}(s)P_{12}(s) + F_2(s)P_{21}(s)P_{22}(s)$$
where the fixed polynomials $F_1(s)$ are

$$F_1(s) = s + f_1, \qquad F_2(s) = s + f_2$$

and the interval polynomials are

$$P_{11}(s) = a_2 s^2 + a_1 s + a_0, \quad P_{12}(s) = b_2 s^2 + b_1 s + b_0, \quad P_{21}(s) = c_2 s^2 + c_1 s + c_0, \quad P_{22}(s) = d_2 s^2 + d_1 s + d_0,$$

37

with all coefficients varying independently. The Kharitonov polynomials corresponding to $P_{11}(s)$, $P_{12}(s)$, $P_{21}(s)$ and $P_{22}(s)$ are:

$$K_{P_{11}}^1(s) = a_2^+ s^2 + a_1^- s + a_0^-, \quad K_{P_{11}}^2(s) = a_2^+ s^2 + a_1^+ s + a_0^-, \quad K_{P_{11}}^3(s) = a_2^- s^2 + a_1^- s + a_0^+,$$

$$K_{P_{11}}^4(s) = a_2^- s^2 + a_1^+ s + a_0^+, \quad K_{P_{12}}^1(s) = b_2^+ s^2 + b_1^- s + b_0^-, \quad K_{P_{12}}^2(s) = b_2^+ s^2 + b_1^+ s + b_0^-,$$

$$K_{P_{12}}^3(s) = b_2^- s^2 + b_1^- s + b_0^+, \quad K_{P_{12}}^4(s) = b_2^- s^2 + b_1^+ s + b_0^+, \quad K_{P_{21}}^1(s) = c_2^+ s^2 + c_1^- s + c_0^-,$$

$$K_{P_{21}}^2(s) = c_2^+ s^2 + c_1^+ s + c_0^-, \quad K_{P_{21}}^3(s) = c_2^- s^2 + c_1^- s + a_0^+, \quad K_{P_{21}}^4(s) = c_2^- s^2 + c_1^+ s + c_0^+,$$

$$K_{P_{22}}^1(s) = d_2^+ s^2 + d_1^- s + d_0^-, \quad K_{P_{22}}^2(s) = d_2^+ s^2 + d_1^+ s + d_0^-, \quad K_{P_{22}}^3(s) = d_2^- s^2 + d_1^- s + d_0^+,$$

$$K_{P_{22}}^4(s) = d_2^- s^2 + d_1^+ s + d_0^+.$$

The sets of segments joining appropriate pairs of Kharitonov polynomials can also be obtained. Here we give only the segments corresponding to the interval polynomial $P_{11}(s)$; others can be similarly obtained.

$$S_{P_{11}}^1(s) = \lambda K_{P_{11}}^1(s) + (1 - \lambda) K_{P_{11}}^2(s), \qquad S_{P_{11}}^2(s) = \lambda K_{P_{11}}^1(s) + (1 - \lambda) K_{P_{11}}^3(s),$$

$$S_{P_{11}}^3(s) = \lambda K_{P_{11}}^2(s) + (1 - \lambda) K_{P_{11}}^4(s), \qquad S_{P_{11}}^4(s) = \lambda K_{P_{11}}^3(s) + (1 - \lambda) K_{P_{11}}^4(s).$$

From the above, we now can write the manifolds:

$$\Delta_1(s) = \left\{ F_1(s) K_{P_{11}}^i(s) K_{P_{12}}^j(s) + F_2(s) S_{P_{21}}^k(s) S_{P_{22}}^l(s) : (i,j,k,l) \in \underline{4} \times \underline{4} \times \underline{4} \times \underline{4} \right\}$$

$$\Delta_2(s) = \left\{ F_1(s) S_{P_{11}}^i(s) S_{P_{12}}^j(s) + F_2(s) K_{P_{21}}^k(s) K_{P_{22}}^l(s) : (i,j,k,l) \in \underline{4} \times \underline{4} \times \underline{4} \times \underline{4} \right\}$$

and

$$\Delta_E(s) = \Delta_1 \cup \Delta_2.$$

As we can see, the total parameter space is of dimension 12. However, our problem is now reduced to checking the stability of 512 two-dimensional manifolds. Notice that each manifold remains of dimension two, even though the dimension of the parameter space can be increased arbitrarily. The dimension of the manifolds is increased only if the number of interval polynomials in a product term is increased.

5.1.1 Dependencies Between the Perturbations

The theorem is stated assuming that the polynomials $P_{ij}(s)$ perturb independently. In an interconnected multiloop control system, it will in general happen that some of the polynomials $P_{ij}(s)$ are in fact identical (see, for example, Exercise 11.1). Such dependencies can be easily handled. To avoid introducing cumbersome notation we illustrate the procedure with an example.

Consider the following multilinear interval polynomial family with dependencies between the perturbations:

$$\delta(s, \mathbf{p}) := F_1(s) P_{11}(s) P_{12}(s) + F_2(s) P_{21}(s) P_{22}(s) + F_3(s) P_{31}(s) P_{32}(s)$$

where $P_{11}(s) = P_{21}(s)$ and $P_{22}(s) = P_{32}(s)$ and each polynomial $P_{ij}(s)$ is interval. If we rewrite embedding the above constraints, we have

$$\delta(s, \mathbf{p}) = F_1(s) P_{11}(s) P_{12}(s) + F_2(s) P_{11}(s) P_{22}(s) + F_3(s) P_{31}(s) P_{22}(s). \tag{44}$$

Let us first fix $P_{11}(s)$ and $P_{31}(s)$ and apply GKT. This tells us that the Hurwitz stability of the set $\Delta(s)$ is equivalent to stability of the sets

$$I_1(s) = \{ F_1(s) P_{11}(s) S_{12}(s) + (F_2(s) P_{11}(s) + F_3(s) P_{31}(s)) K_{22}(s) \}$$

$$I_2(s) = \{ F_1(s) P_{11}(s) K_{12}(s) + (F_2(s) P_{11}(s) + F_3(s) P_{31}(s)) S_{22}(s) \}$$

for each $(P_{11}(s), P_{31}(s)) \in \mathbf{P}_{11}(s) \times \mathbf{P}_{31}(s)$. We now apply GKT again to each of the sets $I_1(s)$ and $I_2(s)$ letting $P_{11}(s)$ and $P_{31}(s)$ now vary. This leads to the condition that the robust stability of $\Delta(s)$ is equivalent to robust stability of the manifolds:

$$\Delta_1(s) = \{ \delta(s, \mathbf{p}) : P_{11} \in S_{11}, \ P_{12} \in S_{12}, \ P_{22} \in K_{22}, \ P_{31} \in K_{31} \}$$

$$\Delta_2(s) = \{ \delta(s, \mathbf{p}) : P_{11} \in S_{11}, \ P_{12} \in K_{12}, \ P_{22} \in S_{22}, \ P_{31} \in K_{31} \}$$

$$\Delta_3(s) = \{ \delta(s, \mathbf{p}) : P_{11} \in K_{11}, \ P_{12} \in S_{12}, \ P_{22} \in K_{22}, \ P_{31} \in S_{31} \}$$

$$\Delta_4(s) = \{ \delta(s, \mathbf{p}) : P_{11} \in K_{11}, \ P_{12} \in K_{12}, \ P_{22} \in S_{22}, \ P_{31} \in S_{31} \} .$$

Since $\Delta_3(s)$ is a polytope, we now can apply the Edge Theorem to conclude that this is stable if and only if its exposed edges are. These exposed edges are

$$\{\delta(s,\mathbf{p}) : P_{11} \in \mathcal{K}_{11}, \ P_{12} \in \mathcal{S}_{12}, \ P_{22} \in \mathcal{K}_{22}, \ P_{31} \in \mathcal{K}_{31}\} \tag{45}$$

$$\{\delta(s,\mathbf{p}) : P_{11} \in \mathcal{K}_{11}, \ P_{12} \in \mathcal{K}_{12}, \ P_{22} \in \mathcal{K}_{22}, \ P_{31} \in \mathcal{S}_{31}\}. \tag{46}$$

It is easy to see that the manifolds (45) and (46) are contained in $\Delta_1(s)$ and $\Delta_4(s)$ respectively. Therefore the set of manifolds that finally need to be checked is

$$\Delta_{\mathrm{E}}(s) := \Delta_1(s) \cup \Delta_2(s) \cup \Delta_4(s). \tag{47}$$

5.1.2 Interval Polynomial Matrix

An important special case of dependent perturbations is that of interval polynomial matrices. Let $M(s)$ be an $n \times n$ polynomial matrix whose ij^{th} entry is the polynomial $P_{ij}(s)$. The characteristic polynomial associated with this matrix is $\det[M(s)]$. We assume that each $P_{ij}(s)$ belongs to an interval family $\mathbf{P}_{ij}(s)$ and the parameters of each $P_{ij}(s)$ are independent of all others. Let $\mathbf{M}(s)$ denote the corresponding set of matrices. We will say that the set is stable if $\det[M(s)]$ is Hurwitz stable for every $M(s) \in \mathbf{M}(s)$. To test Hurwitz stability of the family of characteristic polynomials so obtained we have the following result. Let $\mathbf{T}$ be the set of $n \times n$ permutation matrices obtained from the identity matrix. Corresponding to each $T \in \mathbf{T}$, introduce the set of polynomial matrices $M_T(s)$ where $P_{ij}(s)$ ranges over $\mathcal{K}_{ij}(s)$ if the ij^{th} entry of T is 0 and $P_{ij}(s)$ ranges over $\mathcal{S}_{ij}(s)$ if the ij^{th} entry of T is 1. Let $\mathbf{M}^*(s)$ denote the collection of matrices $M_T(s)$ obtained by letting T range over all permutation matrices $\mathbf{T}$.

Theorem 12. $\mathbf{M}(s)$ *is Hurwitz stable if and only if* $\mathbf{M}^*(s)$ *is Hurwitz stable.*

5.1.3 Boundary Generating Property of the Extremal Manifolds

We have established that Hurwitz stability of the family $\Delta(s)$ is equivalent to the stability of the manifolds $\Delta_{\mathrm{E}}(s)$. This equivalence also follows from the following boundary result relating the image sets $\Delta(j\omega)$ and $\Delta_{\mathrm{E}}(j\omega)$.

Theorem 13.

$$\partial\Delta(j\omega) \subset \Delta_{\mathrm{E}}(j\omega) \tag{48}$$

The boundary result established above implies that the problem of checking robust stability is now reduced to verifying that the origin is excluded from the set $\Delta_{\mathrm{E}}(j\omega)$ for each ω in $[0,\infty)$. This is a great deal simpler than the original problem because of the greatly reduced dimensionality of the set $\Delta_{\mathrm{E}}(s)$ relative to the original set $\Delta(s)$. However, this verification is still not easy because the set $\Delta_{\mathrm{E}}(s)$ is multilinear in the parameters λ_i. At this point, the Mapping Theorem can be brought in and used to approximate $\Delta_{\mathrm{E}}(j\omega)$. Indeed, since $\Delta_{\mathrm{E}}(s)$ depends multilinearly on the parameters λ_{ij} associated with the Kharitonov segments, the vertex set of $\Delta(s)$ can be generated by setting the $P_{ij}(s)$ to the corresponding Kharitonov polynomials. Let

$$\Delta_{\mathrm{K}}(s) = \{\delta(s,\mathbf{p}) \ : \ P_{ij}(s) = K_{ij}^{i_{ij}}(s), \ \ i_{ij} \in \underline{4}, \ \ i \in \underline{m}, \ \ j \in \underline{r_m}\}. \tag{49}$$

We can also introduce the polytopic set consisting of convex combinations of the vertex polynomials:

$$\bar{\Delta}(s) = \{\lambda v_i(s) + (1-\lambda)v_j(s) \ : \ v_i(s), v_j(s) \in \Delta_{\mathrm{K}}(s), \ \ \lambda \in [0,1]\}. \tag{50}$$

It follows from the Mapping Theorem now, that

$$co \ \Delta_{\mathrm{E}}(j\omega) = co \ \Delta_{\mathrm{K}}(j\omega) = \bar{\Delta}_{\mathrm{K}}(j\omega).$$

Therefore, the condition that $\Delta_{\mathrm{E}}(j\omega)$ excludes the origin can be replaced by the sufficient condition that $\bar{\Delta}_{\mathrm{K}}(j\omega)$ exclude the origin. Since this latter set is a polytope, this condition can be verified by checking that the angle subtended by the set $\Delta_{\mathrm{K}}(j\omega)$ at the origin, $\Phi_{\Delta_{\mathrm{K}}}(j\omega)$ is less than π radians. Therefore we have proved the following result.

Theorem 14. *The family* $\Delta(s)$ *is Hurwitz stable if it contains at least one stable polynomial and satisfies*

  1) $0 \notin co \ \Delta(j\omega)$ *for some* ω *2)* $\Phi_{\Delta_{\mathrm{K}}}(j\omega) < \pi,$ *for all* $\omega \in [0,\infty)$.

This result states that the Hurwitz stability of $\Delta(s)$ can be determined by checking the phase difference of the vertex polynomials corresponding to the Kharitonov polynomials along the $j\omega$ axis. This is useful in view of the fact that the number of Kharitonov vertices is fixed whereas the vertices of Π increase exponentially with the dimension of the parameter space. We illustrate these results with examples.

Example 13. Consider the interconnected feedback system shown in Figure 40.
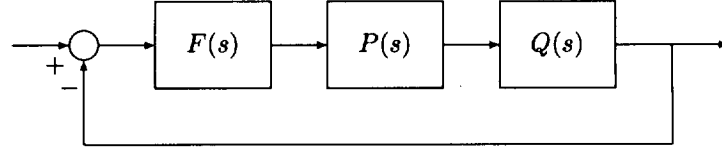
Figure 40: Interconnected Feedback System (Example 13)

Let

$$F(s) := \frac{F_1(s)}{F_2(s)} = \frac{s+2}{s+1}, \quad P(s) := \frac{P_1(s)}{P_2(s)} = \frac{s^2 + s + 1}{s^3 + a_2 s^2 + 4s + a_0},$$

$$Q(s) := \frac{Q_1(s)}{Q_2(s)} = \frac{6.6s^3 + 13.5s^2 + 15.5s + 20.4}{s^3 + b_2 s^2 + 3.5s + 2.4}$$

and let the set of parameters $\mathbf{p} = [a_2, a_0, b_2]$ vary as follows:

$$a_2 \in [a_2^-, a_2^+] = [-3.625, -2.375], \quad a_0 \in [a_0^-, a_0^+] = [1.375, 2.625], \quad b_2 \in [b_2^-, b_2^+] = [2.875, 4.125].$$

The characteristic polynomial of the system is:

$$\delta(s, \mathbf{p}) = s^7 + (7.6 + a_2 + b_2)s^6 + (40.8 + a_2 + b_2 + a_2 b_2)s^5 + (85.7 + a_0 + 3.5a_2 + 4b_2 + a_2 b_2)s^4$$
$$+(137 + a_0 + 5.9a_2 + 4b_2 + a_0 b_2)s^3 + (158.3 + 3.5a_0 + 2.4a_2 + a_0 b_2)s^2$$
$$+(101.8 + 5.9a_0)s + (40.8 + 2.4a_0).$$

We verify that the following polynomial in the family is Hurwitz:

$$\delta(s, \mathbf{p} = [-3, 2, 3.5]) = s^7 + 8.1s^6 + 30.8s^5 + 80.7s^4 + 142.3s^3 + 165.1s^2 + 113.6s + 45.6$$

The parameter sets corresponding to the Kharitonov polynomials are

$$\left\{ (a_2^+, a_0^-, b_2^+), (a_2^-, a_0^+, b_2^+), (a_2^+, a_0^-, b_2^-), (a_2^-, a_0^+, b_2^-) \right\}.$$

The set of Kharitonov vertex polynomials is

$$\Delta_{\mathrm{K}}(s) = \{\delta_{K_1}(s), \delta_{K_2}(s), \delta_{K_3}(s), \delta_{K_4}(s)\}$$

where

$$\delta_{K_1}(s) = s^7 + 9.35s^6 + 32.7531s^5 + 85.4656s^4 + 146.5344s^3 + 163.0844s^2 + 109.9125s + 44.1$$
$$\delta_{K_2}(s) = s^7 + 8.10s^6 + 34.4719s^5 + 83.4344s^4 + 139.8156s^3 + 161.3656s^2 + 109.9125s + 44.1$$
$$\delta_{K_3}(s) = s^7 + 8.10s^6 + 26.3469s^5 + 77.1844s^4 + 145.5656s^3 + 169.6156s^2 + 117.2875s + 47.1$$
$$\delta_{K_4}(s) = s^7 + 6.85s^6 + 29.6281s^5 + 76.7156s^4 + 137.2844s^3 + 166.3344s^2 + 117.2875s + 47.1$$

One approach is to check the Hurwitz stability of all convex combinations of these polynomials. This in turn can be done by using the Segment Lemma. Alternatively, we may check the phase differences of these vertex polynomials. If the maximum phase difference is less than $180°$ (π radians) for all ω, the origin is excluded from convex hull of $\Delta_{\mathrm{E}}(j\omega)$ for all ω. We show the convex hulls of image sets in Figure 41 for illustration.

We confirm robust stability by verifying (see Figure 42) the maximum phase difference never reaches $180°$ for all ω. We also note that if we had applied the Mapping Theorem directly to the three dimensional parameter space $\mathbf{p}$, we would have had to check 8 vertices as opposed to the 4 vertices checked here. This reduction is due to the application of the multilinear version of the Generalized Kharitonov Theorem.

40
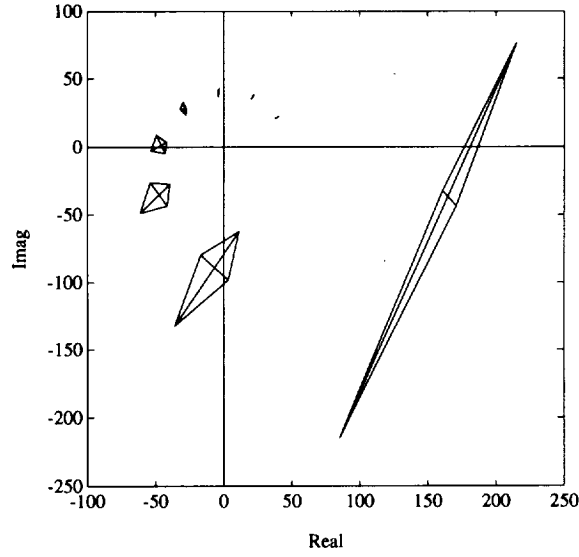
Figure 41: Convex hulls of image sets (Example 13)
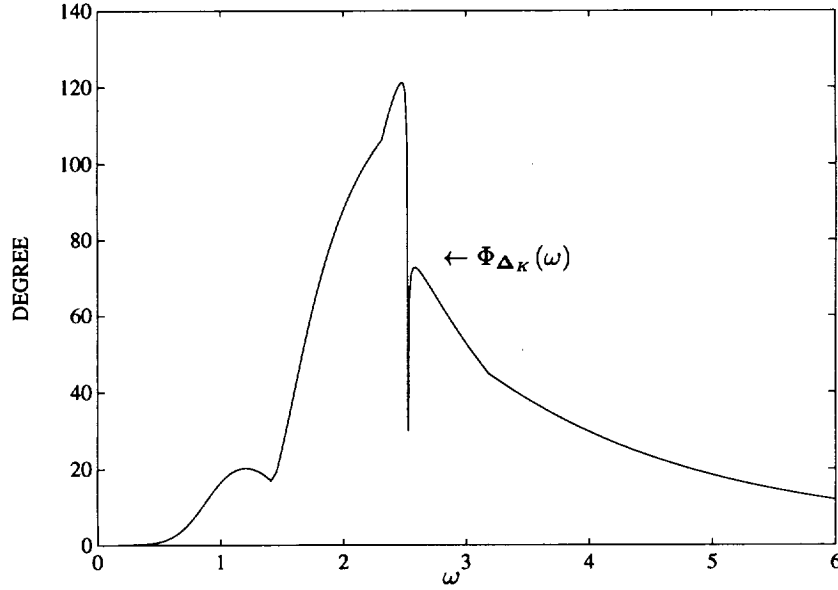
Figure 42: $\Phi_{\Delta_K}(\omega)$ vs. ω (Example 13)

5.2 PARAMETRIC STABILITY MARGIN

Consider again the family of polynomials

$$\Delta(s) = F_1(s)\mathbf{P}_{11}(s)\cdots\mathbf{P}_{1r_1}(s) + \cdots + F_m(s)\mathbf{P}_{m1}(s)\cdots\mathbf{P}_{mr_m}(s). \tag{51}$$

Let $\mathbf{p}_{ij}$ denote the vector of coefficients of the polynomials $P_{ij}(s)$. Each such coefficient belongs to a given interval and the corresponding box of parameters is denoted by $\mathbf{\Pi}_{ij}$. Then the box of uncertain parameters is

$$\mathbf{\Pi} := \mathbf{\Pi}_{11} \times \mathbf{\Pi}_{12} \times \cdots \times \mathbf{\Pi}_{mr_m}. \tag{52}$$

The extremal manifolds $\mathbf{\Delta}_E(s)$ are defined as follows:

$$\mathbf{\Delta}_E^l(s) := F_1(s)\mathcal{K}_{11}(s)\cdots\mathcal{K}_{1r_1}(s) + \cdots + F_{l-1}(s)\mathcal{K}_{l-1,1}(s)\cdots\mathcal{K}_{l-1,r_{l-1}}(s)$$
$$+ F_l(s)\mathcal{S}_{l,1}(s)\cdots\mathcal{S}_{l,r_l}(s) + F_{l+1}\mathcal{K}_{l+1,1}(s)\cdots\mathcal{K}_{l+1,r_{l+1}} + \cdots + F_m(s)\mathcal{K}_{m,1}(s)\cdots\mathcal{K}_{m,r_m}(s) \tag{53}$$

$$\mathbf{\Delta}_E(s) := \cup_{l=1}^m \mathbf{\Delta}_E^l(s). \tag{54}$$

41

The parameter space subsets corresponding to $\mathbf{\Delta}_E^l(s)$ and $\mathbf{\Delta}_E(s)$ are denoted by $\mathbf{\Pi}_l$ and

$$\mathbf{\Pi}_E := \bigcup_{l=1}^{m} \mathbf{\Pi}_l. \tag{55}$$

Let $\mathbf{\Pi}_K$ denote the parameter vector set corresponding to the case where each polynomial $P_{ij}(s)$ set to a corresponding Kharitonov polynomial. We write

$$\mathbf{\Delta}(s) = \{\delta(s, \mathbf{p}) : \mathbf{p} \in \mathbf{\Pi}\}, \qquad \mathbf{\Delta}_E(s) = \{\delta(s, \mathbf{p}) : \mathbf{p} \in \mathbf{\Pi}_E\}, \qquad \mathbf{\Delta}_K(s) = \{\delta(s, \mathbf{p}) : \mathbf{p} \in \mathbf{\Pi}_K\}.$$

In this section, we show that for the family $\mathbf{\Delta}(s)$ in (51) the worst case parametric stability margin over the uncertainty box $\mathbf{\Pi}$ occurs, in fact, on the set $\mathbf{\Pi}_E$.

Let $\| \cdots \|$ denote any norm in $\mathbf{R}^n$ and let $\mathcal{P}_u$ denote the set of points $\mathbf{u}$ in $\mathbf{R}^n$ for which $\delta(s, \mathbf{u})$ is unstable or loses degree (relative to its degree over $\mathbf{\Pi}$). Let

$$\rho(\mathbf{p}) = \inf_{\mathbf{u} \in \mathcal{P}_u} \|\mathbf{p} - \mathbf{u}\|_p$$

denote the radius of the stability ball (measured in the norm $\| \cdot \|$) and centered at the point $\mathbf{p}$. This number serves as the stability margin associated with the point $\mathbf{p}$. If the box $\mathbf{\Pi}$ is stable we can associate a stability margin with each point in $\mathbf{\Pi}$. A natural question to ask is: What is the worst case stability margin in the norm $\| \cdot \|$ as $\mathbf{p}$ ranges over $\mathbf{\Pi}$? The answer to that question is provided in the following theorem.

Theorem 15. (Extremal Parametric Stability Margin)

$$\inf_{\mathbf{p} \in \mathbf{\Pi}} \rho(\mathbf{p}) = \inf_{\mathbf{p} \in \mathbf{\Pi}_E} \rho(\mathbf{p}). \tag{56}$$

Example 14. Consider the system in Example 13 with nominal values

$$a_2^0 = -3, \quad a_0^0 = 2, \quad b_2^0 = 3.5.$$

We compute the maximum parametric stability margin ϵ^* around the nominal values as follows:

$$a_2 \in [a_2^0 - \epsilon, a_2^0 + \epsilon], \quad a_0 \in [a_0^0 - \epsilon, a_0^0 + \epsilon], \quad b_2 \in [b_2^0 - \epsilon, b_2^0 + \epsilon].$$

From the four vertices given in Example 13, we have six segments bounding the convex hull of the images. To check the stability of these segments, we apply the Segment Lemma with incremental
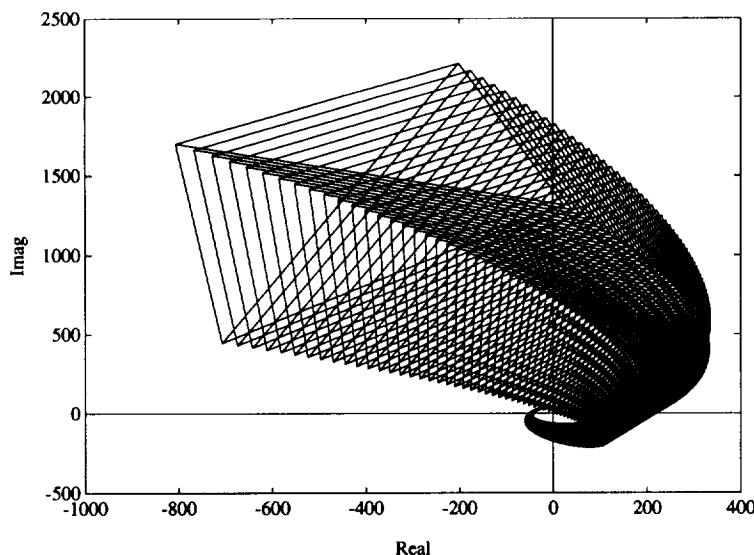

Figure 43: Image set for $\epsilon = 0.63$ (Example 14)

steps of ϵ. This gives $\epsilon^* = 0.63$. The image set of the characteristic polynomial with ϵ^* is shown in Figure 43. The figure shows that the image set is almost touching the origin and thus $\epsilon^* = 0.63$ is the parametric stability margin.

5.3 MULTILINEAR INTERVAL SYSTEMS

In the rest of this section, we will be dealing with transfer functions containing interval parameters with multilinear dependency. The transfer function in question could be embedded in a feedback control system and we will be interested in determining robust stability as well as worst case stability margins and performance measures of such systems. We begin by first focussing on a *multilinear interval system*, namely one whose transfer function is a ratio of multilinear polynomials with independent parameters. To be specific we will consider single-input, single-output, proper, stable systems with transfer function of the form

$$G(s) = \frac{\gamma(s)}{\delta(s)}.$$

Here
$$\gamma(s) = H_1(s)L_{11}(s)L_{12}(s)\cdots L_{1r_1}(s) + \cdots\cdots + H_m(s)L_{m1}(s)L_{m2}(s)\cdots L_{mr_m}(s)$$

where the polynomials $H_i(s)$ are fixed and the polynomials $L_{ij}(s) \in \mathbf{L}_{ij}(s)$ are independent real interval polynomials. Let l denote the ordered set of coefficients of the interval polynomials; l varies in a prescribed axis parallel box Λ; the corresponding family of polynomials $\gamma(s)$ is denoted by $\boldsymbol{\Gamma}(s)$. Similarly we suppose that

$$\delta(s) = F_1(s)P_{11}(s)P_{12}(s)\cdots P_{1r_1}(s) + \cdots\cdots + F_m(s)P_{m1}(s)P_{m2}(s)\cdots P_{mr_m}(s)$$

where the polynomials $F_i(s)$ are fixed, the polynomials $P_{ij}(s)$ are real interval polynomials with the vector of coefficients denoted by p varying in the prescribed box $\boldsymbol{\Pi}$. The resulting family of polynomials $\delta(s)$ is denoted $\boldsymbol{\Delta}(s)$. We also denote explicitly the dependence of $\delta(s)$ on p and of $\nu(s)$ on l by writing $\delta(s, \mathbf{p})$ and $\nu(s, \mathbf{l})$ whenever necessary. We make the standing assumption.

Assumption 1.

A1) Parameters p and l are independent.

A2) $\gamma(s, \mathbf{l})$ and $\delta(s, \mathbf{p})$ are coprime over $(\mathbf{p}, \mathbf{l}) \in \boldsymbol{\Pi} \times \boldsymbol{\Lambda}$.

A3) $\delta(j\omega, \mathbf{p}) \neq 0$ for all $\mathbf{p} \in \boldsymbol{\Pi}$ and each $\omega > 0$.

Later in this section we show how to deal with the situations when assumption A1 does not hold. To display the dependence of a typical element $G(s)$ of G on l and p we write it as $G(s, \mathbf{p}, \mathbf{l})$:

$$G(s, \mathbf{p}, \mathbf{l}) = \frac{\gamma(s, \mathbf{l})}{\delta(s, \mathbf{p})} \tag{57}$$

We form the parametrized family of transfer functions

$$\mathbf{G}(s) = \{G(s, \mathbf{p}, \mathbf{l}) \ : \ (\mathbf{p}, \mathbf{l}) \in (\boldsymbol{\Pi} \times \boldsymbol{\Lambda})\} = \frac{\boldsymbol{\Gamma}(s)}{\boldsymbol{\Delta}(s)}. \tag{58}$$

In order to apply frequency domain methods of analysis and design to the family of systems $\mathbf{G}(s)$ it is necessary to obtain the image set $\mathbf{G}(j\omega)$. We first show how the boundary of this set can be evaluated. We proceed as in the linear case by determining an extremal multilinear interval family of systems $\mathbf{G}_E(s)$. Introduce the Kharitonov polynomials and segments associated with the $P_{ij}(s)$ and $L_{ij}(s)$ respectively, and construct the extremal polynomial manifolds $\boldsymbol{\Delta}_E(s)$ and $\boldsymbol{\Gamma}_E(s)$ and the vertex sets $\boldsymbol{\Delta}_K(s)$ and $\boldsymbol{\Gamma}_K(s)$ as in Section 5.1. Let $\boldsymbol{\Pi}_E$, $\boldsymbol{\Lambda}_E$ and $\boldsymbol{\Pi}_K$, $\boldsymbol{\Lambda}_K$ denote the corresponding manifolds and vertices in $\boldsymbol{\Pi}$ and $\boldsymbol{\Lambda}$ respectively:

$$\boldsymbol{\Gamma}_E(s) = \{\gamma(s, \mathbf{l}) : \mathbf{l} \in \boldsymbol{\Lambda}_E\}, \qquad \boldsymbol{\Gamma}_K(s) = \{\gamma(s, \mathbf{l}) : \mathbf{l} \in \boldsymbol{\Lambda}_K\}$$

$$\boldsymbol{\Delta}_E(s) = \{\delta(s, \mathbf{p}) : \mathbf{p} \in \boldsymbol{\Pi}_E\}, \qquad \boldsymbol{\Delta}_K(s) = \{\delta(s, \mathbf{p}) : \mathbf{p} \in \boldsymbol{\Pi}_K\}.$$

The *extremal set* $\mathbf{G}_E(s)$ is then defined as

$$\mathbf{G}_E(s) := \left\{ \frac{\gamma(s, \mathbf{l})}{\delta(s, \mathbf{p})} : (\mathbf{l} \in \boldsymbol{\Lambda}_K, \ \mathbf{p} \in \boldsymbol{\Pi}_E) \text{ or } (\mathbf{l} \in \boldsymbol{\Lambda}_E, \ \mathbf{p} \in \boldsymbol{\Pi}_K) \right\}. \tag{59}$$

Using our compact notational convention we can write

$$\mathbf{G}_E(s) = \left(\frac{\boldsymbol{\Gamma}_K(s)}{\boldsymbol{\Delta}_E(s)} \right) \cup \left(\frac{\boldsymbol{\Gamma}_E(s)}{\boldsymbol{\Delta}_K(s)} \right).$$

43

Theorem 16. *Under the Assumption 1,*

$$\partial \mathbf{G}(j\omega) \subset \mathbf{G}_E(j\omega)$$

for all $\omega \in [0, \infty)$.

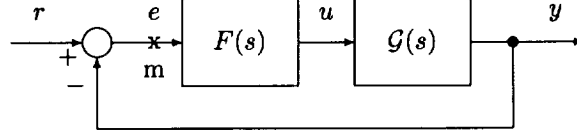Now suppose that $G(s)$ is part of the control system shown in Figure 44.

Figure 44: A unity feedback system

Define transfer functions:

$$\frac{y(s)}{u(s)} := G(s), \qquad \frac{u(s)}{e(s)} = F(s), \tag{60}$$

$$T^o(s) := \frac{y(s)}{e(s)} = F(s)G(s), \qquad T^e(s) := \frac{e(s)}{r(s)} = \frac{1}{1 + F(s)G(s)}, \tag{61}$$

$$T^u(s) := \frac{u(s)}{r(s)} = \frac{F(s)}{1 + F(s)G(s)}, \qquad T^y(s) := \frac{y(s)}{r(s)} = \frac{F(s)G(s)}{1 + F(s)G(s)}. \tag{62}$$

As $G(s)$ ranges over the uncertainty set $\mathbf{G}(s)$, these transfer functions vary in corresponding sets.

$$\mathbf{T}^o(s) := \{F(s)G(s) \ : \ G(s) \in \mathbf{G}(s)\}, \qquad \mathbf{T}^e(s) := \left\{\frac{1}{1 + F(s)G(s)} \ : \ G(s) \in \mathbf{G}(s)\right\}$$

$$\mathbf{T}^u(s) := \left\{\frac{F(s)}{1 + F(s)G(s)} \ : \ G(s) \in \mathbf{G}(s)\right\} \qquad \mathbf{T}^y(s) := \left\{\frac{F(s)G(s)}{1 + F(s)G(s)} \ : \ G(s) \in \mathbf{G}(s)\right\} \tag{63}$$

It turns out that the boundary of the image set, at $s = j\omega$, of each of the above sets is generated by the extremal set $\mathbf{G}_E(s)$. Introduce the *extremal subsets*:

$$\mathbf{T}^o_E(s) := \{F(s)G(s) \ : \ G(s) \in \mathbf{G}_E(s)\}, \qquad \mathbf{T}^e_E(s) := \left\{\frac{1}{1 + F(s)G(s)} \ : \ G(s) \in \mathbf{G}_E(s)\right\} \tag{64}$$

$$\mathbf{T}^u_E(s) := \left\{\frac{F(s)}{1 + F(s)G(s)} \ : \ G(s) \in \mathbf{G}_E(s)\right\}, \qquad \mathbf{T}^y_E(s) := \left\{\frac{F(s)G(s)}{1 + F(s)G(s)} \ : \ G(s) \in \mathbf{G}_E(s)\right\} \tag{65}$$

Theorem 17. *For every $\omega \geq 0$,*
(a) $\partial \mathbf{T}^o(j\omega) \subset \mathbf{T}^o_E(j\omega)$ *(b)* $\partial \mathbf{T}^e(j\omega) \subset \mathbf{T}^e_E(j\omega)$ *(c)* $\partial \mathbf{T}^u(j\omega) \subset \mathbf{T}^u_E(j\omega)$ *(d)* $\partial \mathbf{T}^y(j\omega) \subset \mathbf{T}^y_E(j\omega)$

All the boundary results related to the Nyquist and Bode envelopes given in the previous section carry over to the multilinear case with the corresponding extremal set $\mathbf{G}_E(s)$. In the following subsection we show that these boundary results hold for a much larger class of functions of $\mathbf{G}(s)$.

5.3.1 Extensions of Boundary Results

In defining our multilinear interval system we had assumed that the numerator and denominator parameters of $G(s)$ are independent. However for closed loop transfer functions this assumption of independence does not hold. Nevertheless the boundary generating property of the set $\mathbf{G}_E(s)$ still holds for these closed loop transfer functions. It is natural to attempt to generalize this boundary generating property to a large class of functions where dependencies between numerator and denominator parameters occur. Such dependencies invariably occur in the transfer functions associated with multiloop control systems. We begin with a multilinear function $Q(s)$ of several transfer functions $G^i(s), i = 1, 2 \cdots, q$. Let us assume that each $G^i(s)$ itself lies in a multilinear interval family of systems $\mathbf{G}^i(s)$ defined as in this section, with independent parameters in the numerator and denominator. We also assume that the parameters in $G^i(s)$ are independent of those in $G^j(s)$,

44

$i \neq j$. Note that if we regard $Q(s)$ as a rational function its numerator and denominator polynomials contain common interval parameters. Let

$$\mathbf{Q}(s) := \{Q(s) : G^i(s) \in \mathbf{G}^i(s), \quad i = 1, 2 \cdots q\}.$$

We wish to determine the complex plane image set of the family $\mathbf{Q}(s)$ evaluated at $s = j\omega$:

$$\mathbf{Q}(j\omega) := \{Q(j\omega) : G^i(s) \in \mathbf{G}^i(s), \quad i = 1, 2 \cdots q\}.$$

Let $\mathbf{G}_{\mathrm{E}}^i(s)$ denote the extremal subset of $\mathbf{G}^i(s)$ and introduce

$$\mathbf{Q}_{\mathrm{E}}(j\omega) := \{Q(j\omega) : G^i(s) \in \mathbf{G}_{\mathrm{E}}^i(s), \quad i = 1, 2 \cdots q\}.$$

Then we can state the following boundary result.

Theorem 18.
$$\partial \mathbf{Q}(j\omega) \subset \mathbf{Q}_{\mathrm{E}}(j\omega). \tag{66}$$

We can generalize the above property even further. Let $Q(s)$ be as above and consider a linear fractional transformation (LFT) $T(Q(s))$ defined by arbitrary functions $A(s), B(s), C(s)$ and $D(s)$

$$T(Q(s)) := Q_1(s) := \frac{A(s)Q(s) + B(s)}{C(s)Q(s) + D(s)}.$$

Introduce the set

$$T(\mathbf{Q}(s)) := \left\{ \frac{A(s)Q(s) + B(s)}{C(s)Q(s) + D(s)} : Q(s) \in \mathbf{Q}(s) \right\}.$$

Let us now impose the restriction

$$A(j\omega)D(j\omega) - B(j\omega)C(j\omega) \neq 0. \tag{67}$$

Under the above restriction $T(Q(j\omega))$ is a LFT of $Q(j\omega)$ and thus carries boundaries onto boundaries. Thus we know that the boundary of $\mathbf{Q}_1(j\omega)$ is also generated by the extremal systems $\mathbf{G}_{\mathrm{E}}^i(s)$.

Theorem 19. *Let $\mathbf{Q}(s)$ be as defined above and let $T(Q(s))$ be an LFT. Then, assuming (67) holds*

$$\partial T(\mathbf{Q}(j\omega)) \subset T(\mathbf{Q}_{\mathrm{E}}(j\omega)).$$

Remark 5. We remark that any LFT of $Q_1(s)$ as well as sums and products of LFT's continue to enjoy the boundary generating property of the extremal systems. In this way a large class of transfer functions occurring in closed loop systems can be handled.

5.3.2 Computation of $\mathbf{G}_{\mathrm{E}}(j\omega)$

As we have seen, the determination of the set $\mathbf{G}(j\omega)$ reduces to evaluating $\mathbf{G}_{\mathrm{E}}(j\omega)$, a set of smaller dimension. Nevertheless, $\mathbf{G}_{\mathrm{E}}(j\omega)$ is still a multilinear function of the uncertain segment parameters. The only way to exactly evaluate this set is by gridding over the uncertainty box. In general this procedure is computationally expensive or even infeasible. Fortunately, as we have seen earlier, the "concave" property of the image set of multilinear interval polynomials given by the Mapping Theorem allows us to overbound $\mathbf{G}_{\mathrm{E}}(j\omega)$ by a ratio of unions of convex polygons. Recall that

$$\mathbf{G}_{\mathrm{E}}(j\omega) = \left(\frac{\mathbf{\Gamma}_{\mathrm{K}}(j\omega)}{\mathbf{\Delta}_{\mathrm{E}}(j\omega)} \right) \cup \left(\frac{\mathbf{\Gamma}_{\mathrm{E}}(j\omega)}{\mathbf{\Delta}_{\mathrm{K}}(j\omega)} \right). \tag{68}$$

From the Mapping Theorem we have

$$\mathbf{\Gamma}_{\mathrm{E}}(j\omega) \subset co \; \mathbf{\Gamma}_{\mathrm{K}}(j\omega), \qquad \mathbf{\Delta}_{\mathrm{E}}(j\omega) \subset co \; \mathbf{\Delta}_{\mathrm{K}}(j\omega).$$

Now consider $\bar{\mathbf{G}}_{\mathrm{E}}(j\omega)$ defined by replacing $\mathbf{\Gamma}_{\mathrm{E}}(j\omega)$ and $\mathbf{\Delta}_{\mathrm{E}}(j\omega)$ by $co \; \mathbf{\Gamma}_{\mathrm{K}}(j\omega)$ and $co \; \mathbf{\Delta}_{\mathrm{K}}(j\omega)$ respectively. In other words,

$$\bar{\mathbf{G}}_{\mathrm{E}}(j\omega) = \left(\frac{\mathbf{\Gamma}_{\mathrm{K}}(j\omega)}{co \; \mathbf{\Delta}_{\mathrm{K}}(j\omega)} \right) \cup \left(\frac{co \; \mathbf{\Gamma}_{\mathrm{K}}(j\omega)}{\mathbf{\Delta}_{\mathrm{K}}(j\omega)} \right). \tag{69}$$

It is clear that $\bar{\mathbf{G}}_\mathrm{E}(j\omega)$ overbounds $\mathbf{G}_\mathrm{E}(j\omega)$:

$$\mathbf{G}_\mathrm{E}(j\omega) \subset \bar{\mathbf{G}}_\mathrm{E}(j\omega). \tag{70}$$

The evaluation of $\bar{\mathbf{G}}_\mathrm{E}(j\omega)$ is relatively easy because it consists of a union of one-parameter families of transfer functions of the types

$$\frac{\lambda U_1(j\omega) + (1-\lambda)U_2(j\omega)}{V(j\omega)} \quad \text{or} \quad \frac{U(j\omega)}{\lambda V_1(j\omega) + (1-\lambda)V_2(j\omega)}.$$

The union of these one-parameter families gives rise to $\bar{\mathbf{G}}_\mathrm{E}(j\omega)$ which overbounds the boundary of $\mathbf{G}(j\omega)$. The tightness of the approximation can be improved as we have seen before, by introducing additional vertices in the parameter set $\Pi \times \Lambda$. The guaranteed gain and phase margins of a control system containing parameter uncertainty may be obtained from these overbounded sets as shown in Figure 45. The image at $s = j\omega$ of each of the transfer function sets associated with the feedback
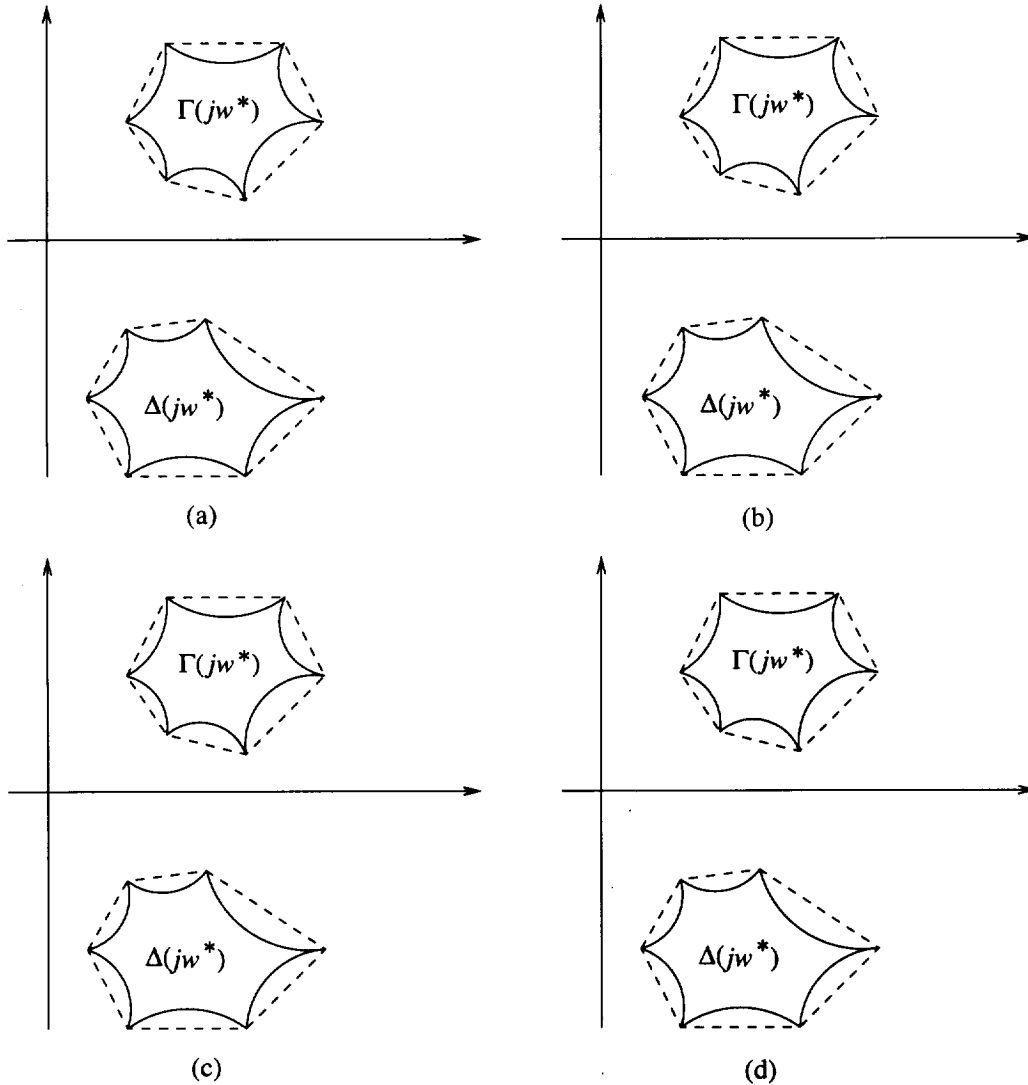

Figure 45: Guaranteed gain and phase margin using overbounded sets

system considered in Figure 44 can be overbounded by replacing $\mathbf{G}(j\omega)$ by $\bar{\mathbf{G}}_\mathrm{E}(j\omega)$, and in fact we can do the same for any linear fractional transformation of $G(s)$. An example of this calculation follows.

Example 15. (**Nyquist, Bode and Nichols Envelopes of Multilinear Systems**) The purpose of this example to show how to construct the frequency domain envelopes (Nyquist, Bode and Nichols envelopes) of the multilinear interval family. Let us recall the system given in Example 12:

$$F(s)\underbrace{P(s)Q(s)}_{G(s)} = \frac{(s+2)(s^2+s+1)(6.6s^3+13.5s^2+15.5s+20.4)}{(s+1)(s^3+a_2s^2+4s+a_0)(s^3+b_2s^2+3.5s+2.4)}$$

where

$$a_2 \in [a_2^-, a_2^+] = [-3.625, -2.375], \qquad a_0 \in [a_0^-, a_0^+] = [1.375, 2.625], \qquad b_2 \in [b_2^-, b_2^+] = [2.875, 4.125].$$

From Theorem 16, it is enough to consider $\mathbf{G}_E(j\omega)$. Since this particular example has parameters only in the denominator, we have

$$\partial \left(F(j\omega)\mathbf{G}(j\omega)\right) \subset F(j\omega)\mathbf{G}_E(j\omega) = \frac{(s+2)(s^2+s+1)(6.6s^3+13.5s^2+15.5s+20.4)|_{s=j\omega}}{\Delta_E(j\omega)}$$

where $\Delta_E(j\omega)$ consists of the six line segments joining the following four vertices:

$$(s+1)(s^3+a_2^+s^2+4s+a_0^-)(s^3+b_2^+s^2+3.5s+2.4)|_{s=j\omega},$$
$$(s+1)(s^3+a_2^+s^2+4s+a_0^-)(s^3+b_2^-s^2+3.5s+2.4)|_{s=j\omega},$$
$$(s+1)(s^3+a_2^-s^2+4s+a_0^+)(s^3+b_2^+s^2+3.5s+2.4)|_{s=j\omega},$$
$$(s+1)(s^3+a_2^-s^2+4s+a_0^+)(s^3+b_2^-s^2+3.5s+2.4)|_{s=j\omega}.$$

Figures 46, 47, and 48 are obtained accordingly.
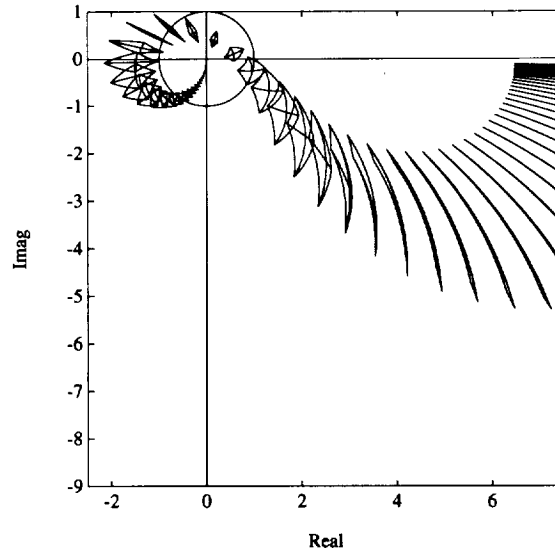
Figure 46: Nyquist envelope (Example 15)

5.4 H_∞ STABILITY MARGIN

In this section we use the boundary results derived above to efficiently deal with many frequency domain measures of performance and, in particular, to determine worst case performance over the parameter set associated with a multilinear interval systems. We will use the standard notation: $\mathbf{C}_+ := \{s \in C : \text{Re}(s) \geq 0\}$, and $H_\infty(\mathbf{C}_+)$ will represent the space of functions $f(s)$ that are bounded and analytic in $\mathbf{C}_+$ with the standard H_∞ norm,

$$\|f\|_\infty = \sup_{\omega \in \mathbf{R}} |f(j\omega)|.$$
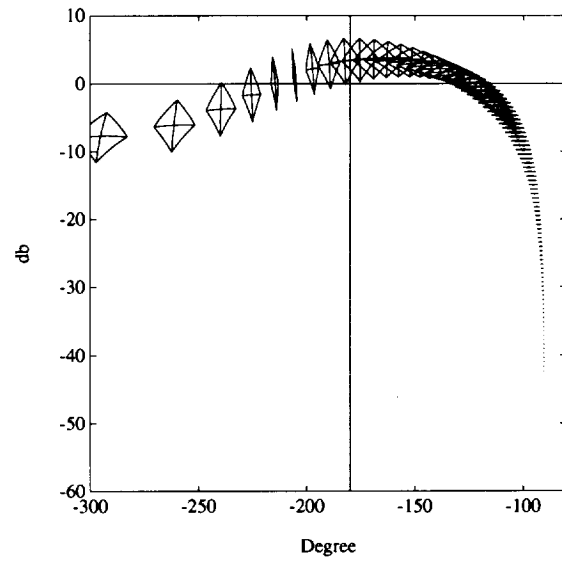
Figure 47: Nichols envelope (Example 15)
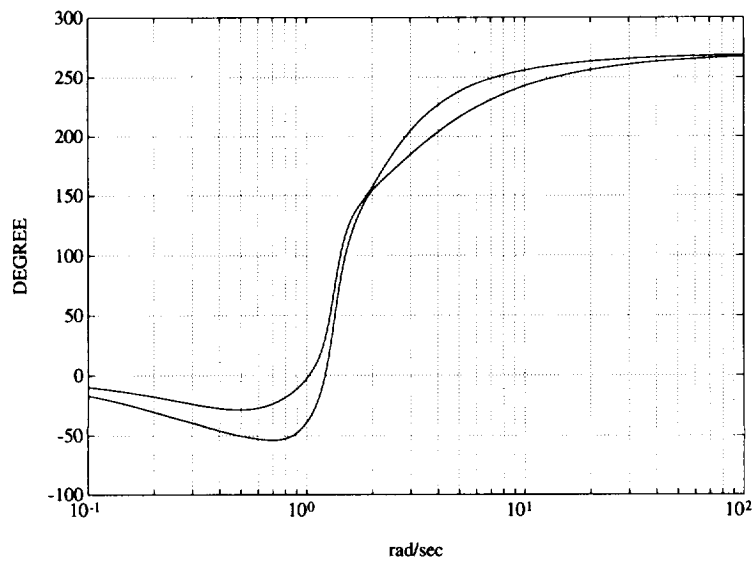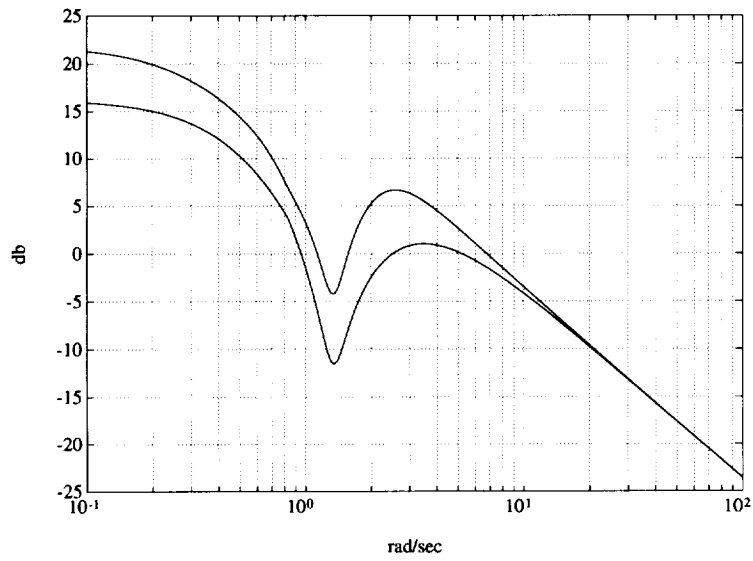
Figure 48: Bode magnitude and phase envelopes (Example 15)

48

Let us consider the multilinear interval family of systems $\mathbf{G}(s)$ defined earlier (see (58)) and let us assume that the entire family is stable. To determine the unstructured stability margin of control systems containing the family $\mathbf{G}(s)$ we need to determine the supremum of the H_∞ norm of certain transfer functions over $\mathbf{G}(s)$. Since the H_∞ norm-bounded perturbations provide uniform perturbations at all frequencies, it is desirable to shape this perturbation by introducing a weight. Let the weight $W(s)$ be a scalar stable proper transfer function

$$W(s) = \frac{n_w(s)}{d_w(s)}.$$

To start with, let us look at two specific robust stability problems involving mixed parametric-unstructured uncertainty:

Problem I: Consider the configuration in Figure 49, where $W(s)$ is a stable proper weight, $\mathbf{G}(s)$ is a stable multilinear interval family of systems, and ΔP is any H_∞ perturbation that satisfies $\|\Delta P\| < \alpha$. Find necessary and sufficient conditions for stability of the family of closed loop systems.
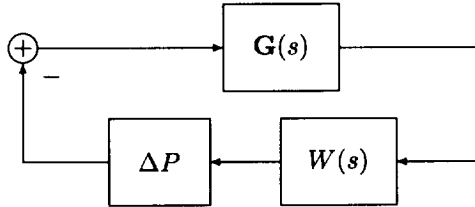
Figure 49:

Problem II: Consider the feedback configuration in Figure 50, where $W(s)$ is a stable proper weight, ΔP is any H_∞ perturbation that satisfies $\|\Delta P\| < \alpha$, and $C(s)$ is a controller that simultaneously stabilizes every element in the set $\mathbf{G}(s)$. Find necessary and sufficient conditions for stability of the family of closed loop systems.
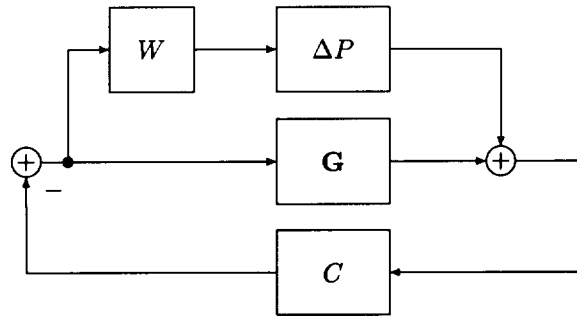
Figure 50:

The above problems are generalized versions of standard H_∞ robust stability problems where a fixed plant is considered. Here, the worst case solution is sought over the parameter set $\Pi \times \Lambda$. We solve this problem by using the Small Gain Theorem and determining the worst case over the uncertainty set. The solution is accomplished by showing that the H_∞ norms in question attain their supremum value over the extremal set of transfer functions $\mathbf{G_E}(s) \subset \mathbf{G}(s)$ defined in (59). We can now state the main result of this section.

Theorem 20. (Unstructured Stability Margins)

1) The configuration of (Figure 49) will be stable if and only if α satisfies

$$\alpha \leq \frac{1}{\sup_{g \in \mathbf{G_E}} \|Wg\|_\infty} := \alpha_o^*.$$

49

2) The configuration of Problem II (Figure 50) will be stable if and only if α satisfies

$$\alpha \le \frac{1}{\sup_{g \in \mathbf{G_E}} \|WC(1+gC)^{-1}\|_\infty} := \alpha_c^*.$$

Remark 6. The quantities α_o^* and α_c^* serve as unstructured H_∞ stability margins for the respective open and closed loop parametrized systems treated in Problems I and II.

Remark 7. In practice we can further replace $\mathbf{G_E}(s)$ by the image set overbounding polytopic family $\mathbf{\bar{G}_E}(s)$, and obtain lower bounds on these margins from $\mathbf{\bar{G}_E}(s)$. We can also obtain upper bounds on these margins from the set of Kharitonov vertex systems of the family. Furthermore, the extremal results stated above also hold for any LFT of $\mathbf{G}(s)$.

5.5 NONLINEAR SECTOR BOUNDED STABILITY MARGIN

We now consider the effect of nonlinear perturbations on the multilinear interval family $\mathbf{G}(s)$ defined in the last section (see (58)). The nonlinear perturbations will consist of all possible nonlinear gains lying in a sector $[0, k]$. In other words, we consider the configurations in Figures 51 and 52.
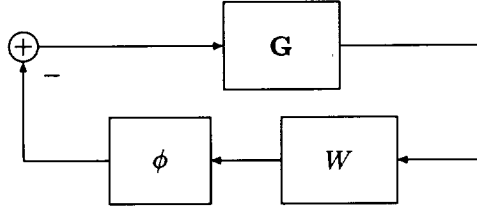
Figure 51:
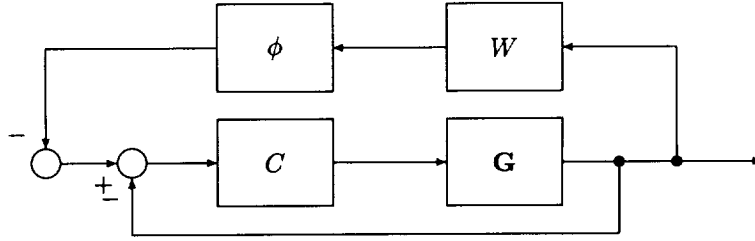
Figure 52:

The gain block ϕ consists of all nonlinear time-varying gains $\phi(t, \sigma)$ satisfying

$$\phi(t, 0) = 0 \quad \text{for all } t \ge 0 \quad \text{and} \quad 0 \le \sigma \phi(t, \sigma) \le k\sigma^2.$$

This implies that $\phi(t, \sigma)$ is bounded by the lines $\phi = 0$ and $\phi = k\sigma$. Such nonlinearities are said to belong to a sector $[0, k]$. $G(s)$ will be assumed to lie in the multilinear interval family $\mathbf{G}(s)$. The problem is to determine the largest size of the sector k for which robust stability is guaranteed. This is the multilinear version of the robust Lur'e problem. As before, the solution depends on the *strict positive realness* (SPR) properties of the family in question. First we have the following.

Lemma 3. (Extremal SPR Properties)

1) Let $\mathbf{G}(s)$ be the multilinear interval family defined in (58) and assume that $\mathbf{G}(s)$ is stable. Then

$$\inf_{G \in \mathbf{G}} \inf_{\omega \in \mathbf{R}} \mathrm{Re}(W(j\omega)G(j\omega)) = \inf_{G \in \mathbf{G_E}} \inf_{\omega \in \mathbf{R}} \mathrm{Re}(W(j\omega)G(j\omega)).$$

2) If $C(s)$ is a controller that stabilizes the entire family $\mathbf{G}(s)$, then

$$\inf_{G \in \mathbf{G}} \inf_{\omega \in \mathbf{R}} \mathrm{Re}\left(W(j\omega)C(j\omega)G(j\omega)(1 + C(j\omega)G(j\omega))^{-1}\right) =$$
$$\inf_{G \in \mathbf{G_E}} \inf_{\omega \in \mathbf{R}} \mathrm{Re}\left(W(j\omega)C(j\omega)G(j\omega)(1 + C(j\omega)G(j\omega))^{-1}\right).$$

Theorem 21. (Nonlinear Stability margin)

1) Let $k^* \geq 0$ be defined by:

$$\sup\left\{k \ : \ \frac{1}{k} + \inf_{G \in \mathbf{G_E}} \inf_{\omega \in \mathbf{R}} \mathrm{Re}(W(j\omega)G(j\omega)) > 0\right\}$$

then the closed loop system in Figure 51 is absolutely stable for all nonlinear gains ϕ lying in the sector $[0, k^*]$.

2) Let $k^* \geq 0$ be defined by:

$$\sup\left\{k \ : \ \frac{1}{k} + \inf_{G \in \mathbf{G_E}} \inf_{\omega \in \mathbf{R}} \mathrm{Re}\left(W(j\omega)C(j\omega)G(j\omega)(1 + C(j\omega)G(j\omega))^{-1}\right) > 0\right\}$$

for the controller C, then the closed loop system in Figure 52 is absolutely stable for all nonlinear gains ϕ lying in the sector $[0, k^*]$.

Example 16. (Stability Sector for Multilinear Interval Systems) Consider the system used in Example 12. We plot the frequency domain image of the closed loop system transfer function

$$\mathbf{M}(s) := \left\{\frac{F(s)G(s)}{1 + F(s)G(s)} : G(s) \in \mathbf{G_E}(s)\right\}.$$

Figure 53 shows that the nonlinear sector is given by $\frac{1}{k} = 20.5012$.
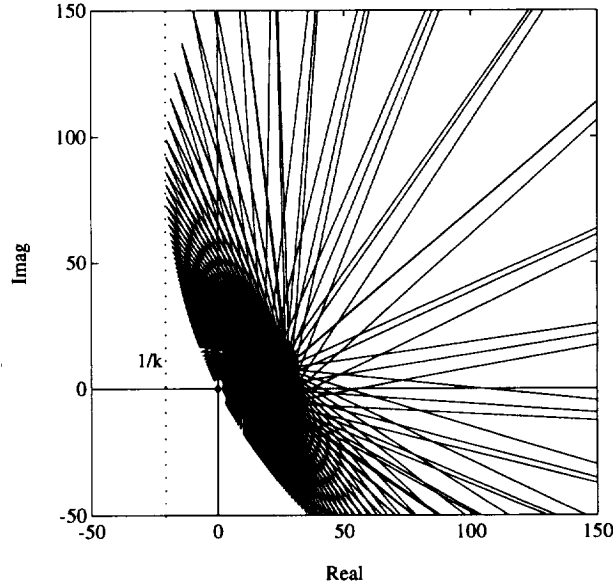
Figure 53: Frequency domain image of $\mathbf{M}(j\omega)$ (Example 16)

5.6 INTERVAL PLANTS AND DIAGONAL REPRESENTATION OF PERTURBATIONS

In the robust control literature it has become customary to represent system perturbations in a signal flow diagram where the perturbations are "pulled" out and displayed in a feedback matrix Δ with independent diagonal or block-diagonal entries Δ_i as shown below in Figure 54. $M(s)$ is a suitably defined interconnection transfer function matrix of appropriate size and Δ is a block diagonal matrix containing all the perturbations affecting the system dynamics. In general this would include real parametric uncertainty as well as norm-bounded uncertainty blocks with the latter representing either actual unmodelled dynamics or fictitious performance blocks. The popularity of this representation is due to the fact that almost all types of uncertainties including parametric and

51
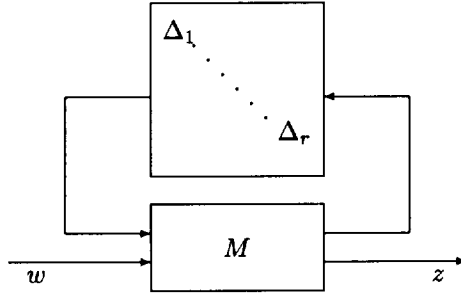
Figure 54: System with uncertainties represented in feedback form

unstructured uncertainties can be accurately and explicitly represented in this framework. Moreover, the feedback representation allows us to use the Small Gain formulation and thus convert robust performance problems into robust stability problems.

Although this formulation does not add anything to the the rich structure of interval systems already developed, it is nevertheless instructive to interpret the solution given by the Generalized Kharitonov Theorem in the linear and multilinear cases in this framework. We begin in the next subsection with the diagonal representation of a single interval system. This is subsequently extended to the case of multiple interval systems and multiple norm-bounded perturbation blocks. This type of mixed perturbation problem arises in systems with several performance specifications. We show how the boundary properties of the extremal systems $\mathbf{G}_E(s)$ established in the GKT play a role in the solution of these problems.

5.6.1 Diagonal Feedback Representation of an Interval System

Let $\mathbf{G}(s)$ be a interval plant

$$\mathbf{G}(s) = \left\{ \frac{N(s)}{D(s)} \ : \ (N(s) \times D(s) \in (\mathbf{N}(s) \times \mathbf{D}(s)) \right\} \tag{71}$$

where $\mathbf{N}(s)$ and $\mathbf{D}(s)$ are interval polynomial families. The four Kharitonov polynomials associated with the interval polynomial $\mathbf{D}(s)$ can be written as follows:

$$K_D^1(s) = D_{\min}^{\text{even}}(s) + D_{\min}^{\text{odd}}(s), \quad K_D^2(s) = D_{\min}^{\text{even}}(s) + D_{\max}^{\text{odd}}(s),$$
$$K_D^3(s) = D_{\max}^{\text{even}}(s) + D_{\min}^{\text{odd}}(s), \quad K_D^4(s) = D_{\max}^{\text{even}}(s) + D_{\max}^{\text{odd}}(s).$$

We know that, as far as frequency domain properties at $s = j\omega$ are concerned, the interval polynomial $\mathbf{D}(s)$ can be replaced by the following reduced 2-parameter family:

$$\mathbf{D}_R(s) = \left\{ D(s) \ : \ D^0(s) + \lambda_1 D_e(s) + \lambda_2 D_o(s) \ \lambda_i \in [-1,1] \right\} \tag{72}$$

where

$$D_e(s) = \frac{1}{2} \left(D_{\max}^{\text{even}}(s) - D_{\min}^{\text{even}}(s) \right), \quad D_o(s) = \frac{1}{2} \left(D_{\max}^{\text{odd}}(s) - D_{\min}^{\text{odd}}(s) \right)$$

and

$$D^0(s) = \frac{1}{2} \left[D_{\max}^{\text{even}}(s) + D_{\min}^{\text{even}}(s) + D_{\max}^{\text{odd}}(s) + D_{\min}^{\text{odd}}(s) \right]$$

is the *nominal* polynomial. Similarly $\mathbf{N}(s)$ can be replaced by:

$$\mathbf{N}_R(s) = \left\{ N(s) \ : \ N^0(s) + \lambda_3 N_e(s) + \lambda_4 N_o(s), \quad \lambda_i \in [-1,1] \right\}. \tag{73}$$

It is clear from the above that an interval plant is completely characterized in the frequency domain by the 4-parameter family $\mathbf{G}_R(s)$:

$$\mathbf{G}_R(s) = \left\{ \frac{N(s)}{D(s)} \ : \ (N(s) \times D(s)) \in (\mathbf{N}_R(s) \times \mathbf{D}_R(s)) \right\}. \tag{74}$$

Now write $y(s) = G(s)u(s)$,

$$y(s) = \frac{N^0(s) + \lambda_3 N_e(s) + \lambda_4 N_o(s)}{D^0(s) + \lambda_1 D_e(s) + \lambda_2 D_o(s)} u(s).$$

52

This may be rewritten as follows:

$$y(s) = \left[D^0(s)\right]^{-1} \left\{ \left(N^0(s) + \lambda_3 N_e(s) + \lambda_4 N_o(s)\right) u(s) - \left(\lambda_1 D_e(s) + \lambda_2 D_o(s)\right) y(s) \right\} \quad (75)$$

or, suppressing s, as

$$y = \left[(D^0)^{-1} N^0 + \lambda_3 (D^0)^{-1} N_e + \lambda_4 (D^0)^{-1} N_o\right] u - \left[\lambda_1 (D^0)^{-1} D_e + \lambda_2 (D^0)^{-1} D_o\right] y. \quad (76)$$

Corresponding to (76), we have the block diagram shown in Figure 55.
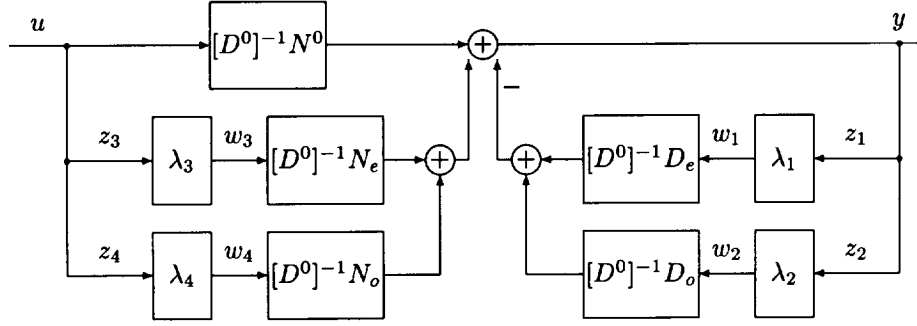
Figure 55: Four parameter structure

This input-output relation may be written as follows:

$$\begin{bmatrix} z_1 \\ z_2 \\ z_3 \\ z_4 \\ y \end{bmatrix} = (D^0)^{-1} \begin{bmatrix} -D_e & -D_o & N_e & N_o & N^0 \\ -D_e & -D_o & N_e & N_o & N^0 \\ 0 & 0 & 0 & 0 & D^0 \\ 0 & 0 & 0 & 0 & D^0 \\ -D_e & -D_o & N_e & N_o & N^0 \end{bmatrix} \begin{bmatrix} w_1 \\ w_2 \\ w_3 \\ w_4 \\ u \end{bmatrix} \quad (77)$$

with

$$w_i = \lambda_i z_i, \quad i = 1, 2, 3, 4. \quad (78)$$

Let $z := [z_1, z_2, z_3, z_4]^T$ and $w := [w_1, w_2, w_3, w_4]^T$. The above equations can then be rewritten as

$$z(s) = M_{11}(s)w(s) + M_{12}(s)u(s), \quad y(s) = M_{21}(s)w(s) + M_{22}(s)u(s), \quad w(s) = \Delta z(s).$$

where

$$M(s) = \quad (79)$$

$$\begin{bmatrix} M_{11}(s) & \vdots & M_{12}(s) \\ \cdots & & \cdots \\ M_{21}(s) & \vdots & M_{22}(s) \end{bmatrix} = \begin{bmatrix} -[D^0]^{-1}D_e & -[D^0]^{-1}D_o & [D^0]^{-1}N_e & [D^0]^{-1}N_o & \vdots & [D^0]^{-1}N^0 \\ -[D^0]^{-1}D_e & -[D^0]^{-1}D_o & [D^0]^{-1}N_e & [D^0]^{-1}N_o & \vdots & [D^0]^{-1}N^0 \\ 0 & 0 & 0 & 0 & \vdots & 1 \\ 0 & 0 & 0 & 0 & \vdots & 1 \\ \cdots & \cdots & \cdots & \cdots & & \cdots \\ -[D^0]^{-1}D_e & -[D^0]^{-1}D_o & [D^0]^{-1}N_e & [D^0]^{-1}N_o & \vdots & [D^0]^{-1}N^0 \end{bmatrix} \quad (80)$$

and

$$\Delta = \Delta^R := \begin{bmatrix} \lambda_1 & & & \\ & \lambda_2 & & \\ & & \lambda_3 & \\ & & & \lambda_4 \end{bmatrix}.$$

Consequently, we have the configuration shown in Figure 56.

The result established from GKT tells us that robust stability of the four parameter feedback structure given in Figure 56 is further equivalent to that of a reduced set of one-parameter extremal
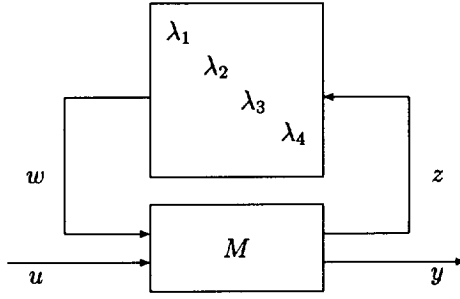
Figure 56: 4-parameter feedback representation of an interval system
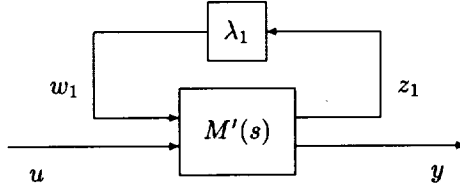
Figure 57: A typical element of the extremal set $\mathbf{G}_E(s)$

feedback structures in which each structure contains a single perturbation block. In Figure 57 we display a typical such extremal system structure where λ_1 is the only perturbation block and the remaining λ's are set to the vertex values $+1$ or -1.

This is denoted in the equations by writing $\lambda_2 = \lambda_2^*$, $\lambda_3 = \lambda_3^*$ and $\lambda_4 = \lambda_4^*$. The system equations assume the form

$$\begin{bmatrix} z_1 \\ y \end{bmatrix} = \underbrace{\begin{bmatrix} M'_{11}(s) \ M'_{12}(s) \\ M'_{21}(s) \ M'_{22}(s) \end{bmatrix}}_{M'(s)} \begin{bmatrix} w_1 \\ u \end{bmatrix} \qquad (81)$$

with

$$w_1 = \lambda_1 z_1$$

where

$$M'_{11}(s) = M'_{21}(s) = (1 + \lambda_2^*[D^0]^{-1}D_o)^{-1}[D^0]^{-1}D_e$$
$$M'_{21}(s) = M'_{22}(s) = (1 + \lambda_2^*[D^0]^{-1}D_o)^{-1}[D^0]^{-1}N^0 + \lambda_3^*[D^0]^{-1}N_e + \lambda_4^*[D^0]^{-1}N_o.$$

The interval plant $\mathbf{G}(s)$ can *always* be replaced by the above set of one-parameter structures $\mathbf{G}_E(s)$ regardless of the rest of the feedback system. If the intervals in which the parameters vary are not fixed *apriori* one can also determine their maximum permissible excursion using the same framework. The only difference in this case is that the Kharitonov polynomials, and therefore the system M' defined from them, have parameters which depend on the dilation parameter ϵ as shown below in Figure 58.
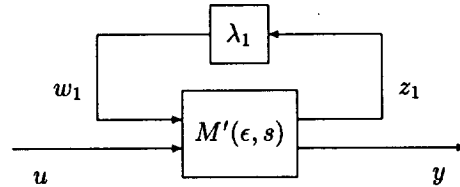
Figure 58: An element of $\mathbf{G}_E(\epsilon, s)$

The limiting value ϵ^* of ϵ is determined as the smallest value of ϵ for which the control system containing one of the one parameter structures representing $\mathbf{G}_E(\epsilon, s)$ acquires a pole on the imaginary axis. Thus ϵ^* can be found using several methods which include the Segment Lemma and the Bounded Phase Conditions. Of course, by restricting attention to the class of controllers which satisfy the vertex conditions given in GKT we get further simplification in that *all* the λ's can be frozen at vertices, and ϵ^* can be found from the vertex systems.

54

The above discussion may be summarized by stating that if $\mathbf{G}(s)$ is an interval plant contained within a control system structure, we can always replace it with the set of one-parameter extremal systems $\mathbf{G_E}(s)$ for the purposes of determining worst case performance and stability margins and for carrying out worst case frequency response analysis. This observation holds also for linear interval systems and polytopic systems. In the case of multilinear interval systems we can again replace the plant set $\mathbf{G}(s)$ by the corresponding set of extremal systems $\mathbf{G_E}(s)$ which now consist of a set reduced dimensional multilinear systems in terms of the interval parameters λ_i. This can in turn be replaced by a polytopic family using the Mapping Theorem. Finally, an extremal one-parameter family can be constructed for this polytopic system as shown in this section.

5.6.2 Interval Plant with H_∞ Norm-Bounded Uncertainty

Now let us consider the mixed uncertainty system in Figure 59.
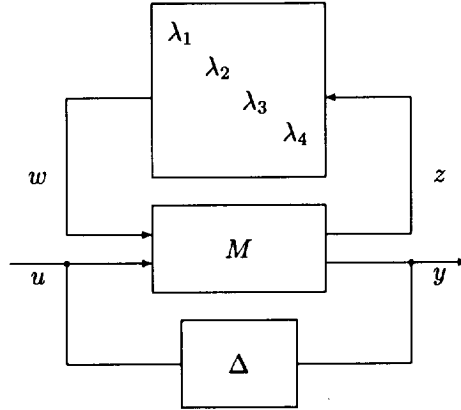
Figure 59: 4-parameter representation of interval system with unstructured uncertainty

It consists of an interval plant with an unstructured perturbation block Δ lying in a H_∞ ball of specified radius. As before, the interval plant can be represented in terms of four feedback parameters around a suitable interconnection transfer matrix $M(s)$. We can now represent all the perturbations, parametric as well as unstructured, in feedback form around a suitably defined system $P(s)$. Thus, we have the structure shown in Figure 60 with an appropriate $P(s)$. This four-parameter system
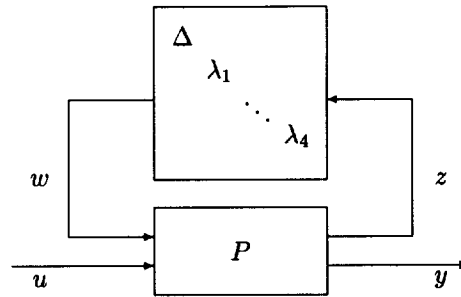
Figure 60: Feedback representation of mixed uncertainties

can be reduced to the extremal set of single parameter uncertainty problems. A typical element of this extremal set is shown in Figure 61 with an appropriate $P'(s)$. By eliminating the feedback loop associated with λ this can also be represented as the structure shown in Figure 62.

5.6.3 Multiple Interval Systems and Unstructured Blocks

Let us now consider the general configuration given in Figure 63.
$M(s)$ is an interconnection transfer function matrix of suitable dimensions and $\Delta^U(s)$ is a diagonal matrix containing all the unstructured system perturbations. The unstructured perturbations can
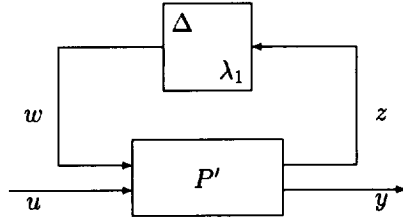
Figure 61: A typical element of the extremal set of systems
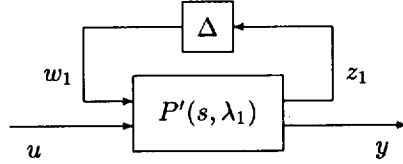
Figure 62: Equivalent representation of an extremal system
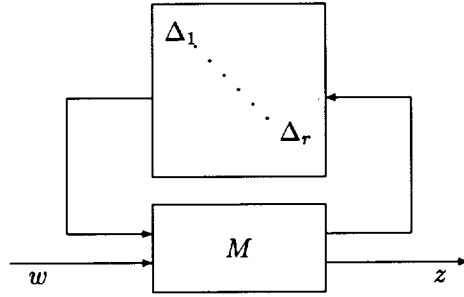
Figure 63: System with uncertainties represented in feedback form

be considered by introducing the class of perturbations $\mathbf{D}^u(r)$ defined as

$$\mathbf{D}^u(r) = \left\{ \Delta^U = \begin{bmatrix} \Delta_1 & & \\ & \ddots & \\ & & \Delta_r \end{bmatrix} \ : \ \Delta_i \in \mathbf{\Delta}_1 \right\} \tag{82}$$

where $\mathbf{\Delta}_1$ is a ball in the space of H_∞ real rational functions, denoted by RH_∞, with radius 1

$$\mathbf{\Delta}_1 = \{ \Delta \ : \ \Delta \in RH_\infty, \ \|\Delta\|_\infty \leq 1 \} .$$

Parametric perturbations or uncertainty can be modeled by letting interval transfer functions represent each physically distinct subsystem. These individual systems can then be "pulled out" and represented in feedback form as described earlier. The result of doing this is the general representation of the system shown in Figure 64.

In this representation, the Δ^U block represents multiple norm-bounded uncertainties, and the Δ^P block accounts for parameter perturbations modeled as the set of independent interval systems $\mathbf{G}^i(s)$ arranged in diagonal form:

$$\mathbf{D}^G(q) = \left\{ \begin{bmatrix} G_1 & & \\ & \ddots & \\ & & G_q \end{bmatrix} \ : \ G_i \in \mathbf{G}^i \right\} . \tag{83}$$

From the discussion of the last subsection we can immediately replace each interval system by a four-parameter set. Further we can also replace each interval system $\mathbf{G}^i(s)$ by the corresponding extremal set $\mathbf{G}_E^i$:

$$\mathbf{D}_E^G(q) = \left\{ \begin{bmatrix} G_1 & & \\ & \ddots & \\ & & G_q \end{bmatrix} \ : \ G_i \in \mathbf{G}_E^i \right\} . \tag{84}$$

56
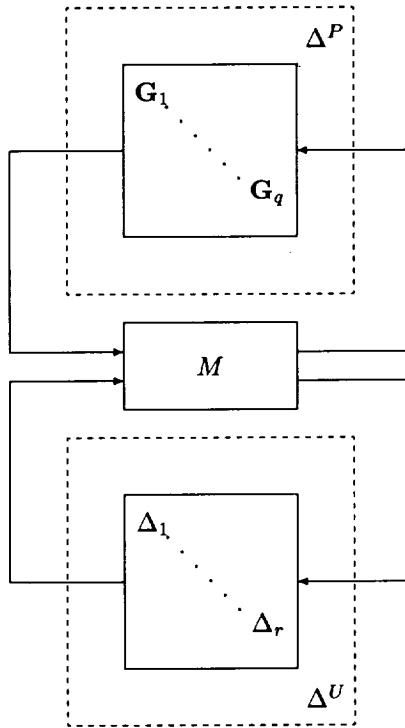
Figure 64: Feedback representation of multiple interval plants and unstructured uncertainties

For carrying out frequency domain analysis, the system in Figure 64 can therefore be replaced by Figure 65 where Δ^{UP} belongs to the mixed complex-real perturbation class $\mathbf{D}^{UP}$ defined as

$$\mathbf{D}^{UP}(r; 4q) = \left\{ \begin{bmatrix} \Delta^U & & & \\ & \lambda_1 & & \\ & & \ddots & \\ & & & \lambda_{4q} \end{bmatrix} \right\}. \tag{85}$$
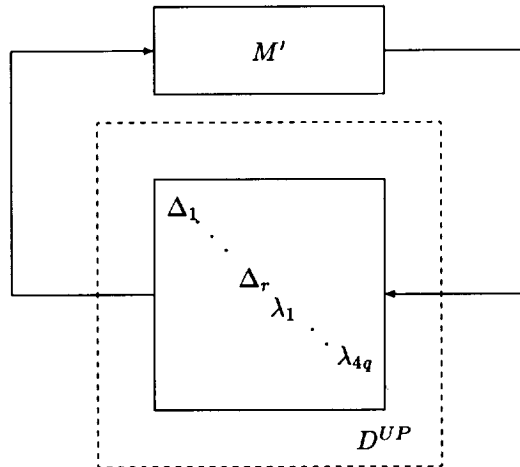
Figure 65: Feedback representation of mixed complex-real block diagonal uncertainties

This representation can be used to formulate a variety of robust stability and performance problems. We illustrate this by considering two specific examples.

Example 17. Consider the control system shown in Figure 66.

57
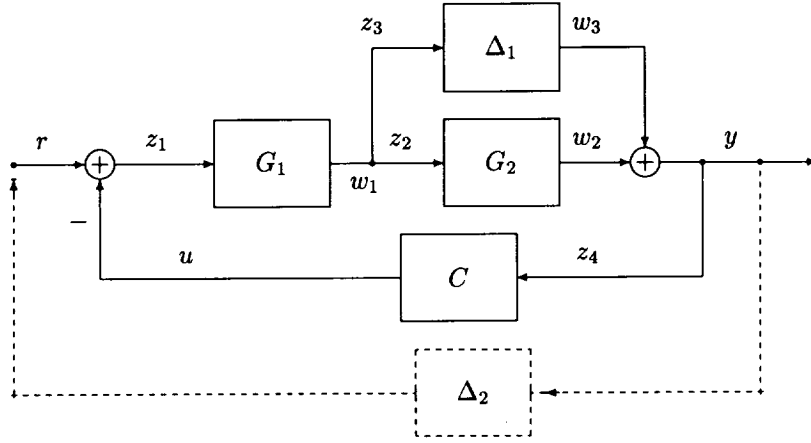
Figure 66: Robust performance problem (Example 17)

In this system there are two independent subsystems containing parametric uncertainty which are modelled by the interval systems $G_1(s) \in \mathbf{G}^1(s)$ and $G_2(s) \in \mathbf{G}^2(s)$. Unstructured perturbations are represented by the block Δ_1, and appropriate scalings have been introduced to allow Δ_1 to belong to $\mathbf{\Delta}_1$, the H_∞ ball of radius unity. The specifications on the system performance are stated as the following requirements:

1) *Robust Stability*   The system must be stable for all $G_1(s) \in \mathbf{G}^1(s)$, $G_2(s) \in \mathbf{G}^2(s)$, $\Delta_1 \in \mathbf{\Delta}_1$ and

2) *Robust Performance*   The worst case H_∞ norm of the closed loop transfer function be bounded by unity:

$$\sup_{\mathbf{G}^1, \mathbf{G}^2, \mathbf{\Delta}_1} \|T_{ry}(G_1, G_2, \Delta_1)\|_\infty < 1,$$

where T_{ry} is the transfer function from r to y.

This problem can be cast in the framework developed above, and treated as a robust stability problem by introducing a fictitious performance block $\Delta_2 \in \mathbf{\Delta}_1$ connected between r and y as shown in Figure 66. The equations describing the system in Figure 66 are

$$\begin{bmatrix} z_1 \\ z_2 \\ z_3 \\ z_4 \\ y \end{bmatrix} = \begin{bmatrix} 0 & 0 & 0 & 1 & -1 \\ 1 & 0 & 0 & 0 & 0 \\ 1 & 0 & 0 & 0 & 0 \\ 0 & 1 & 1 & 0 & 0 \\ 0 & 1 & 1 & 0 & 0 \end{bmatrix} \begin{bmatrix} w_1 \\ w_2 \\ w_3 \\ r \\ u \end{bmatrix}, \qquad \begin{bmatrix} w_1 \\ w_2 \\ w_3 \\ r \\ u \end{bmatrix} = \begin{bmatrix} G_1 & 0 & 0 & 0 & 0 \\ 0 & G_2 & 0 & 0 & 0 \\ 0 & 0 & \Delta_1 & 0 & 0 \\ 0 & 0 & & \Delta_2 & 0 \\ 0 & 0 & 0 & 0 & C \end{bmatrix} \begin{bmatrix} z_1 \\ z_2 \\ z_3 \\ z_4 \\ y \end{bmatrix}.$$

The "feedback" perturbations belong to the class

$$\mathbf{D}^G(2) = \left\{ \begin{bmatrix} G_1 & \\ & G_2 \end{bmatrix} \; : \; G_1 \in \mathbf{G}^1, G_2 \in \mathbf{G}^2 \right\}, \qquad \mathbf{D}^U(2) = \left\{ \begin{bmatrix} \Delta_1 & \\ & \Delta_2 \end{bmatrix} \; : \; \Delta_1, \Delta_2 \in \mathbf{\Delta}_1 \right\}$$

and the interconnection matrix is

$$M = \begin{bmatrix} 0 & 0 & 0 & 1 & -1 \\ 1 & 0 & 0 & 0 & 0 \\ 1 & 0 & 0 & 0 & 0 \\ 0 & 1 & 1 & 0 & 0 \\ 0 & 1 & 1 & 0 & 0 \end{bmatrix}.$$

Example 18.   We consider the system in Figure 67.
Parameter uncertainty is represented by the interval system $G_1(s) \in \mathbf{G}^1(s)$ and unstructured uncertainty consists of two independent blocks $\Delta_1, \Delta_2 \in \mathbf{\Delta}_1$. $W_1(s)$ and $W_2(s)$ represent frequency
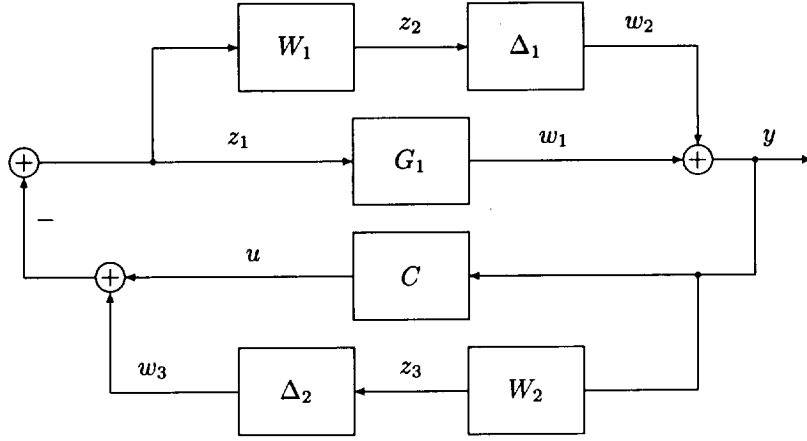
Figure 67: Robust stability problem (Example 11.7)

weightings and consist of fixed stable, proper minimum phase transfer functions. The system equations are

$$
\begin{bmatrix} z_1 \\ z_2 \\ z_3 \\ y \end{bmatrix} = \begin{bmatrix} 0 & 0 & -1 & -1 \\ 0 & 0 & -W_1 & -W_1 \\ W_2 & W_2 & 0 & 0 \\ 1 & 1 & 0 & 0 \end{bmatrix} \begin{bmatrix} w_1 \\ w_2 \\ w_3 \\ u \end{bmatrix}, \qquad \begin{bmatrix} w_1 \\ w_2 \\ w_3 \\ u \end{bmatrix} = \begin{bmatrix} G_1 & 0 & 0 & 0 \\ 0 & \Delta_1 & 0 & 0 \\ 0 & 0 & \Delta_2 & 0 \\ 0 & 0 & 0 & C \end{bmatrix} \begin{bmatrix} z_1 \\ z_2 \\ z_3 \\ y \end{bmatrix}.
$$

This configuration fits the general structure developed above with the "feedback" perturbation classes being

$$
\mathbf{D}^G(1) = \left\{ G_1 \ : \ G_1 \in \mathbf{G}^1 \right\} \quad \text{and} \quad \mathbf{D}^U(2) = \left\{ \begin{bmatrix} \Delta_1 & \\ & \Delta_2 \end{bmatrix} \ : \ \Delta_1, \Delta_2 \in \mathbf{\Delta}_1 \right\}
$$

and the interconnection matrix

$$
M = \begin{bmatrix} 0 & 0 & -1 & -1 \\ 0 & 0 & -W_1 & -W_1 \\ W_2 & W_2 & 0 & 0 \\ 1 & 1 & 0 & 0 \end{bmatrix}.
$$

5.6.4 Extremal Properties

We have shown that parameter uncertainty can be modelled by interval systems and that both parametric and norm-bounded uncertainty can be represented in feedback form. Moreover, each interval system can be replaced, as far as worst case frequency domain analysis is concerned, by the corresponding reduced 4-parameter family.

Let us now consider the system in Figure 64. Suppose that a stabilizing controller for the nominal system has been connected between y and u. The controller is stabilizing when the feedback perturbation is zero. Let $M(s)$ denote the interconnection matrix with the controller attached. We now wish to determine if the control system is robustly stable under the feedback perturbations given. This is a real-complex mixed perturbation robust stability problem with the diagonal "feedback" perturbation matrix (see Figure 65)

$$
\mathbf{D}^{UP} = \left\{ D^{UP} = \begin{bmatrix} \Delta_1 & & & & & \\ & \ddots & & & & \\ & & \Delta_r & & & \\ & & & \lambda_1 & & \\ & & & & \ddots & \\ & & & & & \lambda_{4m} \end{bmatrix} \ : \ \Delta_1 \in \mathbf{\Delta}_1, \ |\lambda_i| \le 1 \right\}.
$$

We make the standing assumption that the McMillan degree of the system remains invariant under the perturbations. The first observation we can make is obvious.

59

Theorem 22. *The system in Figure 64 is Hurwitz stable for all $D^P \in \mathbf{D}^G(m)$ and all $D^u \in \mathbf{D}^U(r)$ if and only if the system in Figure 65 is Hurwitz stable for all $D^{UP} \in \mathbf{D}^{UP}$.*

The above theorem actually applies more generally. For instance a more general formulation could allow for repeated interval system blocks.

As a further simplification in the above result, we can replace each interval system $\mathbf{G}^i(s)$ by the corresponding set of extremal systems $\mathbf{G}^i_E(s)$. This corresponds to replacing each set of 4 λ'_is in Figure 65 by their exposed edges.

Theorem 23. *The system in Figure 64 is Hurwitz stable for all $D^P \in \mathbf{D}^G(m)$ and all $D^u \in \mathbf{D}^U(r)$ if and only if the system in Figure 65 is Hurwitz stable for all $D_P \in \mathbf{D}^G_E(m)$ and all $D^u \in \mathbf{D}^U(r)$.*

Remark 8. The result stated above can be interpreted in terms of the worst case norm-bounded stability margin of the system over the interval parameter uncertainty set. For a prescribed D^P, this stability margin is usually measured as a norm of the smallest destabilizing diagonal perturbation matrix Δ. The norm customarily used is the maximum singular value. The worst case value of this stability margin as D^P ranges over the interval systems can be found by restricting D^P to range over the extremal systems only. This is obviously a tremendous saving in computational effort.

6 INTERVAL MODEL IDENTIFICATION

As demands for the control of flexible structures become more stringent, there arises an increasing need for more precise means of active vibration suppression. However, there is a growing need to develop controllers which are robust; that is the performance of the overall system needs to be insensitive to changes in the plant parameters.

Although passive damping mechanisms such as in-house vibration absorbent materials are helpful, more stringent requirements call for active control schemes. Several types of actuator devices have been developed for applying forces to structures to meet this need. Results in the past have also shown that various design strategies exist for controlling vibration suppression actuators. Some successful local control designs using RMAs are described in various literatures. However, an important issue still remains open; that is maintaining a given level of performance in spite of changes in the plant dynamics. For the past 10 years, an extensive amount of research has been carried out in the area of parametric robust control, which deals with control systems with parametric uncertainties.

Our aim is to apply these theoretical developments to a laboratory experiment, and to achieve meaningful robust control design and analysis of the vibration control of a flexible structure. Therefore, it can be guaranteed that the level of damping will be bounded inside a predicted range. The test structure is a scaled version of a typical flexible truss-like space structure and the parametric uncertainty is represented by mass added to various locations on the structure. This type of structural changes is common in many space-bound dynamic systems. For example, appendage articulation and decreasing fuel weight over the life of a satellite are possible system variations. While inertial changes are chosen for this investigation, this by no means limits the methodology presented herein to only inertial changes. Indeed, the effects of changes of any plant parameter such as structural damping or moduli can be accounted for the interval system techniques.

The structural uncertainties can be modeled in different ways. In the H_∞ approach, the system is described as a nominal model with its corresponding H_∞ error bound transfer function. Minor structural changes may result in the changes of natural frequencies, damping ratios, and mode shapes. For instance, a small change of natural frequency of the lightly damping structures may result in significant frequency domain model error. Consequently, it may be necessary to find an H_∞ error transfer function with large magnitude to bound the model error. Clearly, the choice of largely overbounded H_∞ error bound transfer function results in overly conservative H_∞ control design.

A new model identification scheme has been introduced to overcome this difficulty. The technique introduces a set of artificial parameters to fit the form of interval system framework so that a family of frequency response functions generated by this model contains the dynamics of the actual model. While this technique deals with a single frequency response function, in the work herein, we address the problem of obtaining an interval system model from a set of frequency response functions. These various frequency response functions can be attributed to parameter changes within the structure. Using this identified interval model, a robustness verification is performed to predict the open and closed loop uncertain system behavior. The interval system used in this study is given as a transfer function whose numerator and denominator are linear combinations of polynomials where the coefficients of the linear combinations are bounded with known values.

The paper is organized as follows: first a description of our experimental system including the parameter uncertainty and control strategy is given. Next, a construction of the interval model which captures the system uncertainties due to change of mass is presented. Then detailed analysis of this interval model with the given controller is given. The results are compared with actual experimental data to validate the analysis.

6.1 System Dynamics and Vibration Suppression

6.1.1 Structural Dynamics

A 10-bay aluminum truss structure shown in Figure. 68 is the test article. Each bay of the structure is a 0.5 meter cube made of hollow aluminum tubing joined at spherical nodes with threaded fasteners. The last three bays of the structure form a T-section. This is done so that the torsional modes of vibration will be more pronounced. The final structure has a mass of $31.5kg$ and is cantilevered horizontally from a massive monolithic base. The ANSYS modeling package by Swanson Analysis is used to create a FEM model of the structure as shown in Figure. 69. A modal analysis is performed on the FEM model giving information about the structure's modal frequencies and mode shapes. The results show that 7 modes are within the 100Hz bandwidth.

To verify the FEM model, experimental frequency domain data are collected from the structure using a Tektronix 2642A Fourier Analyzer and compared with the analytically derived transfer function. The input to the structure consists of an impulse applied to Node 40 (see Figure. 69) of the structure, and the output is from an accelerometer mounted at Node 40 as well. The natural
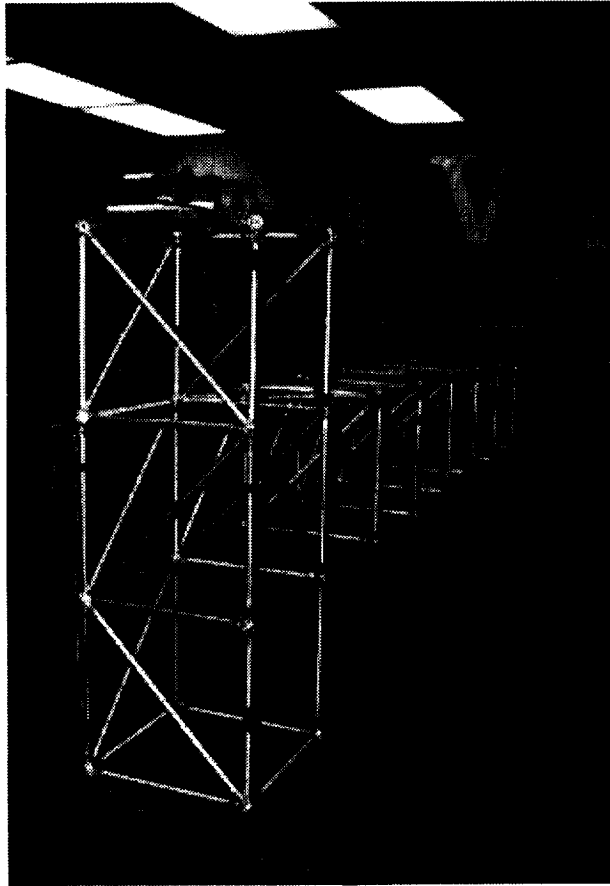
Figure 68: Ten bay MeroForm truss with T-section.

frequencies and damping ratios are obtained by using the Eigensystem Realization Algorithm (ERA) method.

Table 1 shows the results for the first seven modes from the FEM as well as the identified models. From the FEM model we also extract a Guyan reduced order mass matrix M and stiffness matrix K for the structure. Hence the mathematical model of the structure including the ERA identified damping matrix D is represented by

$$M\ddot{x} + D\dot{x} + Kx = Bu. \tag{86}$$

6.1.2 Actuator Dynamics

A reaction mass actuator is used to input force into the structure. This actuator uses a magnet and electrical-coil assembly to accelerate a mass. An amplified signal applied to the stationary electrical-coil creates a magnetic field. The constant field of the magnet inside the moving mass reacts against the new magnetic field causing force and hence movement of the mass. The mass rides on shafts which are limited to linear motion. The mass has a total usable travel length of about 2.5 cm. Any acceleration of the mass caused by force imparted from the coil results in an equal but opposite reaction force on the actuator's housing. When the actuator is mounted on the structure, the force is imparted to the structure. Hence, the actuator is space-realizable, because it requires no inertial reference frame such as the earth.

The actuator contains an internal non-contacting displacement sensor that helps to keep the mass centered with respect to its housing. The block diagram in Figure. 70 shows the local control scheme used to keep the mass centered. The PD type controller contains a proportional feedback loop, which acts as a spring, and a derivative feedback loop, which adds an equivalent viscous damping to the motion of the mass. The resulting system acts like a simple single-degree of freedom mass-spring-damper system. Notice a first-order filter is included to reduce the effects of high frequency noise in the damping loop. Realizing that the force output of the actuator is actually the

62
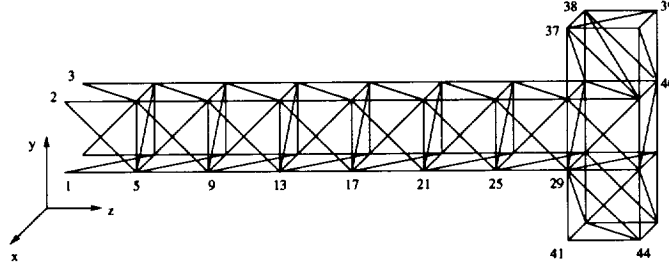
Figure 69: Finite element model of 10 bay truss including node number.

Table 1: Results of FEM model and ERA identified model

Mode	FEM model Freq. (Hz)	ERA model Freq. (Hz)	Damping (ξ)
1 Vertical Bending	9.22	9.45	.0120
2 Horizontal Bending	9.31	9.70	.0140
3 Torsional	18.13	19.69	.0080
4 Vertical Bending	47.43	49.01	.0020
5 Horizontal Bending	55.12	60.30	.0010
6 Torsional	84.73	92.84	.0006
7 Mixed Motion	87.48	98.70	.0003

inertial acceleration of the mass, the output force of the actuator has the following dynamics.

$$\frac{F(s)}{V(s)} = \frac{m\tau s^3 + ms^2}{m\tau s^3 + ms^2 + (c + k\tau)s + k} \tag{87}$$

where m is the mass of the reaction mass, k is the equivalent stiffness, c is the equivalent viscous damping constant, and τ is the time constant of the noise filter. The transfer function represents the force output $F(s)$ with respect to the voltage input $V(s)$.
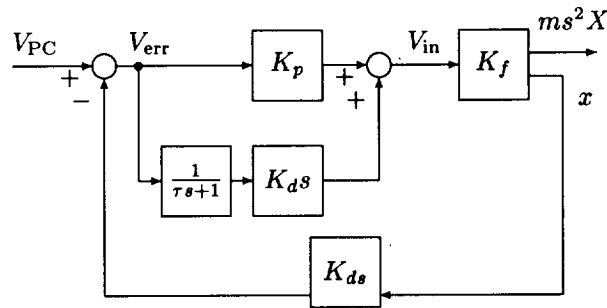
Figure 70: Block diagram of the local centering control system of RMA.

As shown in Figure. 68, the actuator is mounted between Node 39 and Node 40 of the structure. This location on the end of the structure is chosen because the modal participation factors of the first few modes of the structure are large at this location.

It should be noted that several design considerations were enforced when building the actuator and setting the local feedback gains. First, the actuator is designed so that its mass is small compared

to the structure. The reaction mass is approximately 1.67 kg and the parasitic mass is 1.6kg, so that the actuator is just over 10% of the structure's mass. Note also that the efficiency ratio of the actuator itself is 51%. The damping ratio of the actuator affects the damping in the structure for both passively (without active control) and the active control design. This phenomenon has been studied and results in a compromise between damping in the structure and stability of the actuator. These considerations were taken into account when the internal damping in the actuator was chosen.

6.1.3 Parametric Uncertainty

The uncertainty of the structure we consider here is due to added mass to Node 44 and Node 17. We want to examine the structural changes that occur while each added mass varies from 0kg to 2.5kg. In order to observe the frequency domain behavior of the system with respect to the changes of these added masses, we take the following six samples of various added masses as shown in Table 2.

Table 2: Masses added to the structure

Case	1	2	3	4	5	6
Node 17	0	0.5	1.0	1.5	2.0	2.5Kg
Node 44	0	0.5	1.0	1.5	2.0	2.5Kg

Our particular interest is the model uncertainty for the first horizontal mode and the first torsional mode with the natural frequencies ranging from 4 to 24Hz. The output measurement from an accelerometer located at Node 40 in the horizontal direction is used and the input is generated by applying the random signal to the RMA actuator. Figure. 71 illustrates the changes of the experimental data when these inertial parameters change. Therefore, it is reasonable to assume that for any value of added mass ranging from 0 to 2.5kg, the frequency response of the corresponding structure remains inside the thinnest envelope covering the frequency response of these six sampled structures.
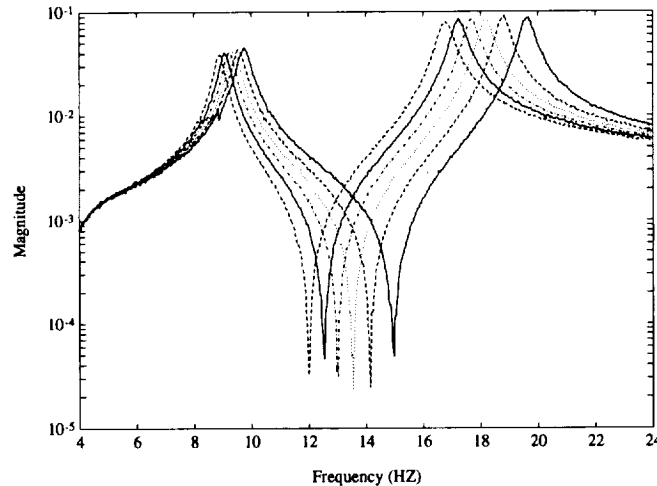
Figure 71: Experimental frequency response function with different added masses: From Right to Left 0Kg, 1Kg, 2Kg, 3Kg, 4Kg, 5 Kg.

By combining Eqs. (86) and (87), we arrive at a transfer function expression of the actuator-structure system

$$G(s,p) = \frac{s^2 X(s,p)}{V(s)} \tag{88}$$

where $V(s)$ is the voltage across the actuator coils and $s^2 X(s,p)$ is the response of an accelerometer. The unknown parameter, p, represents the uncertainty in the structural dynamics. Although we are using inertia to generate a family of perturbed systems, this by no means limits the techniques presented herein to inertial perturbations only.

64

6.1.4 Vibration Suppression Control Law

The controller is designed using classical root loci techniques. However, it is later cast in terms of interval control systems to observe the robustness of the closed loop system. Vibration damping is accomplished with a local velocity feedback (LVF) control scheme. The velocity signal fed into a single actuator from an accelerometer location x at Node 40 horizontal direction is

$$u = -K_v \dot{x}. \tag{89}$$

The control design is based on the model in Eq. (86). Here we consider the first horizontal bending and the first torsional modes. Feeding back velocity multiplied by a feedback gain, K_v, the closed loop pole locations of the system are predicted. After varying the gain, a root locus plot is created. The resulting plot shows a trend of increased damping in all of the modes as the actuator gain is increased.

To implement the controller, a negative velocity signal is fed to the actuator to "cancel out" the motion of the structure, i.e. reduce the velocity of the structure. An accelerometer is mounted on the housing of the actuator and connected to the structure. To get a velocity signal, the acceleration signal from the sensor must be integrated. However, integration of electrical signals results in exponential growth of any DC noise or DC offsets anywhere in the system. Therefore, we use a "velocity estimator". The estimator is formulated as

$$\frac{\hat{V}(s)}{a(s)} = \frac{s}{s^2 + w_c s + w_c^2} \tag{90}$$

where w_c is the break frequency of the filter, $\hat{V}(s)$ is an estimated velocity signal and $a(s)$ is the accelerometer input. The value, w_c, used here is $0.5Hz$, and since the estimator acts like an ideal integrator at frequencies above $6w_c$, the feedback signal should be proportional to the velocity of the structure.

Initially, the controllers are implemented on the structure with no added mass. The control is successful in increasing the system damping, but the question of robustness still remains unanswered. How much will slight changes in the system affect the closed loop control of the structure? The interval system model answers this question.

6.2 Model Identification

6.2.1 Model Structure

The objective of this section is to construct a family of models such that its frequency response contains the six samples of experimental data shown in Figure. 71. Each data set consists of 900 data points over the frequency ranging from 4 to $24Hz$. We first select the structure of the family of transfer functions as follow:

$$\mathbf{G}(s) = \left\{ g(s) \ : \ \frac{n_0(s) + \sum_{i=1}^{m+1} \alpha_i r_i(s)}{d_0(s) + \sum_{i=1}^{m} \beta_i q_i(s)}, \ \alpha_i \in [\alpha_i^-, \alpha_i^+], \ \beta_i \in [\beta_i^-, \beta_i^+], \ \forall \ i \right\} \tag{91}$$

where $n_0(s)$ and $d_0(s)$ are numerator and denominator of the nominal transfer function, and $r_i(s)$ and $q_i(s)$ are base polynomials of degree m and $m - 1$, respectively. The parameters α_i and β_i are the interval parameters which will be determined by their limiting values $\alpha_i^\pm$ and $\beta_i^\pm$. Clearly, upon the determination of the family $\mathbf{G}(s)$, we expect that the frequency response of every structure corresponding to each value of added mass ranging from 0 to 2.5kg remains inside that of the family $\mathbf{G}(s)$.

In the next subsection, we give a brief description of how to determine the desired family of transfer functions $\mathbf{G}(s)$, equivalently determine a set of base polynomials $(r_i(s), q_i(s))$, and the limiting values of interval parameters α_i and β_i. This type of model is called an *interval model*.

6.2.2 Interval Model Identification

The algorithm to generate an interval model starts with identifying a model for each set of data. Any standard identification technique can be used for this purpose and here we use a least-squares based system identification technique which is widely used in practice. We first determine the order of the transfer function:

$$g_i(s) = \frac{n_i(s)}{d_i(s)} = \frac{n_m^i s^m + n_{m-1}^i s^{m-1} + \ldots + n_0^i}{s^m + d_{m-1}^i s^{m-1} + \ldots + d_0^i}, \qquad i = 1, \cdots, 6.$$

Once a judicious choice of the order of the transfer function is made, determination of the coefficients of each transfer function may be easily carried out by solving the least-squares problem. Let $D_i(\omega)$ be the ith sample data set consisting of 900 data points and $W(\omega)$ is a positive weighting function. The coefficients of the transfer function $g_i(s)$ are obtained by minimizing the following index:

$$J_i = \sum_{k=1}^{900} W(w_k) \left[R(\omega_k)^2 + I(\omega_k)^2 \right] \tag{92}$$

where

$$R(\omega_k) := \text{Real} \left[D_i(\omega_k)d_i(j\omega) - n_i(j\omega) \right], \qquad I(\omega_k) := \text{Imag} \left[D_i(\omega_k)d_i(j\omega) - n_i(j\omega) \right].$$

We repeat this procedure for all six data sets to obtain the transfer functions $g_i(s)$, $i = 1, \ldots, 6$. A typical choice for the nominal model $g_0(s)$ is the average of all six of these identified models such as:

$$\underline{n}_0 = \begin{bmatrix} n_0^0 & n_1^0 & \cdots & n_m^0 \end{bmatrix}^T \quad \text{and} \quad \underline{d}_0 = \begin{bmatrix} d_0^0 & d_1^0 & \cdots & d_{m-1}^0 \end{bmatrix}^T \tag{93}$$

where

$$n_l^0 = \frac{1}{6} \sum_{k=1}^{6} n_l^k \quad \text{and} \quad d_l^0 = \frac{1}{6} \sum_{k=1}^{6} d_l^k. \tag{94}$$

The parameter perturbation vectors of the ith identified model are defined as

$$\Delta \underline{n}_i = \underline{n}_i - \underline{n}_0 \quad \text{and} \quad \Delta \underline{d}_i = \underline{d}_i - \underline{d}_0. \tag{95}$$

In order to determine the set of base polynomials $r_i(s)$ and $q_i(s)$ in Eq. (91), we employ a Singular Value Decomposition. To illustrate this SVD technique, we first form a matrix for the uncertainty of the denominator as

$$\Delta D = \begin{bmatrix} \Delta \underline{d}_1 & \Delta \underline{d}_2 & \cdots & \Delta \underline{d}_6 \end{bmatrix}. \tag{96}$$

Then we follow the following procedure:

1) Compute the weighted uncertainty matrix $\Delta D^W = W_d^{-1} \Delta D$ where W_d is a diagonal matrix with its lth diagonal element being the standard deviation of the lth row of ΔD.

2) Using SVD of ΔD^W, compute the basis U of the perturbation matrix ΔD^W (i.e., $\Delta D^W = USV^T$).

3) Compute the basis for ΔD by $U_d = W_d U$ and let

$$U_d = \begin{bmatrix} \underline{u}_{d_1} & \cdots & \underline{u}_{d_m} \end{bmatrix}. \tag{97}$$

4) Compute the base polynomials corresponding to the denominator.

$$q_i(s) = \sum_{l=1}^{m} \underline{u}_{d_i}(l)s^{l-1}, \qquad i = 1, 2, \cdots, 6 \tag{98}$$

where $\underline{u}_{d_i}(l)$ is the lth component of the column vector $\underline{u}_{d_i}$.

5) Determine the coordinate vector of the uncertainty ΔD.

$$\begin{bmatrix} \Delta \underline{q}_1 & \cdots & \Delta \underline{q}_6 \end{bmatrix} = U_d^{-1} \Delta D. \tag{99}$$

6) Determine the upper and lower bounds of the parameters.

$$\beta_l^+ = \max \left\{ \Delta \underline{q}_i(l), \ i = 1, 2, \cdots, 6 \right\}, \qquad \beta_l^- = \min \left\{ \Delta \underline{q}_i(l), \ i = 1, 2, \cdots, 6 \right\}$$

for $l = 1, 2, \cdots, m$.

This interval model represents an optimal linear box of the determined polynomials to cover the perturbation. Similarly, we can obtain $r_i(s)$, α_i^- and α_i^+ for the numerator.

6.3 Interval Model Analysis

The above procedure ensures that every transfer function $g_i(s)$, $i = 1, 2, \cdots, 6$ which represents the system with different added masses, is contained in the interval transfer function $\mathbf{G}(s)$. Consequently, our design and analysis will be performed with this interval model. However, the performance analysis of this type of transfer function cannot be done by traditional techniques such as Bode plots and the root locus method because the transfer function $\mathbf{G}(s)$ represents a family of systems rather than a single system. Here, we give a brief description of how to construct Bode and root locus plots for such systems. Since the interval transfer function represents a family of systems, its Bode plots will form envelopes and the root locus plot will be cluster plots.

In this particular problem, the Bode magnitude plot is obtained as follows: First constructing the set of single parameter transfer functions, let us define the parameter vector which consists of interval parameters

$$\mathbf{p} := [\alpha_1 \ \cdots \ \alpha_{m+1} \ \beta_1 \ \cdots \ \beta_m] := [p_1 \ p_2 \ \cdots \ p_{2m+1}]$$

while the limiting values of each parameter are well-defined for

$$p_i^- \le p_i \le p_i^+, \qquad i = 1, 2, \cdots, 2m + 1.$$

Then the interval model that represents the entire family may be regarded as $\mathbf{G}(s, \mathbf{p})$. A single parameter transfer function is obtained by fixing all parameters at each of their limiting intervals (called *vertices*) except one parameter at a time. For example,

$$\mathbf{G}(s, [p_1 \ p_2^- \ p_3^- \ \cdots \ p_{2m+1}^-])$$

is a single parameter system. This leads us to a total of $(2m + 1)2^{2m}$ single parameter transfer functions. Using this set of single parameter systems, one can construct the Bode magnitude and phase envelopes as well as the plot of root clusters of the entire family $\mathbf{G}(s)$.

Specifically, let $\mathbf{V}_i$ be the set of vertices excluding p_i such as

$$\mathbf{V}_i = \left\{ \begin{array}{c} \left[p_1^-, p_2^-, \cdots, p_{i-1}^-, p_{i+1}^-, \cdots, p_{2m+1}^-\right], \\ \left[p_1^+, p_2^-, \cdots, p_{i-1}^-, p_{i+1}^-, \cdots, p_{2m+1}^-\right], \\ \vdots \\ \left[p_1^-, p_2^+, \cdots, p_{i-1}^-, p_{i+1}^-, \cdots, p_{2m+1}^-\right], \\ \vdots \\ \left[p_1^+, p_2^+, \cdots, p_{i-1}^+, p_{i+1}^+, \cdots, p_{2m+1}^+\right] \end{array} \right\}.$$

It is easy to see that $\mathbf{V}_i$ consists of 2^{2m} components. Let

$$\bar{\mathbf{p}}_i = [p_1 \ p_2 \ \cdots \ p_{i-1} \ p_{i+1} \ \cdots \ p_{2m+1}].$$

Then the boundaries of the Bode magnitude envelope are obtained by collecting

$$\sup_{i=1,\cdots,2m+1} \ \sup_{\lambda \in [0,1]} \left| \mathbf{G}\left(j\omega, [\lambda p_i^- + (1-\lambda)p_i^+, \bar{\mathbf{p}}_i \in \mathbf{V}_i]\right) \right|$$

and

$$\inf_{i=1,\cdots,2m+1} \ \inf_{\lambda \in [0,1]} \left| \mathbf{G}\left(j\omega, [\lambda p_i^- + (1-\lambda)p_i^+, \bar{\mathbf{p}}_i \in \mathbf{V}_i]\right) \right|$$

for every ω. The boundaries of the Bode phase envelope can also be obtained similarly.

The problem of plotting the boundaries of root clusters is nothing but $(2m + 1)2^{2m}$ root locus problem. These boundaries coincide with those of the actual regions in which the poles of the family of systems lie.

6.4 Experimental Results

Utilizing the techniques described earlier, this section gives the design and analysis of the vibration suppression control of the ten-bay truss structure with added mass uncertainty. A reaction mass actuator(RMA) located between nodes 39 and 40 is used to excite and control the structure's motion. An accelerometer located at Node 40 is used to measure the acceleration in the x direction at this position. Here we consider the model for the modes within the $4 - 24\ Hz$ frequency range. There are two modes, one bending mode and one torsional mode, in this bandwidth. The experimental

frequency domain data are collected using a Tektronix 2642A Fourier Analyzer. The 900 point frequency domain experimental data for the system with actuator dynamics is expressed as

$$g_i(\omega_k) = g_a(j\omega_k)g_i^0(\omega_k), \quad k = 1, 2, \ldots, 900 \tag{100}$$

where g_i is the ith set of experimental data and g_i^0 represents the system dynamics excluding actuator dynamics, where the transfer function of the actuator is given by

$$g_a(s) = \frac{n_a(s)}{d_a(s)} = \frac{2.3853 \times 10^{-3}s^3 + 1.6745s^2}{2.3853 \times 10^{-3}s^3 + 1.6745s^2 + 25.781s + 1251.3}. \tag{101}$$

Following the modeling procedure described, we first apply the least squares technique to each set of data g_i^0 to obtain the identified model for each case of added masses given in Table 2. Table 3 shows the structural eigenvalues of these six identified models.

Table 3: Eigenvalues of the identified models

Model No.	First mode	Second mode
1	-1.3864±j61.094	-1.4733±j123.00
2	-1.3065±j59.930	-1.3677±j117.76
3	-1.1854±j58.892	-1.4871±j113.96
4	-1.1081±j57.902	-1.4167±j110.79
5	-1.0424±j56.929	-1.4873±j108.03
6	-0.9581±j55.724	-1.5050±j105.10

After we obtain the identified structural models excluding actuator dynamics, we compute the nominal model as the average of these six models and we have

$$g_0(s) = \frac{n_0(s)}{d_0(s)} = \frac{-3.463 \times 10^{-3}s^4 - 1.173 \times 10^{-3}s^3 - 24.68s^2}{s^4 + 5.241s^3 + 16255s^2 + 40225s + 4.412 \times 10^7}. \tag{102}$$

We now apply the algorithm developed in Section 6.2 to obtain the structural interval model. Table 4 shows the results of the interval model.

Table 4: Results of interval model

	q_1	q_2	q_3	q_4	
s^3	1.4326×10^{-1}	-2.5118×10^{-1}	-1.8767×10^{-2}	-1.0399×10^{-3}	
s^2	8.6678×10^2	5.5011×10^2	-8.0878×10^2	1.1301×10^3	
s^1	4.1568×10^3	1.8545×10^3	6.8649×10^3	8.2205×10^2	
s^0	4.0831×10^6	2.5353×10^6	-2.4265×10^6	-6.1023×10^6	
β^+	3.1117×10^0	2.8036×10^{-1}	2.5123×10^{-2}	2.5140×10^{-3}	
β^-	-2.3396×10^0	-2.1055×10^{-1}	-3.3913×10^{-2}	-2.5161×10^{-3}	

	r_1	r_2	r_3	r_4	r_5
s^4	-8.7360×10^{-4}	-3.2529×10^{-5}	9.2234×10^{-5}	0	0
s^3	-1.3370×10^{-4}	3.8897×10^{-4}	1.0547×10^{-5}	0	0
s^2	-3.3372×10^0	-1.0513×10^0	-3.5316×10^0	0	0
s^1	0	0	0	1	0
s^0	0	0	0	0	1
α^+	2.4339×10^0	1.0485×10^0	6.3217×10^{-2}	0	0
α^-	-1.8816×10^0	-1.3450×10^0	-3.5834×10^{-2}	0	0

The results show that the uncertainty of the denominator is dominated by the uncertainty in the direction of the first singular vector. This phenomenon shows that the perturbation of the denominator coefficients is almost linear due to the changes of the added masses. The perturbation distributed in the direction of the fourth singular vector is around 1000 times smaller than that of the

first singular vector. It also shows that the model uncertainty of the numerator part is dominated by the uncertainty in the directions of the first two singular vectors. Figure. 72 shows the root clusters for the two structural modes of interest. Experimentally identified eigenvalues are also included for our study. These root clusters are generated by evaluating a family of transfer functions (an interval plant), and the method used here is based on the Edge theorem. This means that the poles of every system in the family are found in the regions bounded by the dotted lines in Figure. 72.
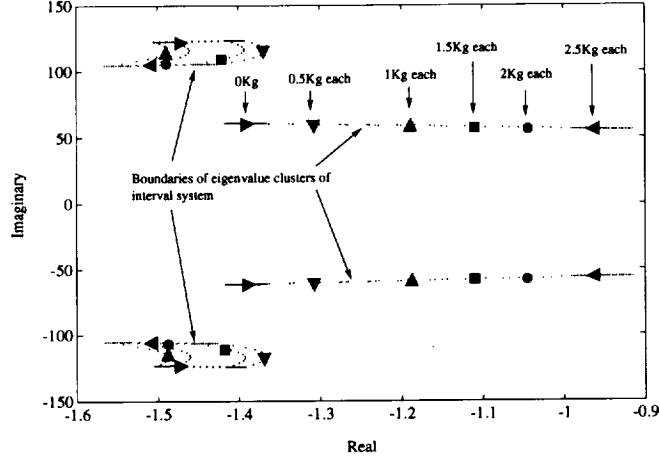

Figure 72: Eigenvalue clusters of interval model and eigenvalues of experimental structure for various added masses.

From the interval model of the structure, one can write the interval model of the system, which includes the actuator dynamics as follows:

$$G(s) = \frac{n_a(s)\left[n_0(s) + \sum_{i=1}^{m+1} \alpha_i r_i(s)\right]}{d_a(s)\left[d_0(s) + \sum_{i=1}^{m} \beta_i q_i(s)\right]} = \frac{n_a(s)n_0(s) + \sum_{i=1}^{m+1} \alpha_i n_a(s)r_i(s)}{d_a(s)d_0(s) + \sum_{i=1}^{m} \beta_i d_a(s)q_i(s)}. \tag{103}$$

To verify the identified interval system by using the closed-loop experiment, we first design a local velocity feedback controller based on the root loci techniques for the vibration suppression of the structure. The transfer function of the controller is

$$K(s) = \frac{n_k(s)}{d_k(s)} = \frac{-110K_v s}{s^2 + \pi s + \pi^2}$$

where K_v is the velocity feedback gain. This controller is designed for the structure without added mass. This controller with $K_v = 30$ increases the damping ratio of the first mode from 2.2% to 6.6% and the damping ratio of the second mode from 1.2% to 3.9%. The closed-loop interval system with the controller $K(s)$ can be computed as

$$T(s) = \frac{d_k(s)\left[n_a(s)n_0(s) + \sum_{i=1}^{m+1} \alpha_i(n_a(s)r_i(s))\right]}{d_k(s)\left[d_a(s)d_0(s) + \sum_{i=1}^{m} \beta_i(d_a(s)q_i(s))\right] + \hat{T}(s)}$$

where

$$\hat{T}(s) = n_k(s)\left[n_a(s)n_0(s) + \sum_{i=1}^{m+1} \alpha_i(n_a(s)r_i(s))\right].$$

This interval system representation may be separated into the fixed and perturbed terms

$$T(s) = \frac{\alpha(s) + \sum_{i=1}^{m+1} \alpha_i \alpha_{1i}(s)}{\beta(s) + \sum_{i=1}^{m} \beta_i \beta_{1i}(s) + \sum_{i=1}^{m+1} \alpha_i \beta_{2i}(s)}. \tag{104}$$

Figure. 73 depicts the magnitude envelope of the closed-loop interval system which shows that the envelope includes the magnitude plots of the experimental transfer functions. We also plot the
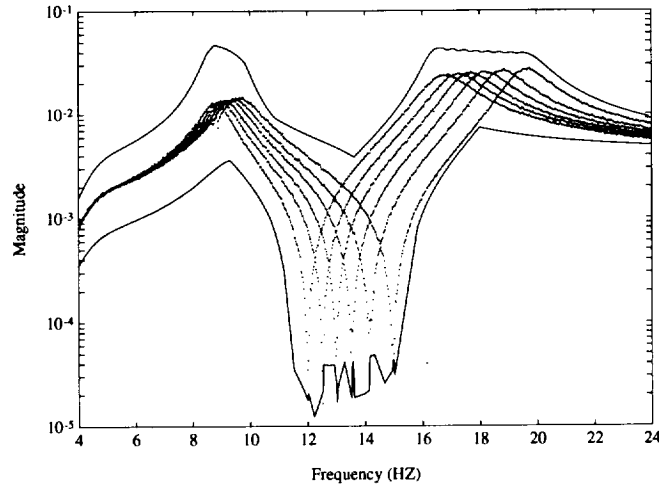
Figure 73: Magnitude envelope (—) of interval model and experimental data (..) for the closed-loop system frequency response functions.

root clusters of the closed-loop interval system in Figure. 74. The damping for each mode of the closed-loop system is increased and it is verified by comparing the boundaries of the root clusters in Figures. 72 and 74. Thus, from this root cluster plot, one can predict the worst case damping of the closed-loop system, while the added mass varies anywhere in between 0 to $2.5Kg$. In other words, as long as the varied system remains inside the interval system family, the poles of the closed-loop system will remain inside the cluster regions shown in Figure. 74.
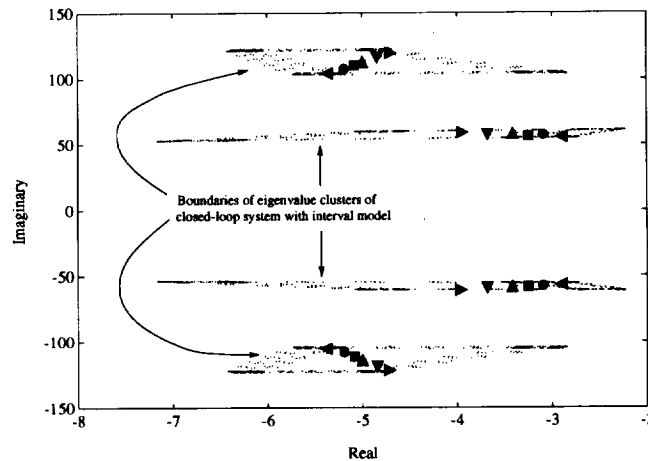
Figure 74: Eigenvalue clusters of closed-loop interval model and eigenvalues of closed-loop experiment for $K_v = 60$.

6.5 Discussion and Remarks

A vibration suppression control law was designed and implemented for an experimental truss structure with parametric uncertainty. It is shown that the system identification technique developed here captures changes in the structural system response due to the parameter variations. Further, the identified interval model was used for robustness verification. That is, the performance bounds of the open and closed loop systems can be mapped with this identified interval model. The robustness verification is independent of the control design methodology and serves over the range of system behavior.

It is worthwhile to note that the number of single parameter systems required to construct the Bode and root cluster plots is relatively large. In fact, this number depends upon the number of interval polynomials for the Bode envelopes and the number of parameters for the root cluster plot. For example, if the interval transfer function is purely a ratio of two interval polynomials, only 32 systems are required to construct the Bode plots regardless of the number of parameters. The transfer function structure chosen here (see Eq. (91)) requires the same number of systems for both plots. This choice is made because our problem is low order and consists of multiple data sets. Nevertheless, since the vibration suppression is achieved by controlling the first few modes of the structure in most cases, the techniques are useful even if the structure is large. As a final note, extension to the case of multivariable system is still an open problem.

7 ROBUSTNESS ANALYSIS OF STATE SPACE MODEL

Most of the results given in this book deal with polynomials containing parameter uncertainty. These results can be directly used when the system model is described by a transfer function whose coefficients contain the uncertain parameters. When the system model is described in the state space framework, the parameters appear as entries of the state space matrices. The polynomial theory can then be applied by first calculating the characteristic polynomial of the matrix as a function of its parameters. In this section, the aim is to provide some computational procedures which can determine robust stability and compute stability margins for the case in which parameters appear linearly in the state space matrices. Under the technical assumption that the perturbation structure is of unity rank the characteristic polynomial coefficients depend on the parameters in multilinear form. This allows us to use the Mapping Theorem to develop an effective computational technique to determine robust stability. This is illustrated with numerical examples.

Next, we describe a Lyapunov based technique to handle perturbations of state space matrices. A stability region in parameter space is determined by this method. While this method does not require us to compute the characteristic polynomial, the stability region obtained from this method is conservative. However, the method gives a direct way to handle perturbations of state space matrices. Furthermore, with these formulas, the stability margin can be increased through optimization over the controller parameter space. This procedure is referred to as robustification. The results are compared with the previously described method, which used the Mapping Theorem, via examples.

In the last part of the section we describe some formulas for the matrix stability margin for the real and complex cases and for some special classes of matrices.

7.1 STATE SPACE PERTURBATIONS

Consider the state space description of a linear system:

$$\dot{x} = Ax + Bu, \qquad y = Cx \tag{105}$$

with the output feedback control

$$u = Ky. \tag{106}$$

The stability of the closed loop system is determined by the stability of the matrix $M := A + BKC$. We suppose that the matrices A, B, K, and C are subject to parameter perturbations. Let

$$\mathbf{p} := [p_1, p_2, \cdots, p_l] \tag{107}$$

denote the parameters subject to uncertainty and set

$$\mathbf{p} = \mathbf{p}^0 + \Delta\mathbf{p} \tag{108}$$

where $\mathbf{p}^0$ is the nominal parameter and $\Delta\mathbf{p}$ denotes a perturbation. Write

$$M(\mathbf{p}) = M(\mathbf{p}^0 + \Delta\mathbf{p}) = M(\mathbf{p}^0) + \Delta M(\mathbf{p}^0, \Delta\mathbf{p}).$$

Assuming that the entries of $\Delta M(\mathbf{p}^0, \Delta\mathbf{p})$ are linear functions of $\Delta\mathbf{p}$, we can write

$$\Delta M(\mathbf{p}^0, \Delta\mathbf{p}) = \Delta p_1 E_1 + \Delta p_2 E_2 + \cdots + \Delta p_l E_l. \tag{109}$$

We shall say that the perturbation structure is of *unity rank* when each matrix E_i has unity rank. The special attraction of unity rank perturbation structures is the fact that in this case the coefficients of the characteristic polynomial of M are multilinear functions of $\Delta\mathbf{p}$ as shown below. When the Δp_i vary in intervals, this multilinear structure allows us to use the Mapping Theorem to develop an effective computational procedure to determine robust stability and stability margins in the parameter space $\mathbf{p}$. The stability margin will be measured as the smallest ℓ_∞ norm of the vector $\Delta\mathbf{p}$ required to make $M(\mathbf{p}^0, \Delta\mathbf{p})$ just unstable.

In the robust stability literature, state space perturbations are often treated by supposing that

$$\Delta M = DUE \tag{110}$$

where the matrix U is regarded as a perturbation. In this formulation, one can calculate the smallest induced norm of U for which $M + \Delta M$ just becomes unstable. We remark that the parametric stability margin, defined as the vector norm of the smallest destabilizing vector $\Delta\mathbf{p}$, has a physical significance in terms of the allowable perturbations of the parameter $\mathbf{p}$. Such a direct significance cannot be attached to the matrix norm. Nevertheless, it has become customary to consider matrix valued perturbations and we accordingly define the *matrix stability radius* as the norm of the smallest destabilizing matrix. We give some formulas for the calculation of the matrix stability radius in the real and complex cases.

7.2 ROBUST STABILITY OF INTERVAL MATRICES

We first establish that the unity rank perturbation structure leads to multilinear dependence of the characteristic polynomial coefficients on the parameter $\mathbf{p}$.

7.3 Unity Rank Perturbation Structure

Let us suppose that

$$M(\mathbf{p}) := \underbrace{M(\mathbf{p}^0)}_{M_0} + \Delta p_1 E_1 + \Delta p_2 E_2 + \cdots + \Delta p_l E_l. \tag{111}$$

Lemma 4. *Under the assumption that* $\mathrm{rank}(E_i) = 1$ *for each* i, *the coefficients of the characteristic polynomial of* $M(\mathbf{p})$ *are multilinear functions of* $\mathbf{p}$.

7.3.1 Interval Matrix Stability via the Mapping Theorem

The objectives are to solve the following problems:

Problem 1   Determine if each matrix $M(\mathbf{p})$ remains stable as the parameter $\mathbf{p}$ ranges over given perturbation bounds $p_i^- \le p_i \le p_i^+$, $i = 1, \cdots, l$.

Problem 2   With a stable $M(\mathbf{p}^0)$, determine the maximum value of ϵ so that the matrix $M(\mathbf{p})$ remains stable under all parameter perturbations ranging over $p_i^0 - w_i\epsilon \le p_i \le p_i^0 + w_i\epsilon$ for predetermined weights $w_i > 0$.

These problems may be effectively solved by using the fact that the characteristic polynomial of the matrix is a multilinear function of the parameters.

The problem 1 can be solved by the following algorithm:

Step 1:   Determine the eigenvalues of the matrix $M(\mathbf{p})$ with $\mathbf{p}$ fixed at each vertex of Π. With this generate the characteristic polynomials corresponding to the vertices of Π.

Step 2:   Verify the stability of the line segments connecting the vertex characteristic polynomials. This may be done by checking the Bounded Phase Condition or the Segment Lemma.

We remark that the procedure outlined above does not require the determination of the characteristic polynomial as a *function* of the parameter $\mathbf{p}$. It is enough to know that the function is multilinear. To determine the maximum value of ϵ which solves the second problem, we may simply repeat the previous steps for incremental values of ϵ. In fact, an upper bound $\bar{\epsilon}$ can be found as that value of ϵ for which one of the *vertices* becomes just unstable. A lower bound $\underline{\epsilon}$ can be determined as the value of ϵ for which a *segment* joining the vertices becomes unstable as follows:

Step 1:   Set $\underline{\epsilon} = \bar{\epsilon}/2$

Step 2:   Check the maximal phase differences of the vertex polynomials over the parameter box corresponding to $\underline{\epsilon}$.

Step 3:   If the maximal phase difference is less than π radians, then increase $\underline{\epsilon}$ to $\underline{\epsilon} + (\bar{\epsilon} - \underline{\epsilon})/2$ for example, and repeat Step 2.

Step 4:   If the maximal phase difference is π radians or greater, then decrease $\underline{\epsilon}$ to $\underline{\epsilon} - (\bar{\epsilon} - \underline{\epsilon})/2$ and repeat Step 2.

Step 5:   This iteration stops when the incremental step or decremental step becomes small enough. This gives a lower bound $\underline{\epsilon}$ and an upper bound $\bar{\epsilon}$.

If $\underline{\epsilon}$ and $\bar{\epsilon}$ are not close enough, we can refine the iteration by partitioning the interval uncertainty set into smaller boxes.

The following examples illustrate this algorithm.

7.3.2 Numerical Examples

Example 19. Consider the interval matrix:

$$A(\mathbf{p}) = \begin{bmatrix} p_1 & p_2 \\ p_3 & 0 \end{bmatrix}$$

where

$$\mathbf{p}^0 = [p_1^0, p_2^0, p_3^0] = [-3, -2, 1]$$

and

$$p_1 \in [p_1^-, p_1^+] = [-3 - \epsilon, -3 + \epsilon], \quad p_2 \in [p_2^-, p_2^+] = [-2 - \epsilon, -2 + \epsilon], \quad p_3 \in [p_3^-, p_3^+] = [1 - \epsilon, 1 + \epsilon].$$

The problem is to find the maximum value ϵ^* so that the matrix $A(\mathbf{p})$ remains stable for all $\epsilon \in [0, \epsilon^*]$. Although the solution to this simple problem can be worked out analytically we work through the steps in some detail to illustrate the calculations involved.

The characteristic polynomial of the matrix is:

$$\delta(s, \mathbf{p}) = s(s - p_1) - p_2 p_3.$$

In general this functional form is not required since only the vertex characteristic polynomials are needed and they can be found from the eigenvalues of the corresponding vertex matrices. Let us now compute the upper bound for ϵ. We have eight vertex polynomials parametrized by ϵ:

$$\mathbf{\Delta}_V(s) := \{\delta_i(s, \mathbf{p}) : \mathbf{p} \in \mathbf{V}\}$$

where

$$\mathbf{V} := \{(p_1^-, p_2^+, p_3^+), (p_1^-, p_2^-, p_3^+), (p_1^-, p_2^+, p_3^-), (p_1^-, p_2^-, p_3^-), (p_1^+, p_2^+, p_3^+),$$
$$(p_1^+, p_2^-, p_3^+), (p_1^+, p_2^+, p_3^-), (p_1^+, p_2^-, p_3^-)\}$$

We found that the vertex polynomial $\delta_3(s)$ has a $j\omega$ root at $\epsilon = 1$. Thus we set $\bar{\epsilon} = 1$. Using the multilinear version of GKT (Theorem 11.1), $\mathbf{\Delta}(s)$ is robustly Hurwitz stable if and only if the following sets are Hurwitz stable:

$$\mathbf{L}_1 = \left\{ s \left[\lambda(s - p_1^-) + (1 - \lambda)(s - p_1^+) \right] - p_2^+ p_3^+ : \lambda \in [0, 1] \right\}$$
$$\mathbf{L}_2 = \left\{ s \left[\lambda(s - p_1^-) + (1 - \lambda)(s - p_1^+) \right] - p_2^- p_3^+ : \lambda \in [0, 1] \right\}$$
$$\mathbf{L}_3 = \left\{ s \left[\lambda(s - p_1^-) + (1 - \lambda)(s - p_1^+) \right] - p_2^+ p_3^- : \lambda \in [0, 1] \right\}$$
$$\mathbf{L}_4 = \left\{ s \left[\lambda(s - p_1^-) + (1 - \lambda)(s - p_1^+) \right] - p_2^- p_3^- : \lambda \in [0, 1] \right\}$$
$$\mathbf{M}_5 = \left\{ s(s - p_1^-) - \left[\lambda_1 p_2^- + (1 - \lambda_1) p_2^+ \right] \left[\lambda_2 p_3^- + (1 - \lambda_2) p_3^+ \right] : (\lambda_1, \lambda_2) \in [0, 1] \times [0, 1] \right\}$$
$$\mathbf{M}_6 = \left\{ s(s - p_1^+) - \left[\lambda_1 p_2^- + (1 - \lambda_1) p_2^+ \right] \left[\lambda_2 p_3^- + (1 - \lambda_2) p_3^+ \right] : (\lambda_1, \lambda_2) \in [0, 1] \times [0, 1] \right\}.$$

The $\mathbf{L}_i$, $i = 1, 2, 3, 4$ are line segments of polynomials, so we rewrite them as follows:

$$L_1 = \lambda(s - p_1^- - p_2^+ p_3^+) + (1 - \lambda)(s - p_1^+ - p_2^+ p_3^+)$$
$$L_2 = \lambda(s - p_1^- - p_2^- p_3^+) + (1 - \lambda)(s - p_1^+ - p_2^- p_3^+)$$
$$L_3 = \lambda(s - p_1^- - p_2^+ p_3^-) + (1 - \lambda)(s - p_1^+ - p_2^+ p_3^-)$$
$$L_4 = \lambda(s - p_1^- - p_2^- p_3^-) + (1 - \lambda)(s - p_1^+ - p_2^- p_3^-)$$

Now we need to generate the set of line segments that constructs the convex hull of the image sets of $\mathbf{M}_5$ and $\mathbf{M}_6$. This can be done by connecting every pair of vertex polynomials. The vertex set corresponding to $\mathbf{M}_5$ is:

$$\mathbf{M}_{5V}(s) := \{M_5 : (\lambda_1, \lambda_2) \in \{(0, 0), (0, 1), (1, 0), (1, 1)\}\}.$$

If we connect every pair of these vertex polynomials, we have the line segments:

$$L_5 = s(s - p_1^-) - \left[\lambda p_2^+ p_3^+ + (1 - \lambda) p_2^+ p_3^- \right] = \lambda(s^2 - p_1^- s - p_2^+ p_3^+) + (1 - \lambda)(s^2 - p_1^- s - p_2^+ p_3^-)$$
$$L_6 = s(s - p_1^-) - \left[\lambda p_2^+ p_3^+ + (1 - \lambda) p_2^- p_3^+ \right] = \lambda(s^2 - p_1^- s - p_2^+ p_3^+) + (1 - \lambda)(s^2 - p_1^- s - p_2^- p_3^+)$$
$$L_7 = s(s - p_1^-) - \left[\lambda p_2^- p_3^+ + (1 - \lambda) p_2^- p_3^- \right] = \lambda(s^2 - p_1^- s - p_2^- p_3^+) + (1 - \lambda)(s^2 - p_1^- s - p_2^- p_3^-)$$
$$L_8 = s(s - p_1^-) - \left[\lambda p_2^+ p_3^- + (1 - \lambda) p_2^- p_3^- \right] = \lambda(s^2 - p_1^- s - p_2^+ p_3^-) + (1 - \lambda)(s^2 - p_1^- s - p_2^- p_3^-)$$
$$L_9 = s(s - p_1^-) - \left[\lambda p_2^+ p_3^- + (1 - \lambda) p_2^- p_3^+ \right] = \lambda(s^2 - p_1^- s - p_2^+ p_3^-) + (1 - \lambda)(s^2 - p_1^- s - p_2^- p_3^+)$$
$$L_{10} = s(s - p_1^-) - \left[\lambda p_2^+ p_3^+ + (1 - \lambda) p_2^- p_3^- \right] = \lambda(s^2 - p_1^- s - p_2^+ p_3^+) + (1 - \lambda)(s^2 - p_1^- s - p_2^- p_3^-).$$

74

Similarly, for $\mathbf{M}_6$ we have the line segments:

$$L_{11} = s(s - p_1^+) - \left[\lambda p_2^+ p_3^+ + (1 - \lambda)p_2^+ p_3^-\right] = \lambda(s^2 - p_1^+ s - p_2^+ p_3^+) + (1 - \lambda)(s^2 - p_1^+ s - p_2^+ p_3^-)$$

$$L_{12} = s(s - p_1^+) - \left[\lambda p_2^+ p_3^+ + (1 - \lambda)p_2^- p_3^+\right] = \lambda(s^2 - p_1^+ s - p_2^+ p_3^+) + (1 - \lambda)(s^2 - p_1^+ s - p_2^- p_3^+)$$

$$L_{13} = s(s - p_1^+) - \left[\lambda p_2^- p_3^+ + (1 - \lambda)p_2^- p_3^-\right] = \lambda(s^2 - p_1^+ s - p_2^- p_3^+) + (1 - \lambda)(s^2 - p_1^+ s - p_2^- p_3^-)$$

$$L_{14} = s(s - p_1^+) - \left[\lambda p_2^+ p_3^- + (1 - \lambda)p_2^- p_3^-\right] = \lambda(s^2 - p_1^+ s - p_2^+ p_3^-) + (1 - \lambda)(s^2 - p_1^+ s - p_2^- p_3^-)$$

$$L_{15} = s(s - p_1^+) - \left[\lambda p_2^+ p_3^- + (1 - \lambda)p_2^- p_3^+\right] = \lambda(s^2 - p_1^+ s - p_2^+ p_3^-) + (1 - \lambda)(s^2 - p_1^+ s - p_2^- p_3^+)$$

$$L_{16} = s(s - p_1^+) - \left[\lambda p_2^+ p_3^+ + (1 - \lambda)p_2^- p_3^-\right] = \lambda(s^2 - p_1^+ s - p_2^+ p_3^+) + (1 - \lambda)(s^2 - p_1^+ s - p_2^- p_3^-).$$

The total number of line segments joining vertex pairs in the parameter space is 28. However the actual number of segments we checked is 16. This saving is due to the multilinear version of GKT (Theorem 11.1), which reduces the set to be checked. By testing these segments we find that they are all stable for $\epsilon < 1$. Since $\epsilon = 1$ corresponds to the instability of the vertex polynomial $\delta_3(s)$ we conclude that the exact value of the stability margin is $\epsilon = 1$. The stability check of the segments can be carried out using the Segment Lemma.

We can also solve this problem by using the Bounded Phase Condition. The set of vertices is

$$\mathbf{\Delta}_\mathbf{V}(s) = \{V_i, i = 1, 2, \cdots, 8\}$$

where

$$V_1(s) = s^2 - p_1^+ s - p_2^+ p_3^+ = s^2 - 2s + 2, \qquad V_2(s) = s^2 - p_1^+ s - p_2^- p_3^+ = s^2 - 2s + 6,$$

$$V_3(s) = s^2 - p_1^+ s - p_2^+ p_3^- = s^2 - 2s, \qquad V_4(s) = s^2 - p_1^+ s - p_2^- p_3^- = s^2 - 2s,$$

$$V_5(s) = s^2 - p_1^- s - p_2^+ p_3^+ = s^2 - 4s + 2, \qquad V_6(s) = s^2 - p_1^- s - p_2^- p_3^+ = s^2 - 4s + 6,$$

$$V_7(s) = s^2 - p_1^- s - p_2^+ p_3^- = s^2 - 4s, \qquad V_8(s) = s^2 - p_1^- s - p_2^- p_3^- = s^2 - 4s.$$

From the vertex set we see that the difference polynomials $V_i(s) - V_j(s)$ are either constant, first order, antiHurwitz or of the form cs and each of these forms satisfy the conditions of the Vertex Lemma. Thus the stability of the vertices implies that of the edges. Thus the first encounter with instability can only occur on a vertex. This implies that the smallest value already found of $\epsilon = 1$ for which a vertex becomes unstable is the correct value of the margin.
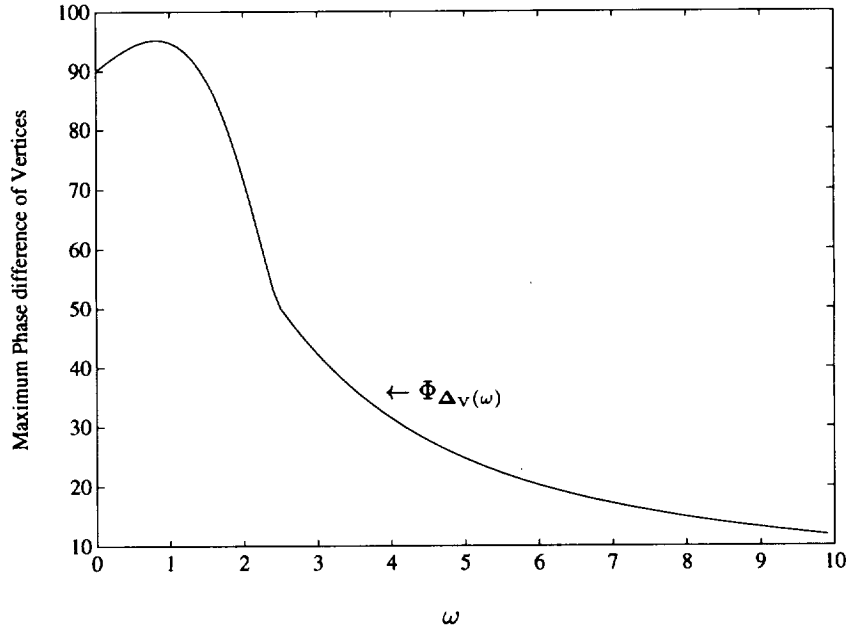

Figure 75: Maximum Phase Differences $\Phi_{\mathbf{\Delta}_\mathbf{V}(\omega)}$ (in degrees) of Vertex Polynomials (Example 19)

This conclusion can also be verified by checking the phases of the vertices. Since there are duplicated vertices, we simply plot phase differences of six distinct vertices of $\Delta(j\omega)$ with $\epsilon = 1$. Figure 75 shows that the maximum phase difference plot as a function of frequency. This plot shows that the maximal phase difference never reaches 180 degrees confirming once again that $\epsilon = 1$ is indeed the true margin.

Remark 9. The phase of a vertex which touches the origin cannot be determined and only the phase difference over the vertex set is meaningful. The phase condition can therefore only be used to determine whether the line segment excluding endpoints, intersects the origin. Thus, the stability of all the vertices must be verified independently.

Example 20. Let

$$\frac{dx}{dt} = (A + BKC)x = \left(\begin{bmatrix} -1 & 0 & 0 \\ 0 & -2 & 0 \\ 0 & 0 & -3 \end{bmatrix} + \begin{bmatrix} 1 & 0 \\ 0 & 1 \\ 1 & 1 \end{bmatrix} \begin{bmatrix} -1+k_1 & 0 \\ 0 & -1+k_2 \end{bmatrix} \begin{bmatrix} 1 & 0 & 1 \\ 0 & 1 & 0 \end{bmatrix} \right) x$$

where

$$k_1 \in [k_1^-, k_1^+] = [-\epsilon, \epsilon] \qquad k_2 \in [k_2^-, k_2^+] = [-\epsilon, \epsilon].$$

We first find all the vertex polynomials.

$$\Delta_V(s) := \{\delta_i(s, \mathbf{k}_i) : \mathbf{k}_i \in \mathbf{V}, \quad i = 1, 2, 3, 4\}$$

where

$$\mathbf{V} := \left\{ (k_1, k_2) : (k_1^+, k_2^+), (k_1^-, k_2^-), (k_1^-, k_2^+), (k_1^+, k_2^-) \right\}.$$

We found that the minimum value of ϵ such that a vertex polynomial just becomes unstable is 1.75. Thus, $\bar{\epsilon} = 1.75$. Then we proceed by checking either the phase condition or the Segment Lemma. If the Segment Lemma is applied, one must verify the stability of six segments joining the four vertices in $\Delta_V(s)$. If the phase condition is applied, one must evaluate the phases of the four vertex polynomials and find the maximum phase difference at each frequency to observe whether it reaches 180°. Again, the calculation shows that the smallest value of ϵ that results in a segment becoming unstable is 1.75. Thus $\underline{\epsilon} = 1.75$. This shows that the value obtained $\epsilon = 1.75$ is the true margin.

The algorithm can also be applied to the robust stability problem for nonHurwitz regions. The following example illustrates the discrete time case.

Example 21. Consider the discrete time system:

$$\underline{x}(k+1) = \begin{bmatrix} -0.5 & 0 & k_2 \\ 1 & 0.50 & -1 \\ k_1 & k_1 & 0.3 \end{bmatrix} \underline{x}(k)$$

For the nominal values of $k_1^0 = k_2^0 = 0$, the system is Schur stable. We want to determine the maximum value of ϵ^* so that for all parameters lying in the range

$$k_1 \in (-\epsilon^*, \epsilon^*) \qquad k_2 \in (-\epsilon^*, \epsilon^*)$$

the system remains Schur stable. Using the procedure, we find the upper bound $\bar{\epsilon} = 0.2745$ which is the minimum value of ϵ which results in a vertex polynomial just becoming unstable. Figure 76 shows that the maximum phase difference over all vertices at each $\theta \in [0, 2\pi)$ with $\epsilon = \bar{\epsilon}$ is less than 180°. Thus we conclude from the Mapping Theorem that the exact parametric stability margin of this system is 0.2745.
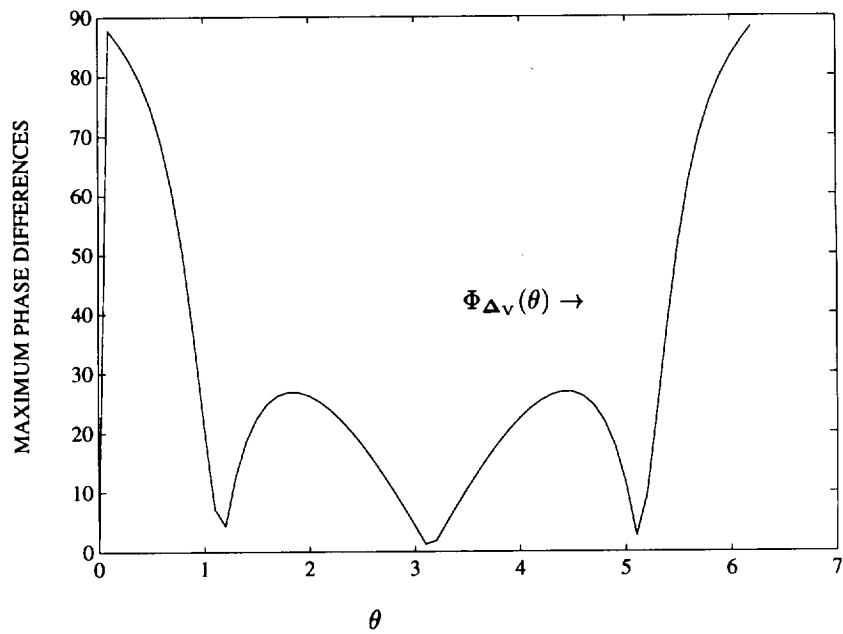
Figure 76: $\Phi_{\Delta_V}(\theta)$ vs θ (Example 21)